THEORETICAL AND EXPERIMENTAL APPROACHES IN SCIENTIFIC STUDIES 2025

Editor

Assist Prof. Dr. Edip TAŞKESEN

Lect. Dr. Canan ÜLGEN

yaz

yayınları

Theoretical and Experimental Approaches in Scientific Studies 2025

Editors

Assist. Prof. Dr. Edip TAŞKESEN

Lect. Dr. Canan ÜLGEN

yaz yayınları

2025

yaz
yayınları

Theoretical and Experimental Approaches in Scientific Studies 2025

Editor: Assist. Prof. Dr. Edip TAŞKESEN

ORCID NO: 0000-0002-3052-9883

Editor: Lect. Dr. Canan ÜLGEN

ORCID NO: 0000-0002-8272-3370

E_ISBN 978-625-8508-84-0

Aralık 2025 – Afyonkarahisar

Dizgi/Mizanpaj: YAZ Yayınları

Kapak Tasarım: YAZ Yayınları

YAZ Yayınları. Yayıncı Sertifika No: 73086

M.İhtisas OSB Mah. 4A Cad. No:3/3
İscehisar/AFYONKARAHİSAR

www.yazyayinlari.com

yazyayinlari@gmail.com

info@yazyayinlari.com

CONTENTS

HYDROELECTRIC ENERGY GENERATION, BASIC PRINCIPLES AND APPLICATIONS

Elif Nur BİLEN[1]

Edip TAŞKESEN[2]

1. INTRODUCTION

Industrialization, economic, social, technological developments and population growth are rapidly increasing the demand for energy [1]. In order to sustain a comfortable life, maintain a modern standard of living, and reach our needs more easily, energy must be consumed directly or indirectly. For the continuity of this comfortable life, energy is needed to create and use the tools that make our lives easier. Fossil fuels, which play a major role in meeting this need, are non-renewable and are harmful to human health and the environment. When producing energy, it is necessary to minimize the negative effects on the environment and human health and to continue the continuity of energy production, it is necessary to turn to renewable energy sources known as environmentally friendly [2]. There are many renewable energy sources such as wind, solar, hydraulic, hydrogen, bioenergy and marine energy. Renewable energy sources are easy to access and are inexhaustible because they are naturally available. One of the most important features of the use of renewable energy sources is that it will reduce the need to purchase energy from foreign countries due to its easy accessibility [3].

[1] Energy System Senior Engineer, Harran University, Mechanical Engineering, Mechanical Engineering Doctorate, ORCID: 0000-0002-7385-3704.

[2] Şırnak University\Faculty of Engineering\Energy Systems Engineering, ORCID: 0000-0002-3052-9883.

Considering the production of electricity from fossil fuels, hydroelectricity, which uses water as fuel, offers a clean, renewable and cheap energy source [4].

In this study, information is given about hydroelectric energy, which is produced by utilizing the potential and kinetic energy of water, which is widely used in our country and in the world.

2. PRINCIPLES OF HYDROELECTRIC ENERGY

Hydraulic Energy is the potential energy of water that has gained some height. Hydroelectric Energy is the electrical energy obtained by converting this potential energy into mechanical energy by various means and then into electrical energy [5]. The basic working principle of hydroelectric power plants is to generate electricity by turning turbines as water falls from a certain level [6]. In storage type facilities, the potential power of water depends on a certain height. Since this water, which has potential energy, gains flow due to falling from a certain level, it creates kinetic energy due to its amount and speed. In the water that is given fluidity, pressure force occurs and converts the pressure force into hydraulic power. The rotation of a hydraulic turbine is provided by passing the water taken through water transmission channels or pipes over the turbine blades. In this way, hydraulic power is converted into mechanical power. Generators that convert mechanical energy into electrical energy are directly connected to the turbine. The rotation of the generator rotor provides mechanical energy formed in the turbine. As the rotor rotates, electrical energy is produced in the stator. The electrical energy in the generators, which is brought to appropriate values using various electrical equipment, is then given to the transmission line [3], [7] .

3. TYPES OF HYDROELECRIC POWER PLANTS

Hydroelectric power plants are divided into various types given below based on their design, location and operating methods.

- **According to the Load Meeting Status of the National Electricity System:**
  - **Base Power Plants:** These are power plants that continuously produce more than 30% of energy with a usage factor.
  - **Peak Power Plants:** These are power plants that have a usage factor below 30% and operate during the times when energy is needed the most [8].
- **According to Storage Structures:**

Run-of-river power plants: They are small or medium-sized power plants that have many advantages such as not having problems such as construction and expropriation of the place where they will be built, not having high investment and operating costs, and being simple to install (Figure 1) [9].

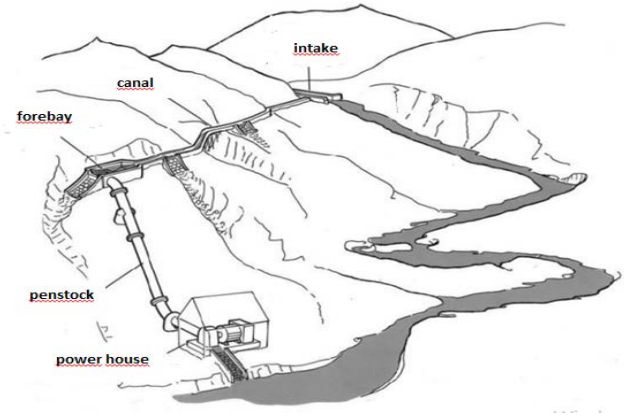

Figure 1. Run-of-river hydroelectric power plant [10].

Channel power plants: It is based on the principle of generating electrical energy by transmitting water to the power plant through a transmission system such as a penstock or canal [9].

Pumped reservoir power plants: Pumped Storage Hydroelectric Power Plants are facilities planned for the storage of electrical energy. They work with the logic of producing and consuming electricity with a large amount of water, and there are two reservoirs in their structures. Electricity is produced by utilizing the height difference between these two reservoirs. When the need for electrical energy is very low, electricity is consumed by pumping water to the upper reservoir with the help of a pump and water is collected in the upper reservoir. When electrical energy is needed the most, water is released from the upper reservoir to the lower reservoir and electricity is produced with the turbined water (Figure 2) [9], [11].

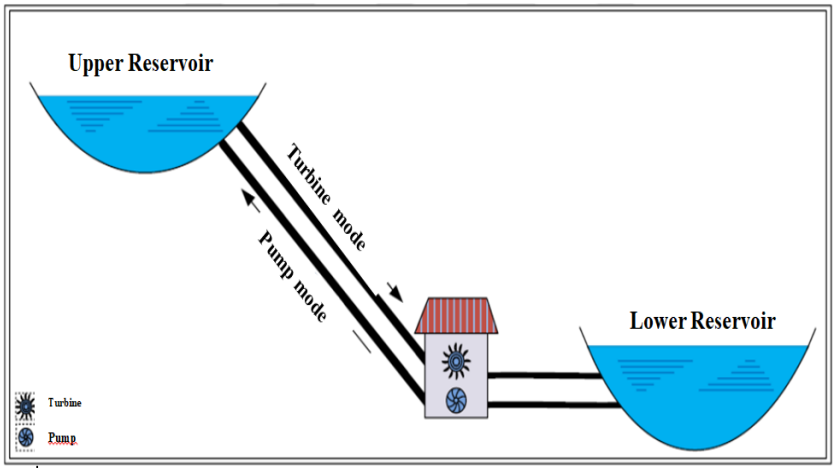

Figure 2. Schematic Representation of Pumped Storage Hydroelectric Power Plant Facility [11].

Dam type power plants: Hydroelectric power plants with reservoirs can store water for later use, usually saving water during the high-flow season and releasing it during the low-flow

season. A reservoir provides greater flexibility and allows the hydroelectric power plant to better adapt to demand, both in the short term and seasonally. Dams have the ability to regulate flow rates [9], [12].

- **According to Your Dreams:**
    - **Low Head Hydroelectric Power Plant (H<15 m):** These are power plants that are built on rivers with a head of less than 15 m, flowing on flat lands, with a low bed slope, generally have a large flow rate, and mostly use Kaplan type turbines. The principle diagram of the Kaplan turbine is given in Figure 3 [13].

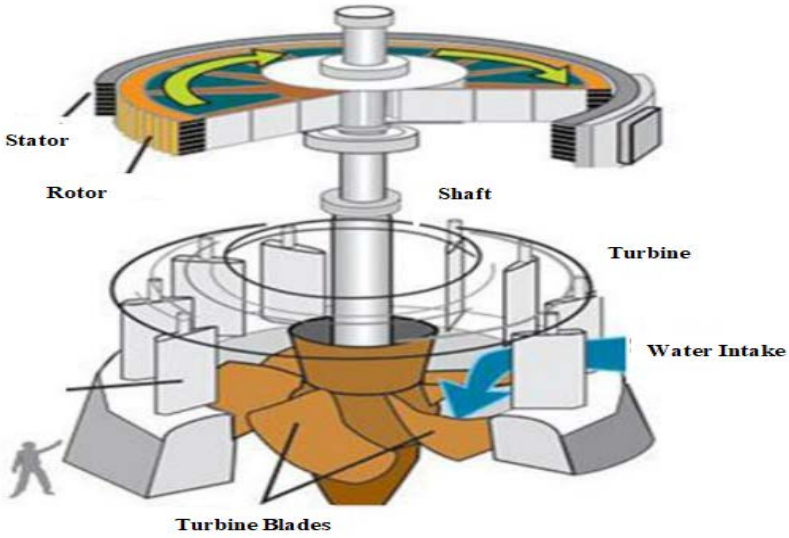

Figure 3. Kaplan turbine principle diagram [13].

- **Medium Head HEPP (H= between 10-50 m) :** These are power plants that are installed on rivers with various flow rates, with a head of 15–50 m, without a long penstock system, and using Kaplan or Francis type turbines. The Francis turbine principle diagram is shown in Figure 4 [13].

Figure 4. Francis türbin [5].

- **High Head HEPP (Head greater than H>50 m):** These are power plants built on rivers or dams with a head greater than 50 m, usually flowing through rugged or mountainous terrain. They have a long penstock, flow rates are variable, there is an approach channel and tunnel, Francis or Pelton type turbines are used. The Pelton turbine principle diagram is shown in Figure 5 [13].

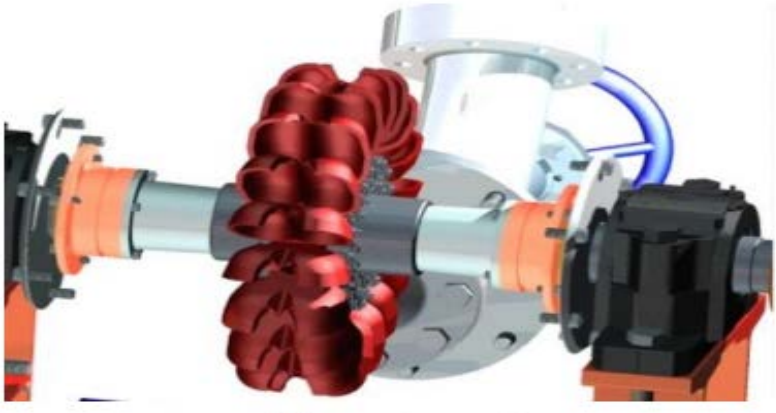

Figure 5. Pelton türbine [13].

- **According to the Type of Dam Body:**

  - **Concrete arch body dam:**

Dams with very long dam bodies are generally made of concrete. They are preferred in valleys with solid foundations and slope conditions [14].

  - **Filled body dam:**

In regions where there are no major geological problems, rock, soil and rock-filled dams with a concrete front face are preferred. These types of dams, which are more frequently preferred in places where earthquakes are likely, are desired to be placed in a larger area [14].

- **According to the Location of the Power Plant Building:**

When selecting one of the power plant building types, the geological and physical conditions of the power plant location should be thoroughly examined, and flood characteristics should be determined in detail together with the hydrological analysis of the tail water. After determining the flood level and examining the physical condition of the settlement, the appropriate one of the mentioned types should be selected.

  - **Above ground:** In above ground power plants, the turbine and generator hall are located approximately at the landscaping level. In order to make such a choice, the turbine type must be suitable and there must be no flood risk.
  - **Semi-buried or submerged:** In semi-buried power plant buildings, there is a difference in elevation between the turbine and generator hall and the landscaping elevation. However, the superstructure is above the environmental elevation. One of the most

important factors in the selection of this type of structure is the high flood level. In addition, since submergence is important in some turbine types, a semi-buried power plant construction is preferred.

- **Underground:** Underground power plants are rare but can be preferred in suitable geological conditions. In these types, the structure is built into a solid rock mass [15].

- **According to Installed Powers:**
  - Very small (micro) capacity (<100 kW),
  - Small (mini) capacity (100-1000 kW; 1MW = 1000 kW),
  - Medium capacity (1000-10000 kW),
  - Large capacity (>10000 kW) [16].

4. HYDRAULIC TURBINES AND TYPES

Turbines are machines that convert the hydraulic energy of a fluid into mechanical energy. The turbines used in hydroelectric power plants are called hydraulic turbines. According to the effect of water, water turbines are classified as action turbines and reaction turbines.

Action turbines: Since the pressures at the turbine inlet and outlet are equal to atmospheric pressure, action turbines are known as isostatic turbines. In this type of turbines, water is passed through a narrowing pipe system and accelerated to create a water jet. The water jet hits the concave bowl-shaped blades on the turbine wheel and the turbine rotates due to the change in water speed. The water jet hits the blades and converts kinetic energy into potential energy. It is preferred at very high

heads. Commonly used action turbines are; Turgo, Pelton and Crossflow (Michell-Banki) turbines.

Reaction turbines: Francis, Kaplan, Uskur, Bulb, Propeller, Straflo, Tube, Water Wheel are examples of reaction turbines. Reaction type water turbines use both kinetic and potential energy of water. Therefore, the pressure at the inlet of the wheel is much greater than the pressure at the outlet and the water has to flow through closed channels. The rotation of the turbine wheel is provided by the reaction force created by the acceleration of the water at the wheel outlet (Figure 6) [17].

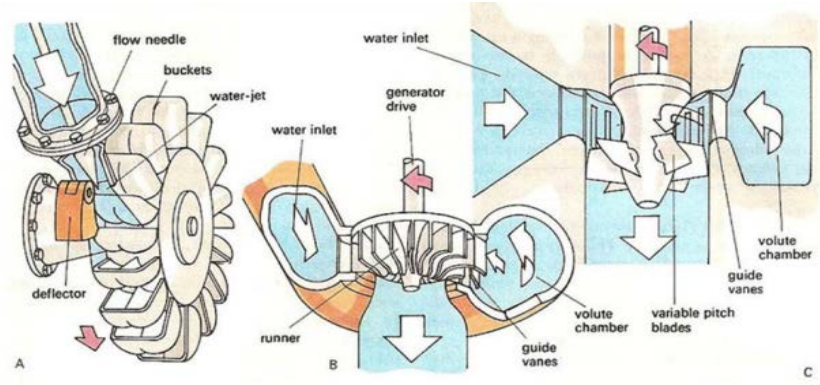

Figure 6. Turbine types (A: Pelton Turbine, B: Francis Turbine, C: Kaplan Turbine) [17].

5. ADVANTAGES OF HYDROELECTRIC ENERGY

The determining factor in preferring hydroelectric power plants is the advantages they provide in electricity production. The energy produced is produced from renewable sources and is domestic energy. Hydroelectric power plant structures are used for drinking water, irrigation and flooding. It has lower operating costs than high-efficiency energy production methods, and it can be efficient in all seasons, and its operating life is

long. It provides cheap energy production, meets daily needs, does not create solid waste and environmental pollution, and has high efficiency. They do not create environmental and air pollution like fuel-fired power plants. It is an ideal system for rural areas that cannot receive energy from the national system. Since it is used regionally, there is no need for long construction processes and long transmission lines. It contributes to tourism, water sports and fishing. It has a positive effect on the climate of the region where it is established. The unit cost of the energy produced is low, and it is not easily affected by economic effects. Energy storage can be done with power plants and energy export can be done with this storage. It creates a softening in the climate [8], [18], [19], [20].

6. DISADVANTAGES OF HYDROELECTRIC POWER PLANTS

Hydroelectric power plants have many disadvantages as well as advantages. Investment costs and total construction process are high and a lot of excavation output occurs during this process. Due to the accumulation of a lot of water, it deteriorates water quality and causes loss of plants and flora. It can cause people to move in places close to the places where it is established. It causes noise in the area where it is established. Misapplications such as errors originating from stream beds, excavation removal errors, etc. can cause environmental pollution and erosion. Electricity production in power plants without storage can be negatively affected by drought. Investment costs for operating expenses of small hydroelectric power plants are higher than large hydroelectric power plants. Since hydroelectric power plant operators have the authority to use water together with the structure, they may not allow the local people to use water, and therefore problems may ocur [18].

7. FUTURE OF HYDROELECTRIC ENERGY IN TÜRKİYE

Hydroelectric power plants are among the renewable energy power plants established in Turkey and electricity is produced in these power plants. The electricity produced in these power plants will provide employment and prevent the current account deficit from increasing due to energy imports, thus supporting production activities. Hydroelectric energy is the basic renewable energy type in Turkey and when its potential is evaluated, the initial installation cost is high and their lifespan is approximately 150 years. The fact that they do not harm the environment and adapt to energy demands are among the reasons why they are preferred. The most prominent hydroelectric power plants in Turkey are Atatürk Dam (1330 mw), Keban Dam (1330 Mw) and Karakaya Dam (1800 mw) [6].

In Türkiye, the lowest electricity consumption is in the spring period and the highest in the summer period. Due to the lack of infrastructure, problems such as unbalanced voltage and frequency changes occur during electricity consumption. Hydroelectric power plants are more numerous and have higher power in the eastern region of Turkey than in the western region (Figure 7) [21].

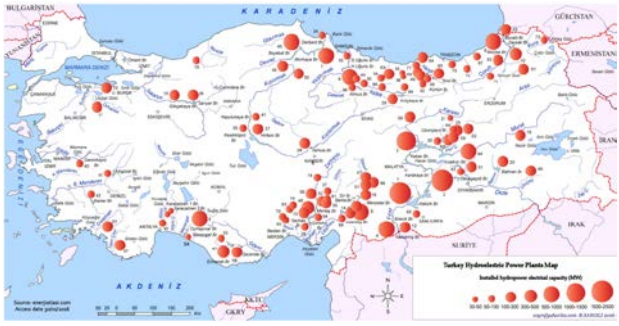

Figure 7. The potential of hydroelectric power plants in Turkey [21].

8. CONCLUSIONS

The potential of hydroelectric energy used in our country and in the world and the results regarding the energy obtained are given below.

- Hydroelectric energy, a sustainable and long-term energy source thanks to the natural cycle of water, significantly reduces greenhouse gas emissions compared to fossil fuels.
- Hydroelectric energy will maintain its importance in the future as a clean and reliable resource. The efficiency of converting the potential and kinetic energy of water into electricity is quite high compared to other renewable sources.
- Thanks to its geographical location and rich river resources, Türkiye has an important place in Europe in hydroelectric energy production.
- Countries such as China, Brazil, the USA and Canada, as well as Turkey, have a significant share in energy production.

REFERENCES

[1] A. Akpinar, “Dünya, Avrupa Birliği ve Türkiyenin toplam elektrik ve hidroelektrik enerji üretim projeksiyonu,” Karadeniz Teknik Üniversitesi / Fen Bilimleri Enstitüsü / İnşaat Mühendisliği Ana Bilim Dalı, 2007.

[2] E. Erkin, “Yenilenebilir enerji kaynaklarının kullanımı ve karabük ili hidroelektrik enerji potansiyelinin araştırılması,” Karabük Üniversitesi / Fen Bilimleri Enstitüsü / Makine Mühendisliği Ana Bilim Dalı, 2019.

[3] E. N. Bilen, “Hidroelektrik santrallerde enerji üretimine etki eden parametreler: Şırnak örneği,” Şırnak Üniversitesi / Lisansüstü Eğitim Enstitüsü / Enerji Bilim ve Teknoloji Ana Bilim Dalı, 2024.

[4] C. Bermann, “Impasses and controversies of hydroelectricity,” *Estud. avançados*, vol. 21, pp. 139–153, 2007.

[5] B. U. Alkan, “Hidroelektrik santrallerinin değerlemesi üzerine model önerisi,” Gebze Teknik Üniversitesi / Fen Bilimleri Enstitüsü / Jeodezi ve Fotogrametri Ana Bilim Dalı, 2015.

[6] E. Şavkar, “Yenilenebilir Enerji Zemininde Hidroelektrik Enerji Ve Türkiye Potansiyeli,” *Oğuzhan Sos. Bilim. Derg.*, vol. 6, no. 1, pp. 51–58, 2024, doi: https://doi.org/10.55580/oguzhan.1484562.

[7] A. Cüce, “Regülatör tipi bir hidroelektrik santralin tasarımı ve ekonomik analizi,” Recep Tayyip Erdoğan Üniversitesi / Fen Bilimleri Enstitüsü / Makine Mühendisliği Ana Bilim Dalı, 2019.

[8] U. Kulak, “Sakarya havzasının hidroelektrik potansiyelinin analizi ve uygun görülen akarsular için HES projesi

yapılması," Sakarya Üniversitesi / Fen Bilimleri Enstitüsü / Yapı Eğitimi Ana Bilim Dalı, 2009.

[9] U. Süğürtin, "Sakaryada bulunan atık su arıtma tesislerinin mikroheslerle kendi elektrik enerjilerini üretme potansiyellerinin incelenmesi," Sakarya Üniversitesi / Fen Bilimleri Enstitüsü / Elektrik-Elektronik Mühendisliği Ana Bilim Dalı / Elektrik Bilim, 2020.

[10] F. Oral, R. Behçet, and K. Aykut, "Hidroelektrik santral rezervuar verilerinin enerji üretimi amaçlı değerlendirilmesi," *Bitlis Eren Üniversitesi Fen Bilim. Derg.*, vol. 6, no. 2, pp. 29–38, 2017.

[11] G. Güney, "Denizsuyu pompaj depolamalı hidroelektrik santraller: Hatay bölgesinde örnek çalışma," Bilecik Şeyh Edebali Üniversitesi / Lisansüstü Eğitim Enstitüsü / Enerji Sistemleri Mühendisliği Ana Bilim Dalı, 2024.

[12] Å. Killingtveit, "Hydroelectric Power," in *Future Energy*, Department of Hydraulic and Environmental Engineering, Norwegian University of Science and Technology, Trondheim, Norway: Elsevier, 2014, pp. 453–470. doi: 10.1016/B978-0-08-099424-6.00021-1.

[13] M. Bozdemir, "Hazneli pompalı hidroelektrik santrallerin Türkiye açısından değerlendirilmesi ve analizi," Bilecik Şeyh Edebali Üniversitesi / Fen Bilimleri Enstitüsü, 2013.

[14] G. Özbek, "Hidroelektrik santrallerinde enerji verimliliğine türbinin etkisi," Bitlis Eren Üniversitesi / Fen Bilimleri Enstitüsü / Elektrik-Elektronik Mühendisliği Ana Bilim Dalı / Elektrik, 2022.

[15] O. V. E. S. U. İ. Bakanliği and D. S. U. İ. G. Müdürlüğü, "Barajlar Ve Hidroelektrik Santraller Yapisal Tasarim

Rehberi," In *Barajlar Ve Hidroelektrik Santraller Yapisal Tasarim Rehberi*, Ankara, 2012.

[16] G. Güney, "Porsuk havzasında küçük ölçekli hidroelektrik enerji potansiyelinin araştırılması," Bilecik Şeyh Edebali Üniversitesi / Fen Bilimleri Enstitüsü / İnşaat Mühendisliği Ana Bilim Dalı / Hidrolik Bilim Dalı, 2017.

[17] M. Yavuzdemir, "Hidroelektrik Santrallerin Siniflandirilmasi Ve Hidrolik Türbin Çeşitleri," Ankara. doi: ISSN : 1308-8262.

[18] V. Süme and S. S. Fırat, "Hidroelektrik santraller ve Rize İlinde bulunan hidroelektrik santrallerin şehir ve Doğu Karadeniz Havzası için önemi," *Türk Hidrolik Derg.*, vol. 4, no. 2, pp. 8–23, 2020.

[19] V. Süme and S. S. Fırat, "Hidroelektrik Santraller ve Trabzon İlinde Bulunan Hidroelektrik Santrallerin Şehir ve Doğu Karadeniz Havzası İçin Önemi," *Türk Hidrolik Derg.*, vol. 4, no. 1, pp. 10–24, 2020.

[20] M. Sönmez, "Türkiyede havzalar bazında hidroelektrik üretiminin istatistiksel yöntemlerle değerlendirilmesi," Yıldız Teknik Üniversitesi / Fen Bilimleri Enstitüsü / İstatistik Ana Bilim Dalı / İstatistik Bilim Dalı, 2019.

[21] L. Saribulut, G. Ok, and A. Ameen, "A case study on national electricity blackout of Turkey," *Energies*, vol. 16, no. 11, p. 4419, 2023.

EMBEDDED SYSTEMS AND TECHNOLOGIES

Sertaç YAMAN[1]

1. INTRODUCTION

Embedded systems are increasingly complex, networked structures comprised of hardware and software components that control the designed system. Development of technological, including the autonomous systems, Internet of Things, smart homes and security, has been more prevalent embedded systems. In contrast, effective design, efficiency, and reliable real-world solutions, these must be equipped with intelligence systems at various levels, including data understanding/collection, processing, and stages for decision-making. Thus, the hardware development efficient and software is necessary to ensure the real-time performance for embedded systems and the same networked devices.

A standalone system obtains input data from the external environment and operates independently of other systems using its own software. These systems transfer their output information independently to output units. Autonomous robotic systems used in the manufacturing sector are examples of embedded systems that can operate independently. Embedded systems that operate in real time receive input data from external systems using their own software and hardware units. They then compare the data and simultaneously control the systems within them. Networked systems can be accessed by multiple users and communicate over

[1] Assist. Prof. Dr., Hakkari University, Faculty of Engineering Department of Electrical-Electronics Engineering Hakkari, TURKEY. ORCID: 0000-0002-0208-8320.

a shared network. Therefore, embedded systems with networking-capable hardware are being developed. These systems can also be controlled via internet access. Examples of these systems include microgrids, smart cities, and smart buildings.

Information of various forms—visual, written, and audio—is generated at a rate of one message per second and processed in a variety of application areas. Presently, the most prevalent intelligent applications are those that are based on visual and image processing. In the contemporary technological landscape, the implementation of image processing algorithms within embedded system platforms has witnessed a marked surge in utilization across a diverse array of domains, including robotics, defense industry, medicine, and intelligent autonomous systems. This proliferation of applications, encompassing unmanned land, sea, and air vehicles, among others, underscores the formidable challenges posed by this field.

In the process of developing such applications for embedded system platforms, it is imperative to take into account factors such as the length of the algorithm, its memory footprint, power consumption, and data processing speed. The construction of each system invariably gives rise to a multitude of issues that must be addressed. The development of suitable algorithms and the selection of an appropriate embedded system platform are essential for the translation of designs into applications.

In applications implemented using embedded systems, the size, nature, and complexity of the algorithms vary depending on the application. The implementation of the complex algorithms employed in these applications necessitates the selection of the most suitable hardware architecture. In real-time image processing applications, the processing load, memory footprint, and power consumption of the algorithms increase significantly.

Consequently, the development of image processing algorithms necessitates a consideration of the distinct RAM structures and power consumption characteristics of each platform intended for utilization.

The detection of image features and their subsequent matching or classification according to predefined characteristics constitutes a subject of extensive research in the domain of video analysis and computer vision systems. The extant studies in this field predominantly concentrate on the impact of diverse embedded system platforms, the role of image processing algorithms in design, and the design of intelligent systems enhanced by deep learning models.

In a study conducted by Kuon and his group [1], system designers compared standard custom integrated circuits (ASIC) with field-programmable gate arrays (FPGA) in terms of logic block density, processing speed, and power consumption. In the course of this study, the Altera Stratix II chip was fabricated using TSMC's Nexsys 90-nm process technology, and STMicroelectronic's CMOS090 Design was used to produce standard cells. For the comparative evaluation, open-source Opencores structures were selected and subjected to experimental testing.

In a study conducted by Pedre and his team [2], they sought to mitigate constraints (power consumption, memory issues, etc.) encountered during the development of real-time image processing applications. The objective was to attain development time that is commensurate with projects that utilize exclusively software interfaces, leveraging hardware and software co-design systems. The implementation of object-oriented recognition was achieved through the integration of a detailed programming language and code generation (HDL) tools in C. This design was implemented in a novel algorithm for multi-

robot localization in vision systems, which demonstrated its efficacy in embedded real-time image processing applications.

In the study conducted by Fradi [3], a programmable chip was designed using Quartus II's Qsys tools and commonly used image processing algorithms were used to test the performance and power consumption of this system. In a comparative study of FPGA architectures and GPUs in data centers, Falsafi and his working group [4] examined four distinct panel programs (Computer Architecture Research Directions).

In their work, HajiRassouliha et al. [5] highlighted important points to consider when selecting hardware accelerators. Due to the fact that central processing units (CPUs) are incapable of performing computations at a sufficient rate, they offer practical information on hardware accelerators such as digital signal processors (DSPs), FPGA platforms, and GPUs, in addition to algorithms that serve to reduce computation time. Additionally, they elucidate the relative merits and drawbacks of DSPs, FPGAs, and GPUs.

2. TECHNICAL SPECIFICATIONS OF EMBEDDED SYSTEM PLATFORMS

Embedded systems are defined as structures with operating systems that are designed for use in various application areas. When formulating system designs, it is imperative to consider factors such as time stability, energy consumption, and memory footprint. This is due to the fact that even the most fundamental tasks demanded by real-time platforms can become arduous. In the process of developing a novel system, the number of planned work packages and the quality of the software required to perform these tasks increase, necessitating the use of different embedded system platforms. The advent of advanced semiconductor technology has led to a proliferation of embedded

system platforms in contemporary devices, with each platform exhibiting a diverse array of functional capabilities.

A comparison of FPGA platforms with computer and GPU-based systems reveals that the former exhibit superior time stability. The rapid processing capabilities of FPGAs are attributable to their programmable logic blocks, which enable the operation of hardware components in parallel. This hardware configuration is advantageous due to its reconfigurability, allowing for adaptability to changing requirements. In the context of embedded systems, the utilization of custom integrated circuits (ASICs) is constrained due to their design for specific structures. These circuits are engineered to execute a defined function or task, which hinders their adaptability to diverse structures [2, 3]. However, FPGAs, or field-programmable gate arrays, are designed with the capacity for post-production reconfiguration, allowing for adaptation to the specific functional requirements of the designer. The significance of reprogrammable logic gates is attributable to the aforementioned characteristics.

A comparative analysis of data classification accuracy, processing speed, memory consumption, and power consumption when employing a neural network model with varying sizes on a Raspberry Pi and Jetson development board reveals that Jetson boards consistently yield superior results. These systems offer several advantages, including faster data processing speeds, lower power consumption, and improved performance as data capacity increases [6]. Embedded systems, state-of-art electronic platforms, can be programmed to perform and control one or more systems/subsystems, depending on the creative design. These embedded platforms based on microprocessor or microcontroller and feature integrated circuits (I2C), serial communication modules, memory, RAM and A/D converters to perform real and time varying operations.

The following items must be taken into consideration to the rate at which data is processed, The memory available, The stability over time, The cost, The size and the duration of use.

Digital Signal Processors (DSPs) systems are microprocessors via a designed architecture for signal processing projects. Texas Instruments' digital signal processors are generally use to utilized predominantly for computer vision and image processing applications. Ultra-low-power digital signal processors (DSPs) are economically advantageous; however, due to their limited computational capabilities, they are predominantly employed in conjunction with rudimentary computer vision and elementary image processing algorithms.

Floating-point operations in digital signal processors (DSPs) facilitate the implementation of algorithms and enhance precision when compared with fixed-point operations. However, fixed-point operations can perform operations with fewer bits, requiring the programmer to carefully reposition the decimal point after each mathematical operation. However, fixed-point DSPs are generally less expensive than their floating-point counterparts. In digital signal processors (DSPs), arithmetic calculations are executed within multiplier-adder (MAC) units. The SYS/BIOS (formerly DSP/BIOS) real-time operating system developed by Texas Instruments has been utilized for programming DSPs, microcontrollers, and ARM processors [7].

Graphics processing units (GPUs) were initially developed for workstations. These accelerators are optimized for matrix calculations in parallel, comprising multiple processor cores. These devices, developed for the gaming industry, are affordable and have gained widespread popularity. Consequently, GPUs have become increasingly prevalent in image processing applications that extend beyond the realm of gaming in recent years. The NVidia GPU series, with its libraries and multi-core

microarchitecture, is extensively utilized in image processing and deep learning applications [8].

The utilization of GPUs offers several advantages, including:

- Graphics processing units (GPUs) are engineered with a primary focus on the processing of images and videos.
- The development and debugging of code on GPUs have been shown to be a more efficient process in comparison to that of FPGA platforms.
- The Peripheral Component Interconnect (PCI) interface between graphics processing unit (GPU) cards and the host computer is characterized by its ease of use by programmers.

The following are some of the disadvantages associated with the utilization of GPUs:

- GPUs exhibit a substantially higher power consumption when we compared with FPGA platforms to operate in the same performance category.
- Graphics processing units (GPUs) are engineered to execute applications that leverage data parallelism. However, it should be noted that GPU performance will undergo a substantial decline if they are required to wait for data or if the processing of data is arduous and protracted.
- The utilization of embedded systems is on the rise, exhibiting a consistent upward trend and accumulating significance in contemporary technological applications.

These technologies find application in a wide range of fields, including intelligent transportation systems, computer-

human interaction, smart agriculture, robotics, the defense industry, medicine, and unmanned land, sea, and air vehicles.

2.1. Field Programmable Gate Array (FPGA)

The inaugural programmable logic circuit element employed in logic circuit design was the PROM (read-only circuit). These are divided into two classes: one-time programmable (PROM, PLA, etc.) and multi- time programmable (EPROM, EEPROM). However, these systems prove insufficient for refined applications. Logic operations that can be used in complex structures can be investigated in four classes [9].

- SPLD: Simple Programmable Logic Circuits
- CPLD, or complex programmable logic circuits, is a specialized circuit configuration that offers a high degree of programmability and flexibility.
- MPGA: Mask-Programmable Logic Gate Arrays

FPGA platforms are a type of state-art electronic circuit that can be programmed in field to perform specific functions. These platforms, introduced to many specific application for developers by Xilinx in 1985, leverages programmable structures such as CPLD and MPGA. The composition of FPGA platforms is typically characterized by the presence of reconfigurable logical blocks, interconnects, and input/output units.

The configuration of FPGA hardware architecture is achieved through the interconnection of FPGA logic gates, which are designed to execute specific tasks. However, it should be noted that this configuration necessitates reconfiguration for each new algorithm. Consequently, FPGAs are frequently designated as reconfigurable devices. FPGAs are distinct from CPUs, DSPs, and GPUs in that they lack a pre-configured chip architecture or a central processing unit. Consequently, the design of custom hardware architectures involves the utilization of components

such as configurable logic blocks (CLBs), lookup tables (LUTs), multiplexers, and flip-flops, which are situated on the FPGA.

The programming languages utilized for FPGA platforms, namely VHDL and Verilog, exhibit notable distinctions from those employed for CPUs, DSPs, and GPUs. In order to facilitate FPGA programming, programming languages such as C and C++ (with structures such as HLS) are employed; however, these languages are seldom preferred due to their limited aptitude for parallel processing logic. The Spartan series of field-programmable gate arrays (FPGA) platforms produced by Xilinx is a line of low-cost field-programmable gate arrays (FPGAs) that have been specifically designed for straightforward applications. The Virtex series is engineered specifically for signal processing applications and is priced higher than competing FPGA platforms.

The Kintex and Artix series are low-performance, inexpensive versions of the Virtex-7. The Zynq series of platforms is a mid-range platform (Artix or Kintex) designed for medium- to high-performance embedded systems incorporating an ARM processor. The UltraScale and UltraScale+ families exemplify the most recent advancements in Xilinx technologies. The Virtex UltraScale+ FPGA represents Xilinx's most advanced FPGA, offering superior performance capabilities [87]. The device has been engineered to support high-performance and high-speed applications. As illustrated in Table 2.1, a range of FPGA platforms is exhibited, along with the planar fabrication technologies and processes associated with them.

Tablo 2.1. Manufacturing technologies of FPGA platforms

FPGA Platforms	Manufacturing technologies
Virtex-4, Spartan-3E	90nm
Virtex-6, Spartan-6	40nm
Virtex-7, Kintex, Artix, Zynq	28nm
UltraScale (Virtex, Kintex, Zynq)	20nm
UltraScale+(Virtex, Kintex, Zynq)	16nm

The following section will provide a concise overview of the most salient features that must be taken into consideration when selecting the most suitable FPGA for computer vision and image processing applications.

CLB: The interconnections of configurable logic blocks form logic circuits that represent user-defined hardware. FPGAs with multiple CLBs are a suitable choice for complex algorithms [88]. As illustrated in Figure 2.4, the Xilinx XC400 FPGA configurable logic block structure is comprised of multiple components.

Digital Signal Processors (DSPs) are specialized electronic circuits that are designed to perform fundamental mathematical operations and signal processing functions. These DSP blocks, when implemented within Field-Programmable Gate Arrays (FPGAs), are engineered to execute these operations with optimal efficiency and precision. These blocks are designated as DSP48 in Xilinx field-programmable gate arrays (FPGAs) and can possess disparate numbers of bits on Xilinx platforms. The performance of a digital signal processor (DSP) is quantified by the maximum number of mathematical operations that a single DSP slice is capable of executing per second. In real-time applications, the implementation of complex structures or the emergence of problems can be contingent upon the performance of the DSPs.

BRAM: Block RAMs are designed with SRAM architecture for storing or buffering data and are particularly important for storing image data on FPGAs. When the write enable input receives a logical value, the address information and data are loaded into memory with a clock pulse. The amount of data to be held in or read from memory depends on the BRAM design and the designer. Traditional image processing algorithms are designed for sequential processors. It is possible to achieve

better performance on FPGA platforms by modifying and optimizing these algorithms for parallel processing [10].

The Xilinx-7 series FPGAs are comprised of four distinct FPGA families that are both cost-effective and capable of meeting the full spectrum of system requirements. The Spartan-7 family of field-programmable gate arrays (FPGAs) offers the most cost-effective solution, requiring the fewest memory and digital signal processing (DSP) units compared to other platforms. The selection of FPGA platforms is a critical component for the successful implementation of the application. During the design process, particular attention must be directed towards the memory, logic blocks, and DSP cell count that will be utilized.

Three general design methods are employed in the design of FPGA embedded system platforms. The following elements are to be considered: a. Hardware Description Language (HDL) b. Schematic diagrams c. Designs based on custom IP cores

The implementation of HDL-based designs typically occurs through the utilization of MATLAB and XSG simulation blocks, or alternatively, through the employment of FPGA programming languages. Schematic diagrams are a powerful design method for representing design hierarchy and signal interconnection. Block structures, ranging from simple logic gates to multifunctional structures, can be incorporated and modified in such designs. The third method utilizes an IP core, otherwise known as an IP block, which generates logic information for the design and forms sections within configurable logic blocks. The utilization of IP cores can be approached in two distinct ways: they can be licensed for implementation in an alternate design or they can be integrated within a single design. Designers of custom integrated circuits (ASICs) and FPGA systems utilize IP cores as fundamental components [11].

The synthesis of HDL-based designs can be accomplished through the utilization of XSG blocks or by employing FPGA programming languages, such as Verilog, VHDL, or SystemVerilog. Schematic diagrams are a powerful design method for representing hierarchy and signal interconnection. In such designs, blocks ranging from simple logic gates to multifunctional ones can be added and edited.

The XSG-MATLAB/Symbol platform facilitates the generation of HDL code automatically, rendering it immediately applicable in FPGA-based applications without necessitating advanced HDL expertise. Utilizing XSG, the comprehensive design created in the simulation environment for the development of any application is converted for JTAG hardware co-simulation [12].

Xilinx System Builder employs the use of Simulation blocks for the purpose of modeling and developing high-performance DSP systems on field-programmable gate arrays. Xilinx simulation blocks encompass arithmetic and logic operations (e.g., OR, NOT, etc.) for digital filtering, spectral analysis, and digital communication, along with real models of memories and DSP functions. XSG has the capacity to transform models constructed from simulation blocks into a hardware implementation of blocks that are prepared to run efficiently in synthesizable VHDL/Verilog languages and on FPGA platforms [14].

IP cores are blocks that perform pre-designed and pre-verified complex functions. The utilization of IP cores is a recommended application development method for designs implemented on FPGAs. In comparison with applications that possess an analogous architectural structure, those implemented with IP cores have also been shown to reduce FPGA resource

utilization [15]. A taxonomy of IP cores can be established by classifying them into three distinct groups based on their features.

• **Soft IP cores:** These modules are characterized by their high degree of resynthesizability and architectural flexibility, which renders them amenable to extensive modification. The design of synthesizable IP cores can be accomplished through the utilization of HDL files for coding purposes. These IP cores can be implemented in a manner that is specific to the user and the design.

• **Robust IP cores:** These are encrypted black boxes integrated into the design flow. These IP cores are immutable and akin to library elements in nature. These elements are situated within the program file, and their utilization does not necessitate alterations to their existing structural design.

• **Hard IP cores:** Hard IP cores are modules that are contingent upon the version of the interface program and the technology employed. The performance and physical properties of IP blocks previously developed by the design company are presented to the user.

2.2. Raspberry Pi

The Raspberry Pi platforms are equipped with a Linux operating system that can be installed on a development board with ARM processor. Raspberry-Pi can be program by using many different programming languages, including C/C++, Python, and Java, among others. The Raspberry Pi is a board that is characterized by its affordability, adaptability, programmability, and the ability. It is specifically well-suited for deployment in the field of sensor networks, where it can leverage its computing abilities to simplify the analyses, and arrangement of data. This feature generates a mobile platform, facilitating its use with a wide variety of external peripherals. [16].

The Raspberry Pi's capacity for manufacturing in reduced dimensions enables its placement in a broader array of locations and utilization in a more extensive range of scenarios. This adaptability is attributable to the influence of physical size on application design. The CPU of the Raspberry Pi is the primary element responsible for implementing the instructions of a computer program through mathematical and logical procedures. The Raspberry Pi's processor is a System-on-Chip (SoC) built on the ARM architecture.

The Raspberry Pi is capable of low power consumption due to its ARM-based Broadcom chip. These boards can be powered by a computer's USB port, an external 5V 1A power supply, or an external solar panel.

The DSI (Display Serial Interface) support facilitates the establishment of a connection between a Raspberry Pi display. In the contemporary era, the Raspberry Pi has emerged as a prominent embedded computer in the domain of robotics, finding application in domains such as object detection. Despite its low-power CPU and absence of a GPU, the Raspberry Pi is employed for certain CNN-based applications and is capable of achieving frame rates ranging from 0.5 to 1.5 FPS [17].

2.3. Jetson Embedded System Platforms

The development of recent embedded system platforms has been informed by the advancements in artificial intelligence and deep learning applications. One such platform is the NVidia Jetson embedded system platform. This platform's low power consumption and compact size it well-suited for real-time applications, GPU-accelerated image processing, object detection, image classification projects, and mobile robotics applications. Its GPU-based architecture usually confers a competitive benefit, making it a selected solution in many applications.

In the context of Jetson embedded system platforms, the GPU can be programmed with CUDA. This feature enables the utilization of deep neural network applications trained on high-end GPUs on Jetson platforms for portable systems (e.g., robots, UAVs). The absence of cuDNN-like structures on other platforms, such as Raspberry Pi and FPGAs, restricts the development of deep learning applications [18].

Tablo 2.2. Comparison of Jetson embedded system platforms

	Jetson-Nano	TK1	TX1	TX2	AGX Xavier
Performans	472GFLOPS	326 GFLOPS	1 TeraFLOPS	1.33TFLOPS	32 TOPS
Production		28nm	20nm	16nm	16nm
GPU	128 Cores Maxwell	192 Cores Keplerr	256 Cores Maxwell	256 Cores Paskal	512 Cores NVIDIA Volta GPU
CPU	4 Cores ARM Cortex-A57	2.32 GHz ARM Cortex A12	1.73 GHz ARM Cortex A57	2 GHz ARM Cortex A52+NVIDIA	Carmel ARM v8.2 64-bit CPU 8MB L2 + 4MB L3
Memory	4GB 64 bit LPDDR4	2GB 64 bit DDR3L	4GB 64 bit LPDDR4	8GB 128 bit LPDDR4	32 GB 256-bit LPDDR4x 136.5GB/s

Table 2.3 presents a comparative analysis of various Jetson embedded system platforms. The prevalence of Jetson embedded systems can be attributed to their performance-efficient and low-power GPU cores. In general, GPUs provide higher throughput than FPGAs, making Jetson embedded system platforms more suitable for deep learning applications. The Jetson AGX Xavier model has been demonstrated to achieve the highest levels of performance, with the capacity to execute 32 tensor operations per second at 32TOPS.

2.4. Programmable System on a Chip (PSoC)

PSoC (Programmable System on Chip) is a low-cost reconfigurable embedded system platform that integrates reconfigurable analog and digital subsystems on a single chip. The PSoC also includes an external memory interface. Internally, it consists of a microprocessor core, configurable analog and digital blocks, and software-configurable and programmable routing and interconnects, which simplifies the design of an

electronic system. Consequently, the integration of applications that facilitate the conversion and management of analog signals within a singular device becomes a viable proposition.

PSoC embedded system platforms are composed of a PSoC core (CPU), digital (PWM, SPI, etc.) and analog (filters, ADC, DAC, etc.) systems, and interfaces (MAC, I2C, etc.).

Tablo 2.3. Comparison of PSoC embedded system platforms

	PSoC-1	PSoC-3	PSoC-4	PSoC-5
ADC	6-14 bit Delta-sigma	8-20 bit Delta-sigma	12 bit SAR	8-20 bit Delta-sigma 2 ad. 12 bit SAR
DAC	2 ad. 6-8bit	4 ad. 8bit	2 ad.8bit	4 d.8-12bit
Working Current	2mA	1.2 mA	1.6 mA	2 mA
CPU	8-bit M8C 24 MHz, 4 MIPS	8-bit 8051 CPU 67 MHz, 33 MIPS	32-bit ARM Cortex-M0 CPU 48 MHz, 100 MIPS	32-bit ARM Cortex- M3 7 MHz, 84 MIPS
SRAM	256b-2Kb	2-8Kb	4Kb	16-64Kb

Table 2.4 provides a comparison of PSoC embedded systems. Depending on the application to be developed, variables such as the importance of the ADC to be used, the number of DACs, or the selection of SRAM based on the scope of the design will be among the factors determining the selection of the PSoC embedded system platform.

3. EVALUATION AND CONCLUSIONS

Embedded system platforms are comprised of software, hardware, input/output interfaces, and user interfaces. The selection of variables, including but not limited to memory, data processing speed, size, and temporal stability, is contingent upon the specific requirements of the application. FPGA, Jetson, and Raspberry Pi platforms are preferred for embedded system platforms that can be operated in real time and independently of a computer. The Jetson and Raspberry Pi models, which are produced with a variety of features, utilize open-source library

functions, support machine learning applications with frameworks, and are small in size. These attributes contribute to their favor. Moreover, the UltraScale and UltraScale+ families, created by Xilinx, are the highest-performance FPGA platforms. These instruments are arranged to perform in high-performance and high-speed applications. The implementation of machine learning applications can be facilitated by frameworks such as Vitis AI or HLS4ML.

In comparison to computer and CPU-based systems, which offer high time stability, FPGA platforms offer significantly faster hardware operations and enable these hardware blocks to be executed in parallel, contingent upon the application under development. The utilization of floating-point operational support within digital signal processors (DSPs) has been demonstrated to facilitate the implementation of algorithms and enhance precision when compared to fixed-point systems. The utilization of GPU architectures is strongly recommended for the purpose of image or video processing.

The programming languages VHDL and Verilog, which are utilized for programming on FPGA platforms, exhibit notable distinctions compared to those employed for CPUs, DSPs, and GPUs.In contrast to computer and CPU-based systems, which are characterized by their high time stability, FPGA platforms offer a significantly faster hardware operation rate and enable the execution of these hardware blocks in parallel, contingent upon the specific application under development.

The utilization of floating-point operational support within digital signal processors (DSPs) has been demonstrated to facilitate the implementation of algorithms and enhance precision when compared to fixed-point systems. The utilization of GPU architectures is strongly recommended for the purpose of image or video processing. The development and debugging of code on

GPUs have been shown to be more efficient and expeditious than on FPGA platforms. However, GPUs have been observed to consume more power than FPGA platforms in the same performance class. The programming languages utilized for FPGA platforms, namely VHDL and Verilog, exhibit notable distinctions from those employed for CPUs, DSPs, and GPUs.

REFERENCES

[1] Kuon and J. Rose, "Measuring the Gap between FPGAs and ASICs," in IEEE Transactions on Computer-Aided Design of Integrated Circuits and Systems, 2007.

[2] S. Pedre, T. Krajník, E. Todorovich, and P. Borensztejn, "Accelerating Embedded Image Processing for Real Time: A Case Study," Journal of Real-Time Image Processing, vol. 11, pp. 349–374, 2016.

[3] M. Fradi, W. E. Youssef, and M. Mohsen, "The Design of an Embedded System (SOPC) for an Image Processing Application," International Conference on Control, Automation and Diagnosis (ICCAD), 2017.

[4] B. Falsafi, B. Dally, D. Singh, D. Chiou, J. J. Yi ve R. Sendag, “FPGAs versus GPUs in Data centers”, IEEE Micro, cilt 37, no. 1, pp. 60-72, 2017

[5] A. HajiRassouliha, A. J. Taberner, M. P. Nash, and P. M. Nielsen, "Suitability of recent hardware accelerators (DSPs, FPGAs, and GPUs) for computer vision and image processing algorithms," Signal Processing: Image Communication, vol. 68, pp. 101–119, 2018.

[6] A. A. Suzen, B. Duman, and B. Sen, "Benchmark Analysis of Jetson TX2, Jetson Nano, and Raspberry PI using Deep-CNN," Human-Computer Interaction, Optimization, and Robotic Applications, Proceedings, 2020.

[7] T. Instruments. [Online]. The tool is available at the following URL: https://www.ti.com/tool/SYSBIOS. April 11, 2021.

[8] NVIDIA, "GPU Applications High Performance Computing |NVIDIA," [Online]. 2021.

[9] S. Brown and J. Rose, "FPGA and CPLD Architectures: A tutorial, Design and Test of Computers", vol. 13, no. 2, pp. 42-56, 1996.

[10] I. Xilinx, "ZCU104 Evaluation Board User Guide (UG1267)," Xilinx, 2018.

[11] N. I. (NI). [Online]. The documentation is available at the following Uniform Resource Locator (URL): https://www.ni.com/documentation/en/labview-comms/5.0/fpga-targets/configurable-logic-blocks/. The data set was last accessed on May 15, 2021.

[12] X. Inc., XC4000E and XC4000X Series Features "System featured Field-Programmable Gate Arrays-SelectRAM TM memory: on-chip ultra-fast RAM with-synchronous write option-dual-port RAM option-Fully PCI compliant (speed grades-2 and faster)",

[13] Y. K. Lim, L. Kleeman and T. Drummond, "Algorithmic methodologies for FPGA-based vision", Machine Vision and Applications, vol. 24, no. 6, pp. 1197-1211, 2013.

[14] Xilinx. [Online]. Available: https://www.xilinx.com/search/site-keyword-search.html#q=ip core. [Accessed: 11 5 2021].

[15] A. M.Ali, H. Cem, A. Hüseyin and U. Ayşegül, "Forming and Co-simulation of Square and Triangular Waveforms by Using System Generator",Balkan Journal of Electrical & Computer Engineering, vol. 3, no. 7, pp. 337-341, 2019.

[16] X. Inc, "Model Composer and System Generator User Guide-UG1483 (v2020.2)", Xilinx Inc, 2020.

[17] M. Geier, M. Brandle, D. Faller and S. Chakraborty, "Debugging FPGA-accelerated Real-time Systems", IEEE Real-Time and Embedded Technology and Applications Symposium, RTAS, 2020.

[18] V. Vujović and M. Maksimović, “Raspberry Pi as a Wireless Sensor node: Performances and constraints”, International Convention on Information and Communication Technology, Electronics and Microelectronics, MIPRO 2014, 2014.

[19] D. Kang, D. H. Kang, J. Kang, S. Yoo and S. Ha, “Joint optimization of speed, accuracy, and energy for embedded image recognition systems”, Design, Automation and Test in Europe Conference and Exhibition, 2018.

[20] M. El Fezazi, A. Achmamad, M. Aqil and A. Jbari, “PSoC-Based Embedded Instrumentation and Processing of sEMG Signals”, Analog Integrated Circuits and Signal Processing, pp. 1-16, 2021.

THE DARK SIDE OF ARTIFICIAL INTELLIGENCE IN MATERIALS SCIENCE: DFT DATA, THE ENERGY DILEMMA, AND THE SUSTAINABILITY PARADOX

Cengiz SOYKAN[1]

1. INTRODUCTION: Beyond the Fanfare – Critical Boundaries of Al-Assisted Discovery

Materials science is in the midst of a profound paradigm shift driven by artificial intelligence (AI) and machine learning (ML). We stand at the threshold of a new era where autonomous laboratories complete experimental cycles within days, inverse design predicts materials with targeted properties, and big data exponentially accelerates the pace of discovery (Long, 2022; MacLeod, 2020). This digital transformation unlocks the potential of a vast chemical space, estimated to be on the order of 10^{60} for potentially synthesizable organic materials, thereby offering a solution to a "discovery crisis" where human lifespans and resources have become inadequate (Aghanim, 2020).

However, every technological revolution also generates systematic limitations and unintended consequences that lurk in the shadow of triumphant narratives and require careful scrutiny. The integration of AI into materials science has introduced critical problems that can be grouped under four main headings. These issues are not merely technical obstacles but also raise

[1] Assoc. Prof. Dr., Kırşehir Ahi Evran University, Health Services Vocational School, Department of Medical Services and Techniques, ORCID: 0000-0003-0897-2384.

profound questions about the philosophy of science, research ethics, and global equity.

First, the quality and reliability of the data fueling AI is a primary concern. While large databases built using Density Functional Theory (DFT) form the backbone of materials discovery, the inherent methodological limitations of DFT and the systematic biases within these databases can lead machine learning models to perpetuate these flaws and trap discovery in a "local optimum" (Allam, 2018).

A second critique arises with the emergence of the sustainability paradox. The training of large AI models and the requirements for high-performance computing (HPC) consume energy on the order of megawatt-hours (Wassermann, 2024). This situation leads to a fundamental paradox: could the energy consumed in the process of developing a greener energy technology potentially exceed the energy saved over the lifetime of the final product?

Thirdly, the ontological constraints of inverse design bring into question the extent to which AI can truly discover the "new." Most current models perform a sophisticated form of interpolation within the data distribution on which they were trained, struggling to generate radical innovations that lie entirely outside this distribution – a true extrapolation (Rittig, 2025).

Finally, this technological progress creates profound ethical and geopolitical dilemmas. Inequality in access to HPC infrastructure and clean data carries the risk of a global "materials divide," intellectual property for materials discovered by autonomous systems challenges current patent law, and the pace of discovery threatens to outstrip thorough ethical and safety assessments (Purificato, 2025).

The aim of this chapter is not to deny the transformative power of AI in materials science, but rather to examine these four critical

areas to contribute to its responsible, sustainable, and equitable advancement. In the following pages, each problem will be analyzed in depth, and potential solutions will be discussed.

2. THE PATTERNS OF DFT DATA: Data Dynamics Shaping the Boundaries of Al- Models

The rise of artificial intelligence in materials discovery has largely been propelled by massive databases calculated using Density Functional Theory (DFT). These datasets constitute an invaluable resource for systematic discovery. However, the inherent methodological constraints of this "gold standard" method, combined with the inevitable structural biases present in the databases, profoundly shape the learning process and generalization capacity of machine learning models.

2.1. The Theoretical Framework of DFT and Its Real-World Complexities

DFT is a revolutionary tool developed to calculate the fundamental properties of materials by solving complex quantum mechanical equations through electron density. However, its practical applications, accuracy, and capacity to capture physical reality depend on the chosen "exchange-correlation functional". Widely used functionals such as LDA (Local Density Approximation) and GGA (Generalized Gradient Approximation) exhibit known systematic discrepancies, such as underestimating the band gaps of materials (Allam, 2018). More importantly, standard DFT calculations operate under idealized conditions, such as zero absolute temperature (0 K) and perfect crystal structures. This imposes inherent limitations on modeling real-world phenomena like temperature fluctuations, chemical defects, amorphous structures, and complex surface chemistry (Lejaeghere, 2016). Consequently, DFT data represents an approximate and idealized representation of physical reality.

2.2. Systematic Focus and Relative Deficiencies in Database

While large-scale open databases such as the Materials Project, AFLOWLIB, and OQMD promise a democratic revolution in materials science, their content inevitably exhibits a focus on specific classes of materials. This focus stems primarily from the computational priority given to material classes that are relatively easier and faster to simulate. Consequently, while inorganic crystalline oxides and intermetallic compounds are well-represented, there is a relative data deficiency for materials that are computationally challenging or structurally ambiguous, such as complex polymers, metal-organic frameworks (MOFs), amorphous solids, and liquid systems (de Pablo, 2019; Jain, 2013). This systematic compositional distribution shapes the discovery landscape, naturally steering researchers toward the well-characterized regions of chemical space.

2.3. Dependence of Model Inferences on Data Distribution

By fundamental principle, a machine learning model learns the statistical distribution of the dataset presented to it. If the training data is concentrated within specific material families, the model's inferences will inevitably reflect this data distribution. While the model may be highly successful at optimizing compositions within well-represented material families in the database, its capacity to predict entirely new and unconventional material candidates in regions where the data distribution is sparse becomes limited (de Pablo, 2019). This situation risks concentrating the discovery process on only a specific subset of the search space, potentially causing broader chemical possibilities to be overlooked.

2.4. Methods for Balanced Discovery

Fortunately, methods are being actively researched to overcome these data-centric challenges and enable a more balanced discovery process:

• **Active Learning:** In this method, the ML model actively queries which subsequent experiment or calculation would yield the highest information gain (typically where its own predictive uncertainty is highest), rather than just passively consuming data. This targets sparse regions in the data distribution, thereby expanding the dataset in a more balanced and comprehensive manner (de Pablo, 2019).

• **Physics-Informed Neural Networks (PINNs):** This approach incorporates physical laws (e.g., quantum mechanical equations or conservation laws) as constraints during the model's training. This helps the model learn not only correlations from the existing data but also fundamental physical principles, enabling it to make more reliable predictions in regions with little or no data (Karniadakis, 2021).

In conclusion, while DFT and the data ecosystem built upon it provide an invaluable starting point for AI-assisted materials discovery, it is crucial to be critically aware of the methodological and structural biases inherent in this system. Truly inclusive and innovative discovery requires an approach that understands these data dynamics and actively adopts methods to balance the discovery process.

3. THE SUSTAINABILITY PARADOX: Al's Energy Dilemma

While artificial intelligence in materials science is praised for its potential to accelerate the discovery process, a growing concern is emerging in the background of this digital revolution:

energy consumption. The sustainability of AI-assisted discovery is not merely a matter of economic cost but is also at the heart of a profound environmental and ethical paradox. This paradox raises the question: *could the research conducted for a greener future potentially undermine that very future due to its own energy footprint?*

3.1. The Hidden Cost of Large-Scale Computation

The role of AI in materials discovery revolves around intensive DFT calculations, the training of large language models, and the optimization of complex neural network architectures. These processes require thousands of high-performance processors (GPUs/CPUs) to operate continuously for days or even weeks. For instance, training a large-scale language model can consume electricity on the order of hundreds of megawatt-hours (MWh); this is equivalent to the annual energy consumption of dozens of households or the emission of hundreds of tons of carbon dioxide (CO_2) (Strubell, 2019). Autonomous laboratories further increase the total energy burden by adding not only computational demands but also the energy requirements of robotic systems operating for synthesis and characterization (Montoya, 2022).

3.2. The Anatomy of the Sustainability Paradox

This extraordinary energy consumption creates a paradox, particularly in the context of energy technology-focused materials discovery. Consider a concrete scenario: the search for a new generation of solar cell materials. The process might begin with an AI-driven screening campaign, running thousands of industry-standard GPUs for months to identify this material. This is followed by the synthesis and characterization of the most promising candidates in autonomous laboratories. Could the total carbon footprint of all these activities potentially exceed the carbon emissions that the ultimately discovered and

commercialized solar cell would "save" over its lifetime by displacing energy generated from fossil fuels? This constitutes a fundamental sustainability paradox that is attracting increasing attention within the field (Lynn, 2022). In short, the process itself can, to a certain extent, consume the environmental benefit of its ultimate goal.

3.3. Novel Approaches for Energy Efficiency

Fortunately, researchers aware of this dilemma are developing various strategies to improve the energy efficiency of AI-driven discovery:

• Targeted and Efficient Models: Using smaller, specialized neural networks trained for specific material classes, rather than universal, massive models, can significantly reduce energy consumption (Anthony, 2020).

• Active Learning and Smart Data Usage: The active learning strategies mentioned in the previous section improve not only data bias but also energy efficiency. By targeting points where the model is most uncertain and can learn the most, unnecessary and energy-intensive computations are avoided.

• Green Computing (Green HPC) and Hardware Innovation: Cloud computing providers and supercomputing centers are developing more energy-efficient processors and shifting towards powering their facilities with renewable energy sources. Researchers opting for carbon-neutral or low-carbon footprint HPC resources is critical to reducing the overall impact (Wassermann, 2024).

In conclusion, while AI-assisted materials discovery holds the potential to find solutions to urgent global problems like the climate crisis, it cannot ignore the environmental cost of its own operational processes. A sustainable discovery ecosystem requires attention not only to which materials are found but also

to how we find them. The future will belong not only to smarter algorithms but also to more energy-conscious research paradigms.

4. THE BOUNDARIES OF CREATIVITY: Ontological Constraints of Inverse Desing

Inverse design stands as one of the most impressive applications of AI in materials science. However, beyond the data and energy issues addressed in previous sections, this approach raises a profound ontological question: *Can a machine truly create something "new"?*

4.1. The Dominance of Interpolation

Most current inverse design models (GANs, VAEs) perform a sophisticated form of interpolation, navigating between points within the data distribution on which they were trained (Sanchez, 2018). The model generates new candidates by recombining the existing building blocks present in the training data (e.g., specific molecular groups or crystal symmetries). This is analogous to an artist mixing a limited palette of colors to create new shades; the result may appear novel, but the underlying pigments remain the same.

4.2. The lack of Radical Innovation and “Black Swans”

The problem lies in the model's difficulty in generating radical innovations—a true extrapolation—that fall entirely outside the distribution of its training data, such as a completely new type of chemical bond or crystal structure (Gómez, 2018). Such "black swan" discoveries typically emerge through human intuition, serendipity, or unexpected observations during traditional experiments. Although AI excels at optimization and efficiency, its capacity to capture this unpredictable "leap" remains limited.

4.3. The Future: Human-Al Partnership

This does not mean that AI has failed. On the contrary, it indicates that the most efficient discovery model of the future will be a symbiotic partnership that combines AI's speed and optimization power with the human researcher's intuition, creativity, and ability to forge interdisciplinary connections (Segler, 2018). The role of AI is evolving into that of a "catalyst" that nourishes and guides human creativity, rather than being the ultimate decision-maker.

5. CONCLUSION: Towards a Responsible and Sustainable Discovery Paradigm

While the age of artificial intelligence in materials science began with the promise of extraordinary speed and efficiency, it has become clear that significant undercurrents swirl beneath these seemingly transparent waters. The triple crisis examined in this chapter—structural biases in DFT data, the sustainability paradox, and the creativity limits of inverse design—reveals that AI-assisted discovery is not a neutral tool but a complex socio-technical system with its own constraints and side effects.

These technical limitations inevitably raise profound ethical and societal questions. Energy consumption is not merely an environmental cost but also a matter of equitable access to resources and the ecological responsibility of research (Wassermann, 2024). The focused compositional distribution in DFT databases risks deepening a "materials divide," thereby exacerbating inequalities within the global scientific ecosystem (Purificato, 2025). Furthermore, the speed of autonomous systems carries the potential to outpace the ethical and safety evaluation of discovered materials and to challenge existing intellectual property frameworks (Resnik, 2025). Confronted by these challenges, the fundamental skill set expected of the future

materials scientist is undergoing a radical transformation. It is no longer sufficient to be solely an experimental designer or data analyst.

The future researcher must also be:

- A data critic, capable of questioning the origin, scope, and limitations of the datasets they use.
- An energy auditor, aware of the ecological cost of computational processes and striving to minimize it.
- An ethics overseer, considering the broader societal and environmental impacts of their work.

In conclusion, awareness of the "dark side" is not a reason for rejection or pessimism, but rather a sign of maturity. The true and lasting success of artificial intelligence in materials science will depend not on blindly embracing it nor on rejecting it outright, but on our courage to grasp both its power and its flaws simultaneously, and to thereby construct a discovery paradigm that is more responsible, transparent, sustainable, and fair (Segler, 2018). This will be a step forward not only for better materials but also for a better understanding of science itself.

REFERENCES

Aghanim, N., Akrami, Y., Ashdown, M., Aumont, J., Baccigalupi, C., Ballardini, M., Zonca, A. (2020). Planck2018 results: VI. Cosmological parameters. *Astronomy & Astrophysics, 641*, A6. doi:10.1051/0004-6361/201833910

Allam, N. K., Tolba, S. A., Gameel, K. M., Ali, B. A., & Almossalami, H. A. (2018). The DFT+U: Approaches, Accuracy, and Applications. In G. Yang (Ed.), *Density Functional Calculations - Recent Progresses of Theory and Application*. London: IntechOpen.

Anthony, L. F. W., Kanding, B., & Selvan, R. (2020). Carbontracker: Tracking and Predicting the Carbon Footprint of Training Deep Learning Models. doi:arXiv:2007.03051

de Pablo, J. J., Jackson, N. E., Webb, M. A., Chen, L.-Q., Moore, J. E., Morgan, D., Zhao, J.-C. (2019). New frontiers for the materials genome initiative. *npj Computational Mathematics, 5*, 41. doi:10.1038/s41524-019-0173-4

Gómez-Bombarelli, R., Wei, J. N., Duvenaud, D., Hernández-Lobato, J. M., Sánchez-Lengeling, B., Sheberla, D., Aspuru-Guzik, A. (2018). Automatic Chemical Design Using a Data-Driven Continuous Representation of Molecules. *ACS Central Science, 4*(2), 268–276. doi:10.1021/acscentsci.7b00572

Jain, A., Ong, S. P., Hautier, G., Chen, W., Richards, W. D., Dacek, S., Persson, K. A. (2013). Commentary: The Materials Project: A materials genome approach to accelerating materials innovation. *APL Materials, 1*(1). doi:10.1063/1.4812323

Karniadakis, G. E., Kevrekidis, I. G., Lu, L., Perdikaris, P., Wang, S., & Yang, L. (2021). Physics-informed machine learning. *Nature Reviews Physics, 3*(6), 422-440. doi:10.1038/s42254-021-00314-5

Lejaeghere, K., Bihlmayer, G., Björkman, T., Blaha, P., Blügel, S., Blum, V., Cottenier, S. (2016). Reproducibility in density functional theory calculations of solids. *Science, 351*(6280), aad3000. doi:10.1126/science.aad3000

Long, T., Zhang, Y., Fortunato, N. M., Shen, C., Dai, M., & Zhang, H. (2022). Inverse design of crystal structures for multicomponent systems. *Acta Materialia, 231*, 117898. doi:https://doi.org/10.1016/j.actamat.2022.117898

Lynn, H. K., Priya, L. D., Emma, S., George, K., Felix, C., & David, R. (2022). [Aligning artificial intelligence with climate change mitigation]. *Nature Climate Change*(6), 518-527. doi:10.1038/s41558-022-01377-7

MacLeod, B. P., Parlane, F. G. L., Morrissey, T. D., Häse, F., Roch, L. M., Dettelbach, K. E., Berlinguette, C. P. (2020). Self-driving laboratory for accelerated discovery of thin-film materials. *Sci Adv, 6*(20), eaaz8867. doi:10.1126/sciadv.aaz8867

Montoya, J. H., Aykol, M., Anapolsky, A., Gopal, C. B., Herring, P. K., Hummelshøj, J. S., Storey, B. D. (2022). Toward autonomous materials research: Recent progress and future challenges. *Applied Physics Reviews, 9*(1). doi:10.1063/5.0076324

Purificato, E., Bili, D., Jungnickel, R., Ruiz Serra, V., Fabiani, J., Abendroth Dias, K., Gómez, E. (2025). *The Role of Artificial Intelligence in Scientific Research: A Science for Policy, European Perspective*. Retrieved from

Luxembourg: https://www.astrid-online.it/static/upload/jrc1/jrc143482_01.pdf

Resnik, D. B., & Hosseini, M. (2025). The ethics of using artificial intelligence in scientific research: new guidance needed for a new tool. *AI and Ethics, 5*(2), 1499-1521. doi:10.1007/s43681-024-00493-8

Rittig, J. G., Dahmen, M., Grohe, M., Schwaller, P., & Mitsos, A. (2025). Molecular Machine Learning in Chemical Process Design. In.

Sanchez-Lengeling, B., & Aspuru-Guzik, A. (2018). Inverse molecular design using machine learning: Generative models for matter engineering. *Science, 361*(6400), 360-365. doi:doi:10.1126/science.aat2663

Segler, M. H. S., Preuss, M., & Waller, M. P. (2018). Planning chemical syntheses with deep neural networks and symbolic AI. *Nature, 555*(7698), 604-610. doi:10.1038/nature25978

Strubell, E., Ganesh, A., & McCallum, A. (2019). Energy and Policy Considerations for Deep Learning in NLP. doi:arXiv:1906.02243

Wassermann, C., Bielert, M., Vanberg, G., Hackenberg, D., Terboven, C., & Müller, M. S. (2024, 24-27 Sept. 2024). *Calculating User-Centric Carbon Footprints for HPC.* Paper presented at the 2024 IEEE International Conference on Cluster Computing Workshops (CLUSTER Workshops).

PHYSICAL CHARACTERISTICS OF THE STRAWBERRY FRUIT (*Arbutus unedo*) GROWING IN THE BLACK SEA REGION[1]

Seyhun YURDUGÜL[2]

Canan ÜLGEN[3]

1. INTRODUCTION

Arbutus unedo is a perennial shrub or small tree species belonging to the Ericaceae family, native to Greece, Lebanon, Ireland, Southern Europe, and Anatolia, and considered a typical Mediterranean climate species. The regions where populations exist both globally and in Turkey are provided in the study conducted by Sarikaya and colleagues in 2024. In Turkey, this species is particularly widespread in the Black Sea region and is also present in the Marmara, Aegean, and Mediterranean coastal regions, as well as in provinces such as Sinop, Trabzon, Ordu, Giresun, Bolu, Düzce, Zonguldak, Artvin, Balıkesir, Kocaeli, Sakarya, Hatay, Mersin, Muğla, and Antalya. As the plant is generally found in places quite close to sea level, at low altitudes and in maquis formations, it occurs in small and scattered populations, and these populations are shrinking over time. In terms of its botanical characteristics, the species usually grows to a height of 2 to 6 meters, rarely reaching 8 meters. The species' leaves are thick, dark green, elliptical or oval in shape, and

---

1 This book chapter has been developed from a Master's thesis.

2 Prof. Dr., Bolu Abant İzzet Baysal University, Faculty of Science, Department of Biology, ORCID:0000-0002-3652-9737.

3 Dr. Lecturer, Şırnak University Technology and Research Center Laboratory, ORCID: 0000-0002-8272-3370.

serrated at the edges. The leaves are evergreen. The strawberry tree fruit (Kocayemiş) flower blooms in the fall and winter months. Small, white-pink bell-shaped flowers are found in clusters.

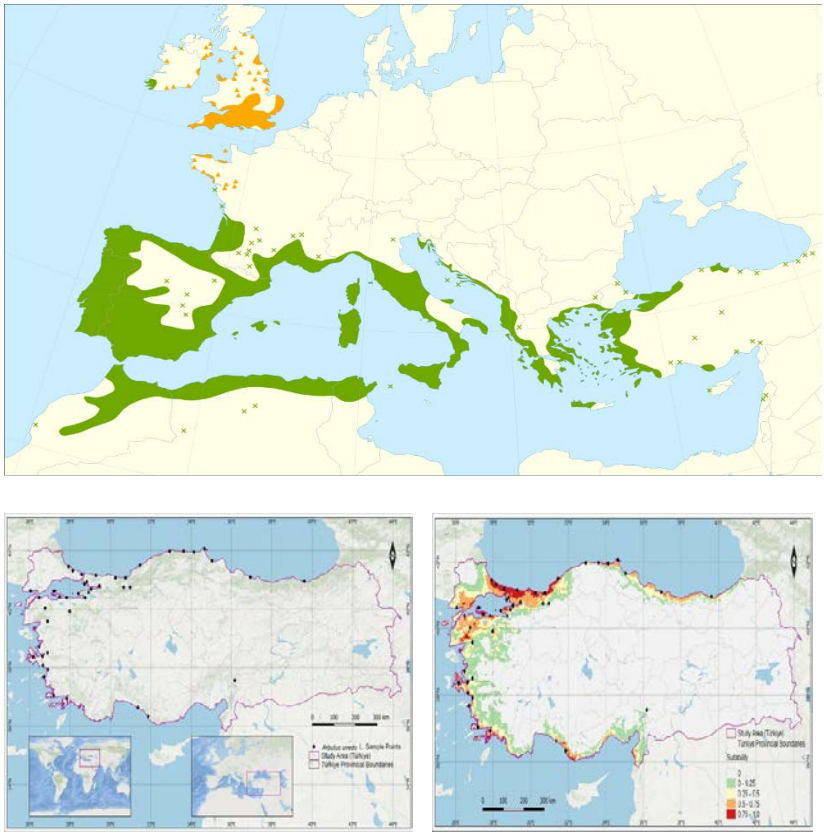

Figure 1. The World and Turkey Distribution of *Arbutus unedo* (Sarikaya et al., 2024)

The strawberry tree fruit (Kocayemiş) produces round, nut-sized berries of a red-orange color, which can take 6 to 12 months to ripen (see Figure 2). The fruit is sweet and mildly aromatic, while its root and stem are barked, and its branches are reddish-brown. Furthermore, the most significant species of the genus Arbutus are *Arbutus unedo* L. and *Arbutus andrachne* L.

Both of these species are present in the natural flora of Turkey (Anşin and Özkan, 1993). The genus Arbutus is naturally distributed along the coastal regions of the Mediterranean, Black Sea, Marmara, and Aegean Seas (Yaltırık and Erdinç, 2002).

Figure 2. Strawberry Tree Fruit (*Arbutus Unedo*) Grown in the Black Sea Region

Regarding the ecological characteristics of the strawberry tree fruit (*Arbutus unedo*) (Figure 2), its micro-site requirements allow it to be resistant to drought and poor soils. Its flowers are an important nectar source for bees, and its seeds are dispersed due to the consumption of its fruit by birds and mammals. This fruit is a plant with high aesthetic and ecological value, playing a significant role in its natural habitat. The fruit can be consumed fresh and is used in the production of jam, marmalade, etc. It is also often preferred as an ornamental plant in gardens and parks. In some traditional medicine practices, it has been used for its diuretic and antiseptic properties.

In this study, the freeze-drying (lyophilization) method was applied to the fruit in question with the aim of extending its shelf life, and the changes in the physical properties of the fruit after this process were investigated. Thus, fresh and freeze-dried *Arbutus unedo* fruits were evaluated comparatively.

Furthermore, this study aimed to increase the value of the strawberry tree fruit in terms of food technology and functional food production, and to incorporate the natural products of our country into industrial use.

2. MATERIALS AND METHOD

The strawberry tree fruits (*Arbutus unedo*) used in the study were naturally collected from the surrounding areas of Zonguldak and Düzce provinces (within the district borders of Akçakoca). The collected fruits were selected according to their maturity level and washed. Subsequently, both fresh and freeze-dried (lyophilized) strawberry tree samples were prepared in comparison. For the freeze-drying process, the fruits were initially frozen at −80°C and then dried for 48 hours under a vacuum of 0.25 mbar.

The dried samples were stored at room temperature in airtight containers. The analyses conducted within the scope of the research were performed on both fresh and freeze-dried fruit samples. Thus, for the physical analyses, color measurement was performed first, followed by surface morphology analysis using a Scanning Electron Microscope (SEM) (JEOL JSM-5600 LV model).

The color properties of the fruit samples were determined using a Minolta CR-300 colorimeter (Minolta Co., Japan). For the surface morphology, samples were first coated with gold and subsequently observed at an acceleration voltage of 15 kV. The SEM images were evaluated to examine surface roughness, pore structure, and the morphological changes dependent on the drying process.

The data obtained from all analyses were statistically evaluated, and the effects of the freeze-drying process on the

properties of the strawberry tree fruit were comparatively investigated. Experiments were initiated with two types for each treatment, consisting of at least three replicates of fresh and freeze-dried (CHRIST Epsilon 2-6D) fruit. Statistical analysis was performed using ANOVA (STATISTICA 6), and significantly different means ($P \leq 0.05$ or $P \leq 0.01$) were determined using Duncan's test.

3. RESULTS AND DISCUSSION

The physical analysis results obtained from fresh and freeze-dried samples of *Arbutus unedo* (strawberry tree) fruit were presented and discussed comparatively with the relevant literature. The color parameters and surface morphologies of the fresh and freeze-dried *Arbutus unedo* fruits were evaluated.

The colors of the fresh and freeze-dried samples were measured using a Minolta Chroma Meter CR-400 portable colorimeter (Minolta Corp., Osaka, Japan) and recorded in terms of the Commission Internationale de l'Éclairage (CIE) color space coordinates (L^*, a^* and b^*). Prior to measurement, the colorimeter was calibrated daily using the Minolta calibration plate CR.A43. The hue angle (or color angle) was calculated using the formula: $\arctan(b^*/a^*) \times 57.3$.

For the fresh and freeze-dried *Arbutus unedo* samples, the L^* value indicates lightness ($L^*=0$ is black, $L^*=100$ is white), the a^* value represents the red-green axis (+60=red, −60=green), and the b^* value shows the yellow-blue axis (+60=yellow, −60=blue).

Samples collected from Akçakoca and Zonguldak were designated as TazeAkc¸ or TazeZon for fresh fruit samples, and Don-Akc¸ or Don-Zon for freeze-dried fruit samples. The color measurements performed on the fresh and lyophilized (freeze-dried) strawberry tree fruit samples are presented in Table 1.

According to Table 1, the L^*, a^*, and b^* values for the fresh strawberry tree fruit collected from Akçakoca were statistically calculated as 21.93,1.02, and 1.58, respectively (Ulgen, C. 2013). The corresponding values for the freeze-dried samples were 21.51,0.81, and 1.80, respectively. Similarly, while the L^*, a^*, and b^* values for the fresh strawberry tree samples collected from Zonguldak were 22.69,−0.95, and 1.91, respectively, the data for the freeze-dried samples were 22.59,−0.95, and 1.03.

Table 1. Color Measurement Values of Fresh and Freeze-Dried Akçakoca and Zonguldak Samples.

	TazeAkç1	TazeAkç2	TazeZon1	TazeZon2
L* value	20.66 20.75 20.88	22.08 22.28 22.42	21.41 21.56 21.61	23.14 23.63 24.19
a* value	0.79 0.67 0.59	1.01 0.91 0.89	-0.52 -0.58 -0.58	-1.17 -1.36 -1.52
b* value	1.23 1.28 1.31	2.27 2.34 2.38	0.17 0.26 0.28	1.51 1.51 2.05
	Don-Akç1	Don-Akç2	Don-Zon1	Don-Zon2
L* value	21.77 21.79 22.17	21.89 21.97 22.01	22.55 22.58 22.63	22.38 22.79 22.81
a* value	1.13 1.03 0.99	1.00 0.96 0.97	-0.79 -0.80 -0.84	-0.99 -1.12 -1.18
b* value	1.44 1.50 1.52	1.67 1.67 1.73	1.66 1.73 1.74	2.11 2.11 2.15

As shown in Table 1, the L^* (lightness) value of the freeze-dried samples exhibited a slight increase compared to the fresh fruits. This finding is attributed to the formation of micro-pores on the fruit surface during the drying process, which results in greater light reflection. Conversely, a slight decrease was observed in the a^* (redness) and b^* (yellowness) values.

Furthermore, the Scanning Electron Microscopy (SEM) images of the fresh and freeze-dried strawberry tree fruit samples are presented in Figure 3, Figure 4, Figure 5, and Figure 6.

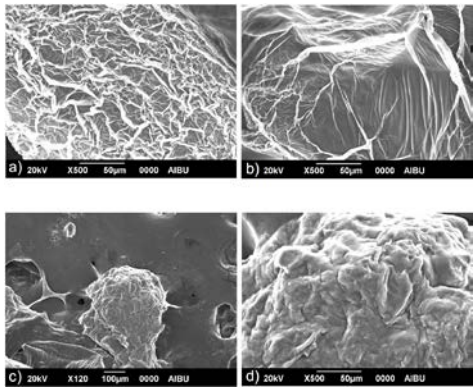

Figure 3. SEM Images of Fresh Strawberry Tree Fruit Collected from Akçakoca a) and b) Fiber part, c) and d) Surface part.

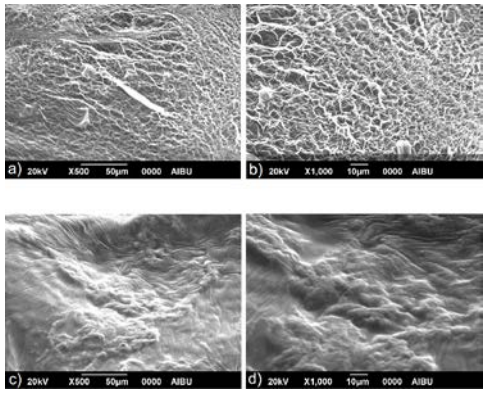

Figure 4. SEM Images of Fresh Strawberry Tree Fruit Collected from Zonguldak a) and b) Fiber part, c) and d) Surface part.
The SEM images of the fresh strawberry tree fruit collected from Akçakoca are presented in Figure 2, and the images of the fresh strawberry tree fruit collected from Zonguldak are presented in Figure 3. The images related to the freeze-dried strawberry tree fruit are those collected from Akçakoca in Figure 4 and those collected from Zonguldak in Figure 5.

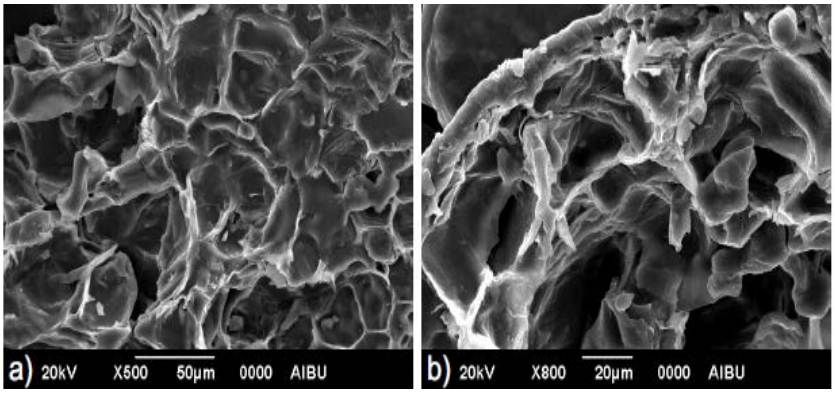

Figure 5. SEM Images of Freeze-Dried Strawberry Tree Fruit Collected from Akçakoca a) at 500x magnification and b) at 800x magnification

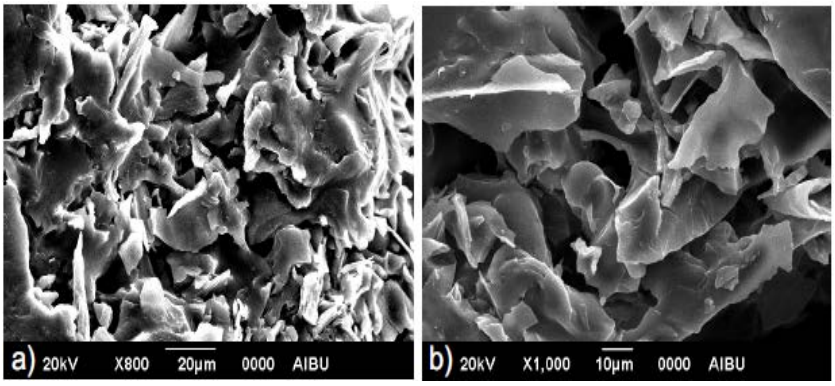

Figure 6. SEM Images of Freeze-Dried Strawberry Tree Fruit Collected from Zonguldak a) at 800x magnification and b) at 1000x magnification.

In fresh fruit samples, the surface structure was observed to be smooth, dense, and the intercellular connection regular. In contrast, the lyophilized samples were determined to have a porous and loose structure, with partially collapsed cell walls. This morphological change is attributed to the voids formed in the tissue as a result of the direct sublimation of ice crystals during

the drying process. This porous structure can enhance the fruit's water holding capacity and rehydration properties. Similar morphological changes have also been reported by Malheiro et al. (2012) in *Arbutus unedo* leaves and by Basu et al. (2009) in freeze-dried strawberries.

4. CONCLUSION AND RECOMMENDATION

In this research, the physical properties of the fresh and freeze-dried (lyophilized) forms of *Arbutus unedo* (strawberry tree) fruit were investigated, and the results are summarized:

- Physical analyses determined that the L^* (lightness) value slightly increased in the freeze-dried fruits, while a limited decrease occurred in the a^* (redness) and b^* (yellowness) values.
- SEM images showed the formation of a porous structure on the fruit surface after drying. This revealed that lyophilization largely preserved the structural integrity of the tissue but created a micro-porous texture internally.

This study demonstrated that the freeze-drying method is a suitable technique for *Arbutus unedo* fruit and, based on the physical analysis results, indicates that this fruit can be utilized in the development of functional foods, natural preservatives, and health-supporting products.

ACKNOWLEDGEMENT

This work was derived from a Master's thesis study. I extend my gratitude to my advisor, Prof. Dr. Seyhun Yurdugül, from the Department of Biology, Faculty of Arts and Sciences, Bolu Abant İzzet Baysal University.

REFERENCES

Anşin, R., & Özkan, Z. C. (1993). *Tohumlu bitkiler (Spermatophyta) odunsu taksonlar* [Seed plants (Spermatophyta) woody taxa]. KTÜ Orman Fakültesi Yayınları.

Basu, A., Wilkinson, M., Penugonda, K., Simmons, B., Betts, N. M., & Lyons, T. J. (2009). Freeze-dried strawberry powder improves lipid profile and lipid peroxidation in women with metabolic syndrome: Baseline and post intervention effects. *Nutrition Journal*, *8*(1), 43.

Malheiro, R., Sá, O., Pereira, E., Aguiar, C., Baptista, P., & Pereira, J. A. (2012). *Arbutus unedo* L. leaves as source of phytochemicals with bioactive properties. *Industrial Crops and Products*, *37*(1), 473–478.

Sagbaş, H. I., İlhan, G., Zitouni, H., Anjum, M. A., Hanine, H., Nečas, T., Ondrašek, I., & Ercisli, S. (2020). Morphological and biochemical characterization of diverse strawberry tree (*Arbutus unedo* L.) genotypes from Northern Turkey. *Agronomy*, *10*(10), 1581. doi:10.3390/agronomy10101581

Sarikaya, A. G., Uzun, A., & Turan, F. D. (2024). Effect of climate change on current and future potential distribution of Strawberry tree (*Arbutus unedo* L.) in Türkiye. *Scientific Reports*, *14*(1), 17408.

Ulgen, C. (2013). “Certain Chemical, Physical and Microbiological Properties of The Freeze-Dıed (Lyophılızed) Apple of Cain/Cane Apple (*Arbutus Unedo*) Fruit” Msc Thesis, Bolu Abant Izzet Baysal Univesity.

Yaltırık, T., & Erdinç, S. (2002). *Trees*. The Foundation of Challenge with Erosion, Forestation and Protection of Natural Resources of Turkey.

Yıldırım, N., Atar, F., Turna, H., Bayraktar, A., & Turna, İ. (2018). Floristic characteristics of *Arbutus unedo* L. and *Arbutus andrachne* L. as medicinal plants. *Works of the Faculty of Forestry University of Sarajevo, 48*(1), 56–63. doi:10.54652/rsf.2018.v48.i1.52

RISK ASSESSMENT IN A FAMILY HEALTH CENTER USING THE L-TYPE MATRIX METHOD

Emre Can UĞUR[1]

Mehmet HASKUL[2]

1. INTRODUCTION

Health constitutes a fundamental human right that has remained paramount throughout history. Family Health Centers, which serve as cornerstones of healthcare maintenance, represent primary healthcare services in our country and function as the initial touchpoint for health-related concerns. Within this context, their significance in terms of occupational health and safety must be emphasized. Every individual in our country is assigned a family physician, and healthcare examinations are conducted at the family health center where these physicians practice. Family health centers serve as facilities where individuals with immediate health concerns seek care; consequently, they are critically important regarding occupational injuries, diseases, and workplace accidents that may result in injuries or fatalities. Therefore, identifying and assessing hazards and risks in family health centers is essential (Öngel ve Zaloğlu 2017).

Implementing measures to ensure the health and safety of employees and healthcare workers at family health centers reduces operational costs and enhances workplace efficiency by

[1] Graduate Student, Sirnak University, Graduate Education Institute, Master's Degree (Thesis) - Occupational Health and Safety, ORCID: 0009-0009-6503-9030.

[2] Associate Professor, Sirnak University, Faculty of Engineering, Department of Mechanical Engineering, ORCID: 0000-0001-8671-4597.

maintaining workforce health. Occupational health and safety hold multifaceted importance, as the illness of a healthcare worker at a family health center can adversely affect workflow and disrupt healthcare service delivery (Öngel ve Zaloğlu 2017). When workplaces are classified as family health centers according to their hazard classes, the classification is as indicated in Table 1.

Table 1. Family Health Center Hazard Classification

NACE CODE	DEFINITION	HAZARD CLASS
86.21.02	Described as general medical practice activities without accommodation, provided by family and community health units (RG, 28509 2012).	HAZARDOUS

According to legislation, risk assessments conducted in HAZARDOUS workplaces must be renewed every four years (RG, 28512 2012).

This study addresses the potential hazard factors that patients, visitors, employees, and interns may encounter at family health centers throughout the day, as well as the risks that may arise from these hazards. The current hazards, risks, at-risk groups, severity, probability, and risk scores were determined, and preventive strategies were developed using the L-type matrix method, a widely recognized risk assessment methodology.

2. L-TYPE MATRIX METHOD

Risk assessment and analysis are conducted using the 5×5 L-type matrix method, a frequently employed analysis technique in healthcare institutions that is easily applicable and compliant with legislation. This matrix method evaluates both the probability of an event occurring and the consequences should a hazardous event materialize, determining its extent and nature within the scope of regulatory and preventive activities (Karan Buturak ve Yapıcı 2022).

The L-type matrix method (5×5 matrix diagram) is particularly useful for evaluating cause-effect relationships and enables risk analysts to work independently (Karan Buturak 2019).

Table 2. L-Type Matrix Severity Scale (Ünverdi ve Çetinyokuş 2021)

Severity Level	Description
1 - Very Mild	No loss of work time; initial intervention may be required.
2 - Mild	No loss of work days; outpatient care may be required.
3 - Moderate	Minor injuries may require inpatient treatment.
4 - Severe	Severe injuries, long-term treatment, or occupational diseases.
5 - Very Severe	Death or permanent disability.

Table 3. L-Type Matrix Probability Scale (Ünverdi ve Çetinyokuş 2021)

Probability Level	Occurrence Frequency
1 - Very Low	Almost never
2 - Low	Very rarely (approximately once a year)
3 - Medium	Rarely (approximately once a year)
4 - High	Frequently (approximately once a month)
5 - Very High	Very often (once a week to daily)

Table 4. L-Type Risk Matrix (Ünverdi ve Çetinyokuş 2021)

	SEVERITY				
PROBABILITY	**1**	**2**	**3**	**4**	**5**
1	(1)	(2)	(3)	(4)	(5)
2	(2)	(4)	(6)	(8)	(10)
3	(3)	(6)	(9)	(12)	(15)
4	(4)	(8)	(12)	(16)	(20)
5	(5)	(10)	(15)	(20)	(25)

Risk Score = Severity × Probability

Risk Level Classification:

- □ **Low Risk (1-6)**: Acceptable
- □ **Medium Risk (8-12)**: Considerable
- ■ **High Risk (15-25)**: Unacceptable

Table 5. Risk Score Action Requirements (Ünverdi ve Çetinyokuş 2021)

RISK SCORE	RISK LEVEL	ACTION REQUIRED
1, 2, 3, 4, 5, 6	**LOW** - Acceptable Risk	May not require immediate action (Within 1 year)
8, 9, 10, 12	**MEDIUM** - Considerable Risk	These hazards must be addressed as quickly as possible (Within 6 months)
15, 16, 20, 25	**HIGH** - Unacceptable Risk	Corrective and protective actions are mandatory (Immediate action required)

3. RESEARCH AND FINDINGS

In this study, a family health unit was examined, and risk analysis and assessment were conducted using the L-type matrix method.

Table 6. Risk Analysis and Assessment in Family Health Center

No	Identified Hazard	Potential Risk	At-Risk Groups	Severity	Probability	Risk Score	Control Measure
1	Unsafe exterior area	Falls, injuries, and death	Patients, employees, guests, interns	5	5	**25**	Install safety railings in accordance with legislation (RG, 28710 2013).
2	Exposed electrical cable	Electric shock, injury, and death	Employees, patients, guests, interns	5	5	**25**	Ensure all electrical cables are properly secured and insulated in accordance with legislation (RG, 28628 2013; RG, 28786 2013).
3	Unfixed infant weighing scale	Falls, injuries, and death	Infants coming for examination	4	5	**20**	The infant weighing scale must be securely fixed (RG, 28628 2013).
4	Improper worker posture during blood collection	Falls, injuries, and musculoskeletal disorders	Employees, interns	4	5	**20**	Provide ergonomic equipment and training to employees in accordance with legislation (RG, 28628 2013).

5	Sharps container filled beyond capacity	Injury and infectious disease	Employees, interns	4	5	**20**	Ensure the container is filled in accordance with legislation (¾ capacity maximum) (RG, 29959 2017).
6	Stairs without railings	Falls and injuries	Guests, employees, patients, interns	4	5	**20**	Install stair railings that comply with legislation (RG, 28710 2013).
7	Open electrical panel cover	Electric shock, injury, and death	Employees, interns, patients, guests	5	4	**20**	The electrical panel cover must be secured and protected in accordance with legislation (RG, 28786 2013).
8	Disorganized workplace	Injuries and infectious diseases	Employees, interns, patients	4	5	**20**	Ensure the workplace is organized and maintained in accordance with legislation (RG, 28710 2013).
9	Emergency exit door opens inward	Injury and death due to blocked exit	Guests, patients, employees, interns	5	3	**15**	The emergency exit door must open outward (RG, 28710 2013).
10	Fire hose and hose reel system not maintained	Injuries, deaths, and material losses due to inadequate firefighting equipment	Patients, employees, guests, interns	5	3	**15**	Ensure regular maintenance of fire hose and hose reel systems (RG, 26735 2007).
11	Lack of access to portable fire extinguisher	Injuries, deaths, and material losses due to inability to respond to fire	Guests, patients, employees, interns	5	3	**15**	Install portable fire extinguishers in accessible locations in accordance with legislation (RG, 26735 2007).
12	Improperly managed electrical cables	Injury, death, and material loss due to tripping or electrical hazards	Employees, interns, guests, patients	5	3	**15**	Implement cable management measures to ensure proper organization (RG, 18565 1984; RG, 28628 2013).
13	Antenna and camera cables not properly arranged	Electric shock and fire due to improper wiring	Patients, guests, interns, employees	5	3	**15**	Ensure all cables are properly organized and secured (RG, 18565 1984; RG, 28628 2013).

14	Holes and slopes in interior building area	Injury due to tripping and falling	Patients, staff, interns, guests	5	3	**15**	Eliminate holes and slopes or provide appropriate warnings (RG, 28710 2013; RG, 28786 2013).
15	Lack of emergency exit signage	Injury due to inability to locate exit during emergency	Patients, staff, interns, guests	3	4	**12**	Install permanent emergency exit signs in accordance with legislation (RG, 28710 2013; RG, 28762 2013).
16	Unsafe stairs	Falls and injuries	Employees, interns, guests, patients	3	4	**12**	Repair and secure stairs to meet safety standards (RG, 28710 2013).
17	Wheelchair blocking emergency exit door	Falls, injuries, and death due to blocked emergency exit	Employees, patients, interns, guests	4	3	**12**	Ensure emergency exit doors remain unobstructed and accessible in accordance with legislation (RG, 28710 2013).
18	Cleaning equipment positioned in inappropriate area	Infection and disease transmission	Patients, employees, guests, interns	2	5	**10**	Ensure cleaning equipment is stored in designated areas by authorized personnel (RG, 28698 2013).
19	Needle tip on ground after injection	Injury, infection, and contamination from sharps	Employees, interns, guests, patients	3	3	**9**	Ensure proper disposal of sharps waste immediately after procedures (RG, 29959 2017).
20	Inadequate lighting	Falls and injuries	Patients, employees, guests, interns	3	3	**9**	Provide adequate lighting throughout the facility (RG, 28710 2013).
21	Inadequate ventilation in toilet and sink area	Infectious diseases and infection transmission	Patients, employees, guests, interns	3	3	**9**	Install appropriate ventilation system in toilet and sink areas (RG, 28710 2013).
22	Lack of protection on stair steps	Falls and injuries	Patients, guests, employees, interns	3	3	**9**	Install slip-resistant surfaces or edge protection on stairs in accordance with legislation (RG, 28710 2013).
23	Sharps waste container positione	Injuries and infectious diseases due	Patients, guests, employees, interns	3	3	**9**	Position sharps containers in appropriate locations in accordance with

	d inapprop riately	to container spillage					legislation (RG, 29959 2017).
24	Deforme d work table base	Injury due to table collapse	Employe es	3	3	**9**	Replace damaged work table with new equipment (RG, 28628 2013).
25	Open garbage can without lid	Infection and disease transmission	Patients, guests, employee s, interns	3	3	**9**	Ensure all garbage bins have proper lids (RG, 28786 2013).
26	Dirty basemen t door (full of garbage)	Obstruction and infection	Employe es	3	3	**9**	Clean doorway and maintain hygiene standards (RG, 28698 2013).
27	Broken and unstable stair steps	Falls and injuries	Employe es	3	3	**9**	Repair or replace broken stairs to ensure stability (RG, 28710 2013).
28	Waste transport vehicle positione d in unsuitabl e location	Infection and contaminati on due to contact with waste	Patients, guests, employee s, interns	4	2	**8**	Position waste transport vehicle in designated area in accordance with legislation (RG, 29959 2017).
29	Generato r maintena nce not performe d	Vaccine cold chain disruption leading to financial loss and inability to vaccinate on time	Patients requiring vaccinati on	2	3	**6**	Ensure periodic maintenance of generator (RG, 28628 2013).
30	Air conditio ning maintena nce not performe d	Respiratory system disorders due to breathing contaminate d air	Patients, guests, employee s, interns	2	3	**6**	Conduct air conditioning maintenance annually in accordance with legislation (RG, 28628 2013; RG, 28786 2013).

Risk Level Classification:

- ■ **High Risk (15-25)**: Unacceptable - Immediate action required
- ■ **Medium Risk (8-12)**: Considerable - Action within 6 months
- □ **Low Risk (1-6)**: Acceptable - Action within 1 year

4. CONCLUSION

In this study, a family health center underwent comprehensive risk assessment using the L-type matrix risk assessment method. Thirty hazards were identified and systematically analyzed. These hazards and associated risks were documented, and necessary control measures were recommended.

The risk assessment identified 14 unacceptable (high) risks, 4 considerable (medium) risks, and 2 acceptable (low) risks.

This study demonstrates that hazards and risks exist within family health centers, and the importance of occupational health and safety in mitigating these risks is critical. Therefore, systematic risk assessment is essential. The greatest advantage of proactive risk assessment is that hazards can be prevented before they result in adverse outcomes. Implementing control measures in accordance with legislation is crucial for ensuring the health and safety of employees, employers, patients, interns, and visitors. Consequently, family health centers must prioritize occupational health and safety (OHS) and ensure sustainable progress in workplace safety management.

REFERENCES

Akpınar, T., & Çakmakkaya, B. Y. (2014). İş sağlığı ve güvenliği açısından işverenlerin risk değerlendirme yükümlülüğü. *Çalışma ve Toplum Dergisi*, (3), 273-304.

Kafkas Üniversitesi Sağlık Araştırma ve Uygulama Merkezi. (n.d.). İş sağlığı ve güvenliği ilkeleri. Kafkas Üniversitesi. Retrieved May 5, 2025, from https://hastane.kafkas.edu.tr/TR/index.php/2020-05-04-09-47-29/isg-ilkeleri

Kantarcıoğlu, H., Kantarcıoğlu, A., & Dinç, H. (2020). Sağlık kurumlarında iş sağlığı ve güvenliği: Kamu hastanelerinde risk değerlendirme yöntemlerine yönelik bir inceleme. *Sağlık Akademisyenleri Dergisi*, 7(1), 61-67.

Karan Buturak, G. (2019). *Bir sağlık kurumunda L matris ve Finne-Kinney risk analiz yöntemlerinin kıyaslanması* (Master's thesis). Çukurova Üniversitesi, Adana.

Karan Buturak, G., & Yapıcı, N. (2022). Kamu sağlık kurumlarında farklı risk analiz yöntemlerinin incelenmesi: Örnek bir uygulama. *Çukurova Üniversitesi Mühendislik Fakültesi Dergisi*, 37(3), 753-764. https://doi.org/10.21605/cukurovaumfd.1190398

Öngel, K., & Zaloğlu, A. (2017). Aile hekimliğinde iş güvenliği. *Klinik Tıp Aile Hekimliği Dergisi*, 9(4), 42-44.

Tekeli, S., & Oral, A. İ. (2022). *İş Sağlığı ve Güvenliği Temelleri* (1st ed.). Anadolu Üniversitesi Yayınları.

RG. (1984). *Elektrik İç Tesisleri Yönetmeliği*. Official Gazette Date: 04.11.1984, Official Gazette No: 18565.

RG. (2007). *Binaların Yangından Korunması Hakkında Yönetmelik*. Official Gazette Date: 19.12.2007, Official Gazette No: 26735.

RG. (2012). *İş Sağlığı ve Güvenliğine İlişkin İşyeri Tehlike Sınıfları Tebliği*. Official Gazette Date: 26.12.2012, Official Gazette No: 28509.

RG. (2012). *İş Sağlığı ve Güvenliği Risk Değerlendirmesi Yönetmeliği*. Official Gazette Date: 29.12.2012, Official Gazette No: 28512.

RG. (2013). *İş Ekipmanlarının Kullanımında Sağlık ve Güvenlik Şartları Yönetmeliği*. Official Gazette Date: 25.04.2013, Official Gazette No: 28628.

RG. (2013). *Hijyen Eğitimi Yönetmeliği*. Official Gazette Date: 05.07.2013, Official Gazette No: 28698.

RG. (2013). *İşyeri Bina ve Eklentilerinde Alınacak Sağlık ve Güvenlik Önlemlerine İlişkin Yönetmelik*. Official Gazette Date: 17.07.2013, Official Gazette No: 28710.

RG. (2013). *Sağlık ve Güvenlik İşaretleri Yönetmeliği*. Official Gazette Date: 11.09.2013, Official Gazette No: 28762.

RG. (2013). *Yapı İşlerinde İş Sağlığı ve Güvenliği Yönetmeliği*. Official Gazette Date: 05.10.2013, Official Gazette No: 28786.

RG. (2017). *Tıbbi Atıkların Kontrolü Yönetmeliği*. Official Gazette Date: 25.01.2017, Official Gazette No: 29959.

RG. (2019). *Kişisel Sağlık Verileri Hakkında Yönetmelik*. Official Gazette Date: 21.06.2019, Official Gazette No: 30808.

Tekeli, S. (2021). *İş Sağlığı ve Güvenliği Mevzuatı* (1st ed.). Anadolu Üniversitesi Yayınları.

Ünverdi, Ş., & Çetinyokuş, S. (2021). Bir kamu kurumunda bulunan asbest uygulama merkezi ve SEM laboratuvarında L tipi matris yöntemi ile risk değerlendirmesi. *Karaelmas İş Sağlığı ve Güvenliği*

Dergisi, 5(2), 99-107. https://doi.org/10.33720/kisgd.977714

AVAILABILITY OF MoS_2 THIN FILM BIOSENSORS FOR DIAGNOSING SOME DISEASES WITH DNA

Hamit ÖZTÜRK[1]

1. INTRODUCTION

With this study, it is aimed to explain to the reader from different perspectives that MoS_2 biosensor can be used in medical disease diagnosis using DNA and that it is both an interesting and promising field of study in terms of the future. When we look at the last 10 years, it is possible to reach countless applications of MoS_2 biosensors in medical diagnosis, especially in critical areas, from the literatüre (Lee et al., 2014; Wang et al., 2021; Yadav et al., 2023; Tao et al., 2025).

In this study, we aim to draw attention to disease diagnosis with DNA and to present the physicochemical capabilities of MoS_2 in terms of its interaction with biomolecules to the reader. In addition to the achievements that have been achieved today in the field of nanomaterial-based biosensor technology, it is also aimed to provide the reader with ideas in terms of developments that can be made to meet future expectations and to draw a clear roadmap between today and the future.

MoS_2 has sensitive Van der Waals forces and offers a significant surface-to-volume ratio, which produces positive results in terms of physicochemical reactions that will occur on the sensor surface and the ability to detect biomolecules. In

[1] Assist. Prof. Dr., Isparta University of Applied Sciences, Technology Faculty, Basic Sciences, Isparta/Turkey, ORCID: 0000-0002-9968-6377.

addition, the absence of dangling bonds in MoS_2 minimizes surface defects. This increases the desired sensor stability and sensitivity in sensors. Considering these features regarding MoS_2, MoS_2 is among the best candidate biosensors that can be considered ideal, especially in terms of detecting biological analytes (Wen et al., 2024). Here, in order to draw attention to the usability of the biosensor properties of MoS_2 in disease diagnosis using DNA and as a result of its potential features for the future in this field, the diagnosis of Down syndrome, the diagnosis of Hepatitis-B and the examination of some human diseases such as Monkeypox Virus and Human Papillomavirus via DNA-MoS_2 interaction are discussed.

2. DNA SENSITIVE MoS_2 BIOSENSORS

It has been reported that MoS_2 nanosheets exhibit strong adsorption affinity to single-stranded nucleic acid (ssDNA) due to π–π stacking interactions via aromatic rings of nucleobases with the MoS_2 surface having van der Waals forces (Zhu et al., 2013). However, it is known that there is hybridization between complementary strands on the surface of MoS_2 nanosheets. It has also been reported that the hybridization here weakens the binding affinity and negatively affects the binding of double-stranded nucleic acid (dsDNA) and causes desorption of DNA from the surface (Zhang et al., 2019). Using this adsorption ability of MoS_2 nanosheets, Asefifeyzabadi and colleagues reported that they developed a sensitive detection method for the repeated structures of guanine and cytosine and stated that this development could be used to distinguish pathogenic and non-pathogenic sequences (Asefifeyzabadi et al., 2020).

Considering the outstanding features of MoS_2 such as the absence of dangling bonds on its surface, its scalable and controllable thickness parameter during the production phase, and

the ability to impart the desired sensor feature to the structure with this adjustable thickness feature, as well as its physical and electrical properties, as well as its compatibility with DNA and some other biological agents in terms of excellent physicochemical reactions, it stands out in terms of its use as a biosensor.

2.1. Ultra-Sensitive MoS_2-Based DNA Sensors for Screening for Down Syndrome

Prenatal screening and controls performed using traditional ultrasound or biochemical methods have some limitations in terms of accuracy or precision of the results. This situation paves the way for incorrect diagnosis. For more accurate results, non-invasive prenatal tests using whole-genome sequencing (WGS) can provide more accurate results. However, these tests are both more complex and often inaccessible to many people due to their cost. Therefore, obtaining more accurate results due to being both cost-effective and DNA-based is one of the broad research areas.

Table 1. Chromosome 21 sequences used related research (Liu et al., 2023)

ssDNA (chromosome 21)	sequence (30mer)
thiolated DNA probe	HS-C6-TGAGTTCCTTCTAGGGAGTCACATTGATGA
complementary DNA target	TCATCAATGTGACTCCCTAGAAGGAACTCA
mismatched DNA	TCATCAATGTGACTGGGTAGAAGGAACTCA

Liu and colleagues (Liu et al., 2023) addressed this issue and produced MoS_2 films with a thickness of approximately 1nm with the CVD method, and silver nanoparticles were added to the structure in order to improve the sensor properties. When the working mechanism of the sensor is examined, it is in the form of monitoring the change in the electrical surface conductivity of

MoS_2 via immobile probes on the target DNA attached to the MoS_2 surface. The DNA biosensor that was made showed the detection limit for target DNA at a concentration as low as 100 aM (attomolar). In addition to the sensor's high sensitivity and fast detection features, they reported that the response rate was 240%.

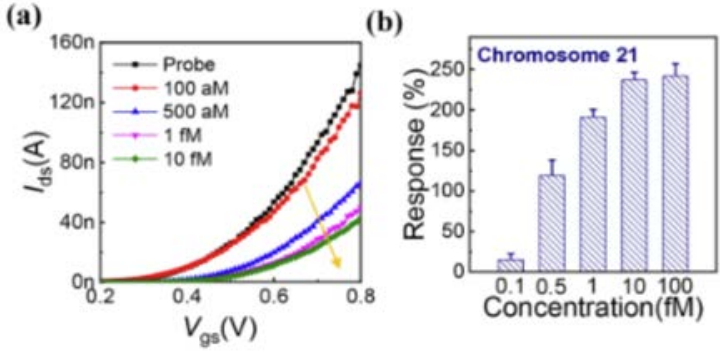

Figure 1. (a) Response curves about chromosome 21 target for DNA solutions having concentrations of 100 aM, 500 aM, 1 fM, and 10 fM. (b) Relationship between response and concentration taken from Figure 1a (Liu et al., 2023).

The study highlights the potential of nanomaterials such as MoS_2 in terms of their usability as biosensors, paving the way for diagnostic tools that can provide more sensitive results in the prenatal period, are affordable, and are user-friendly due to the use of a non-invasive method.

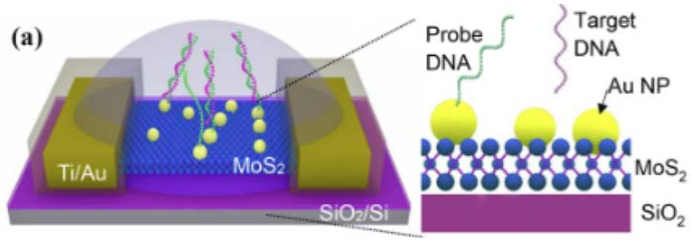

Figure 2. MoS_2 biosensor schmetic structure (Liu et al., 2023).

The study states that FET-based MoS_2 may be a promising alternative as a DNA detection biosensor (Liu et al., 2023).

2.2. Some disease viruses can be detected through DNA using MoS_2 Quantum Dots

Monkeypox and human papillomaviruses serious threats for human health moreover require complex and laborious processes involving professionals to detect them (Tao et al., 2025).In this study, the biosensor works the CRISPR-Cas12a system. The working principle of this system is as follows: it binds to the target DNA and activates the trans-splicing activity. This activity cleaves the probe DNA, resulting in a decrease in catalytic activity as a result of inhibiting the adsorption of a DNA peroxidase mimic onto MoS_2 QDs.

The selectivity of the MoS_2-QD biosensor was evaluated by comparing the colorimetric responses to perfectly matched and mismatched DNA targets. The results showed a significant decrease in absorbance for perfectly matched targets. The sensor also demonstrated high selectivity and sensitivity in detecting HPV and MPXV DNA.Monkeypox and human papillomaviruses pose serious threats to human health and require complex and laborious processes involving professionals for their detection (Tao et al., 2025).

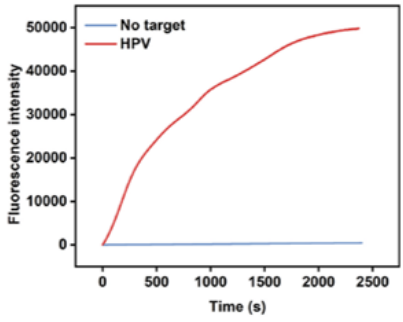

Figure 3. time-dependent fluorescence plot (in the presence of target DNA) (Tao et al., 2025).

Various instruments such as fluorescence spectroscopy, UV-Vis spectrophotometry for absorbance, and transmission electron microscopy (TEM) were used to characterize MoS_2 QDs.

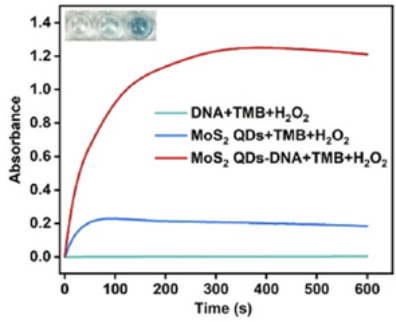

Figure 4. This graph shows the time-dependent change of absorbance in tetramethylbenzidine (TMB) solutions containing H2O2 with different reaction systems such as DNA, MoS_2 QDs and MoS_2 QDs-DNA (Tao et al., 2025).

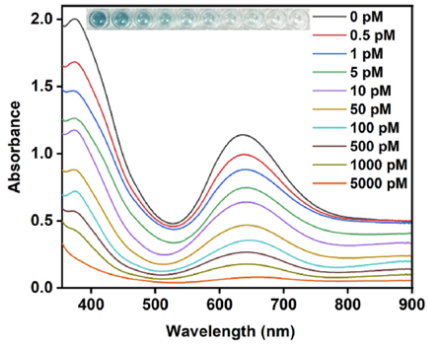

Figure 5. Absorption spectrum of Tetramethylbenzidine towards different amounts of target MPXV DNA by imlementation of MoS_2 QDs-DNA nanohybrids (Tao et al., 2025).

The probe DNA successfully increases the peroxidase which has mimetic activity belonging to MoS_2 QDs with the absence of some target which could be MPXV or HPV DNA. DNA probes are degraded when MPXV or HPV targets are

present because the Cas12a also having trans-cleavage property is activated. Minimal catalytic ability results from this degradation, which inhibits the probe DNA with enzyme activity increase the activity of adsorbed on MoS_2 QDs.

When the nanohybrid MoS_2 QDs probe (which does not require DNA target amplification) is examined against DNA, the CRISPR-Cas12a detection system reagents function as a signal amplification detection system. This paves the way for highly sensitive and accurate detection of MPXV and HPV DNA, providing a simple and innovative method (Tao et al., 2025).

Finally, in this study, they reported the development of a novel colorimetric method that enables the highly sensitive detection of HPV and MPXV DNA by combining the CRISPR-Cas12a system with a colorimetric nanoplatform with DNA nanohybrid MoS_2 QDs probe-assisted amplification. This nanosensor triggers Cas12a trans-cutting activity using DNA targets. As a result, the probe DNA is fragmented. This prevents the peroxidase-mimicking DNA structure from adhering to the MoS_2 QDs. This process results in low catalytic activity.

First, due to the biosensor platform's fast operation and simple design, mandatory requirements such as high-cost equipment and some complex experimental procedures are eliminated to some extent. Second, the advanced colorimetric nanoplatform presented in this study enables HPV and MPXV targets to be evaluated with high sensitivity, even with the naked eye.

2.3. Diagnosis of Viral Hepatitis B with MoS_2 Nanowire Field-Effect Transistors

This research is reported in the literature regarding a field-effect transistor (FET) form using molybdenum disulfide (MoS_2) nanowires (NWs).

The challenging detection of HBV, a global health problem, with sensitive and specific diagnostic tools demonstrates the need for such biosensors. This study describes the feasibility of a field-effect transistor (FET) form composed of molybdenum disulfide (MoS_2) nanowires (NWs), which can detect HBV DNA with high sensitivity and is also robust to multiple repetitions (Shariati et al., 2021).

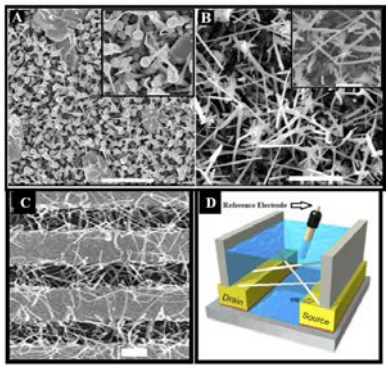

Figure 6. (A) ZnO NPs doped with MoS_2 for the growth of MoS_2-NWs. (B) Illustration of the wire form (MoS_2 NWs). (C) FESEM image of the FET sensor fabricated with MoS_2-NWs. (D) Schematic of the HBV sensor fabricated based on the MoS_2-NWs-FET sensor (Shariati et al., 2021).

To investigate the sensitivity of the biosensor, electrochemical impedance spectroscopy (EIS) was used to investigate the DNA-embedded HBV. The biosensor was further examined for sensitivity and detection limits. This study reported that the limit of detection (LOD) for HBV DNA was within 1 femtomolar (fM) for a linear concentration range of 0.5 picomolar (pM) to 50 micromolar (µM). The meaning of this result is that it has also been shown and stated in this study that the device can detect viral DNA even at very low concentrations.

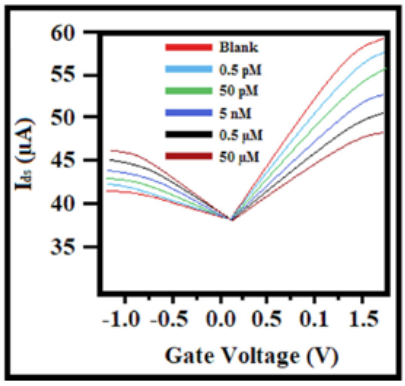

Figure 7. Sensitivity responses of the fabricated biosensor (HBV-doped MoS_2-NWs) (Shariati et al., 2021).

The biosensor response time was reported to be 25 seconds. When the sensor was examined for repeatability, it was reported that the measurement taken after an eight-week period showed only a 4% loss compared to the initial measurement.

3. CONCLUSION AND FUTURE PERSPECTIVE

As a result, MoS_2 biosensors have become a focal point of interest and research for researchers in medical diagnostic applications, which have gained importance in the last decade, particularly with the increasing global population, due to their electrical, optical, and flexible mechanical properties. Significant advances in this field continue to appear in the literature, with an increasing number of studies.

As a result of all these advances, the use of these sensors for diagnostic purposes in clinical applications has been paved and they will start to serve humanity.

REFERENCES

Asefifeyzabadi, N., Alkhaldi, R., Qamar, A. Z., Pater, A. A., Patwardhan, M., Gagnon, K. T., ... & Shamsi, M. H. (2020). Label-free electrochemical detection of CGG repeats on inkjet printable 2D layers of MoS_2. *ACS Applied Materials & Interfaces*, *12*(46), 52156-52165.

Lee, J., Dak, P., Lee, Y., Park, H., Choi, W., Alam, M. A., & Kim, S. (2014). Two-dimensional layered MoS_2 biosensors enable highly sensitive detection of biomolecules. *Scientific reports*, *4*(1), 7352.

Liu, J., Chen, X., Wang, Q., Xiao, M., Zhong, D., Sun, W., ... & Zhang, Z. (2019). Ultrasensitive monolayer MoS_2 field-effect transistor based DNA sensors for screening of down syndrome. *Nano letters*, *19*(3), 1437-1444.

Shariati, M., Vaezjalali, M., & Sadeghi, M. (2021). Ultrasensitive and easily reproducible biosensor based on novel doped MoS_2 nanowires field-effect transistor in label-free approach for detection of hepatitis B virus in blood serum. *Analytica Chimica Acta*, *1156*, 338360.

Tao, Y., Wang, H., Ju, E., Lao, Y. H., Zhang, Y., & Li, M. (2025). CRISPR-Cas12a-regulated DNA adsorption on MoS_2 quantum dots: Enhanced enzyme mimics for sensitive colorimetric detection of human monkeypox virus and human papillomavirus DNA. *Talanta*, *283*, 127153.

Wang, J., Sui, L., Huang, J., Miao, L., Nie, Y., Wang, K., ... & Ai, K. (2021). MoS_2-based nanocomposites for cancer diagnosis and therapy. *Bioactive Materials*, *6*(11), 4209-4242.

Wen, X., Zhao, X., Shan, X., Lu, H., Gao, X., & Zhuang, S. (2024). Biofunctionalization-optimized MoS_2-based FET

biosensors for the detection of Tau protein. *Applied Surface Science*, *670*, 160616.

Yadav, A. K., Verma, D., & Solanki, P. R. (2023). Enhanced Electrochemical Biosensing of the Sp17 Cancer Biomarker in Serum Samples via Engineered Two-Dimensional MoS_2 Nanosheets on the Reduced Graphene Oxide Interface. *ACS Applied Bio Materials*, *6*(10), 4250-4268.

Zhang, F., Wang, S., Zou, R., Xiang, L., & Cai, C. (2019). MoS_2-loaded G-quadruplex molecular beacon probes for versatile detection of MicroRNA through hybridization chain reaction signal amplification. *Talanta*, *202*, 342-348.

Zhu, C., Zeng, Z., Li, H., Li, F., Fan, C., & Zhang, H. (2013). Single-layer MoS_2-based nanoprobes for homogeneous detection of biomolecules. *Journal of the American Chemical Society*, *135*(16), 5998-6001.

AT THE FRONTIERS OF SIMULATION: EPISTEMOLOGICAL RUPTURE, THE SINGULARITY ILLUSION, AND THE END OF THE HUMAN-INTUITION PARADOX IN ARTIFICIAL INTELLIGENCE AND MATERIALS SCIENCE

Cengiz SOYKAN[1]

1. INTRODUCTION: The New Mechanism of Prophecy

Materials science has historically been a discipline encompassing the epistemological stages of human intelligence's endeavor to penetrate nature. The initial stage was the "experiment → theory" cycle. This process, spanning from Aristotle's logic to Bacon's induction, involved humans recording material behaviors through senses and systematic observation, then formulating physical laws based on these observations (Gribbin, 2002). The hardening of steel, the fracture of glass, or the conductivity of copper were first observed in workshops and laboratories before being framed within theoretical constructs. This era was founded on the pursuit of understanding and the search for causality.

With the second half of the century, the advent of the computer initiated the second major paradigm shift: the "computation → simulation" phase. Observation and theory were no longer sufficient; it became possible to solve theoretical

[1] Assoc. Prof. Dr., Kırşehir Ahi Evran University, Health Services Vocational School, Department of Medical Services and Techniques, ORCID: 0000-0003-0897-2384.

models and complex equations using numerical methods to mimic, i.e., simulate, material properties in a virtual environment. Methods like Density Functional Theory (DFT) revolutionized the calculation of a material's electronic structure (Kohn, 1965). The aim here was not so much to create a copy of nature, but to construct its mathematical model and see "what would happen" through this model. Simulation did not entirely replace experiment but became a powerful tool complementing and guiding it. Knowledge was now produced not only for understanding but also for modeling and emulating (Sholl, 2009).

Now, in this first quarter of the 21st century, we are witnessing the third and perhaps most disruptive epistemological rupture: the "data → artificial intelligence → prophecy" stage. This new paradigm is qualitatively different from its predecessors. The ultimate goal is no longer to solve fundamental physical laws or simulate a process in detail, but to train an artificial intelligence model that captures statistical patterns from vast amounts of data (thousands of DFT calculations, experimental databases) and to use this model to predict the properties of materials not yet synthesized, or even simulated. This is a mechanism of prophecy rather than simulation. The system tells us that "material X will possess property Z under condition Y," but it often fails to provide a transparent explanation of how it reached this conclusion. The black box is not merely an engineering problem; it is an epistemological problem (Castelvecchi, 2016).

This situation brings about a profound transformation in scientific methodology, an "epistemological rupture." Causality, the cornerstone of traditional science, risks being supplanted by powerful correlations (Domingos, 2015). The scientist now dialogues not with nature itself, but with an algorithm trained on its digital twin. We are no longer just understanding nature; we are predicting its future through a data-driven model based on its

digital representation. While this promises incredible speed and efficiency, it also harbors a profound paradox: As the accuracy of our prophecies increases, could our capacity to understand the physical reality underpinning these prophecies diminish?

This book chapter will examine the profound effects of this rupture on the practice of materials science. We will question the limits of AI-aided prophecies, what lies behind the "singularity illusion," and the potential role of human intuition and critical thinking within this new ecosystem. Our aim is not to reject this powerful tool, but to understand its impact on how we construct knowledge, and to reposition humans not as mere spectators, but as central actors in the process—those who still hold wisdom at the core.

2. EPISTEMOLOGICAL RUPTURE: The Triumph of Correlations and the End of Causality?

The infiltration of artificial intelligence into materials science has triggered a quiet yet profound shift in the discipline's epistemological foundations. This shift has brought an ancient distinction concerning the nature of knowledge – the distinction between correlation and causality – back to the forefront. The fundamental operating logic of AI models, particularly deep learning, is built upon statistical patterns and correlations. While these models are exceptionally successful at discovering complex relationships within massive datasets, they are not designed to uncover the underlying physical causal mechanisms (Hutson, 2018). In other words, these systems make powerful predictions of the type "when X occurs, Y happens," but fall short of answering the question "why does X cause Y?"

This creates a fundamental tension with the traditional understanding of science. Since the time of Galileo and Newton, traditional science has been built upon the effort to uncover

fundamental physical principles and causal laws governing phenomena, rather than merely observing them. A material's strength, electronic band gap, or catalytic activity are explained by fundamental causal mechanisms such as its atomic structure, chemical bonds, and electron dynamics. AI-aided prophecies, however, do not treat such deep understanding as a prerequisite. They prioritize statistical power over explanatory power.

The greatest danger here lies in the fact that the ability of "black box" models to make near-perfect predictions elevates them to the status of an "incomprehensible oracle." A model might predict with high accuracy that a material will exhibit superconductivity at a certain temperature, yet it does not explain the quasiparticle interactions, spin-orbit coupling, or electron-phonon pairing behind this behavior (Carvalho, 2019). This presents a paradox with the potential to radically transform scientific practice: as predictive success increases, could the drive for understanding diminish? Consequently, science risks being reduced from an intellectual discipline striving to comprehend phenomena in depth to an "engineering discipline" focused solely on finding materials with desired properties (Marcus, 2018). This reflects the danger of the means supplanting the ends.

To consider a concrete example: An AI model might correctly predict, based on existing databases, that a new material with a specific crystal structure and chemical composition will exhibit high-temperature superconductivity. This is a significant achievement in itself and provides valuable guidance for researchers. However, while making this prediction, the model does not develop the BCS theory or other theoretical frameworks for high-temperature superconductivity, nor does it even reference them. It does not provide new physical insight into why the process works. In this scenario, AI functions not as a creative theorist, but as an extraordinarily skilled empiricist. It makes discoveries, but leaves the understanding to the critical

intelligence of the human researcher and their ability to use this prediction as a starting point for constructing new physical models.

Therefore, the role of the materials scientist in the age of AI must evolve from being a technician who blindly accepts model outputs to that of a sage who critically interprets these outputs, persists in the quest for causality, and ultimately forges the link between "what happens" and "why it happens."

3. THE SINGULARITY ILLUSION: Is a Complete Simulation of the Materials Universe Possible?

The most alluring promise of big data and artificial intelligence in materials science is the potential to eventually create a complete, digital catalog of the materials universe, encompassing the stability, electronic properties, and functional performance of all possible chemical compositions and structures. This vision is sometimes heralded as a "singularity in materials science," imagining a future where the entire discovery process becomes automated, yielding an endless number of perfect materials from a database (Trehern, 2022). However, looking beyond this exciting vision, profound conceptual and practical limitations at its core reveal the risk of this being an "illusion."

One of the most fundamental obstacles to constructing this digital catalog is the quality of the very bricks we use to build it: the data. The vast majority of AI models in materials science are trained on computational data, particularly from Density Functional Theory (DFT). Yet, DFT is an approximation containing systematic errors. For instance, the bandgap problem and the inadequate description of van der Waals forces are known limitations of DFT (Medvedev, 2017). This situation brings to mind the adage, "you can't reach heaven with dirty data." A model

trained on flawed and approximate data, no matter how complex, will inherently inherit these flaws, and its predictions will only be as reliable as the quality of the input data. This means the digital catalog would represent not the entire materials universe, but a subset constrained by the approximations of DFT.

A second, and perhaps more insidious, limitation is the predictivity trap. Machine learning models typically perform best within the statistical distribution of the data on which they were trained. However, genuine scientific innovation and discovery often rely on unusual chemical compositions or structural configurations that lie outside this distribution. This is known as the "out-of-distribution" (OOD) problem, which often causes deep learning models to fail at identifying and predicting samples that are radically different from their training data (Yang, 2024). Consequently, a model confined to the data distribution of existing materials may be inadequate for predicting an entirely new class of material. Truly revolutionary innovation lies precisely where the model is weakest: beyond the boundaries of the known data distribution.

Finally, the reality of chaos and complexity fundamentally challenges the premise of this digital catalog. Real-world materials that are synthesized and used are filled with a range of complex properties that idealized simulations fail to capture. Defects at the single-atom level, the dynamic nature of surface chemistry, grain boundary interactions, and stochastic variations in manufacturing processes are fundamental factors determining a material's macro-scale behavior. Encoding all these complex, multi-scale, and often chaotic phenomena digitally with current computational methods and datasets is nearly impossible (Cao, 2018). Simulations often focus on cleaned, ideal systems, filtering out these "imperfections" as noise; yet, the true "soul" of a real material often lies hidden within these very imperfections.

In conclusion, the idea of a "singularity in materials science" is largely an illusion. AI and big data offer powerful tools that tremendously accelerate our rate of materials discovery, but these tools do not possess the capacity to create a complete digital twin capable of capturing the infinite complexity and uncertainty of the physical world. It is more realistic and productive to view this digital catalog not as a holy grail, but as an extremely valuable yet ultimately limited and flawed roadmap that must be guided by human intuition and creativity.

4. THE END OF THE HUMAN-INTUITION PARADOX: The Disappearance of a Master Guide

In the traditional practice of materials science, forged in workshops and laboratories, the acquired experience, deep intuition, and that often-indefinable grasp sometimes termed "material feel" of the master researcher have always been a critical component of the discovery process. This intuition ranges from understanding a material's internal state from the colour of a furnace during heat treatment to sensing the presence of a brand-new phase from a specific pattern in a microscope image. It is a difficult-to-codify expertise, born from years of observation, failure, and intellectual accumulation.

Artificial intelligence promises to automate this intuitive process in the name of efficiency, ostensibly removing the human from the loop. However, this situation introduces a dangerous paradox: the sharpening of our tools could simultaneously dull our own cognitive and intuitive capacities. This could signify the "end of the human-intuition paradox." The general principle concerning the effect of automation on human skills becomes critically important here: the more a skill is automated, the more our capacity to maintain and develop it diminishes (Carr, 2014). In the context of materials science, increasing reliance on AI risks

eroding researchers' abilities for critical thinking, making unexpected connections, and performing intuitive leaps. The statement "the machine says so" can become a sufficient explanation, or even a dogma. This can reduce scientific practice to a "black box functionalism," where algorithmic authority replaces critical inquiry and results are accepted without being understood (Saltelli, 2017).

Yet, beyond this bleak picture lies a window of opportunity. The ultimate role of AI should not be to replace human intuition, but to augment and complement it. This symbiotic relationship, combining AI's power with human comprehension, can create a new discovery paradigm. In particular, the anomalies predicted by AI but left unexplained by it offer fertile ground for this collaboration. When a model predicts a material exhibiting an unexpected property that cannot be explained by existing theoretical frameworks, it creates a new area for in-depth investigation by human researchers. This anomaly could be the harbinger of a new physical phenomenon or structural mechanism (Klenam, 2023). Here, AI functions as an "anomaly detector," guiding the human researcher to the most promising, yet least understood, frontiers of discovery.

Another dimension of this collaboration involves using AI as a "thought partner" or "intuition accelerator." When a researcher formulates a hypothesis, AI can rapidly screen thousands of its variations through simulation, testing and enriching the researcher's intuition. This accelerates the process of validating or refining an intuitive idea, freeing human intelligence to focus on more creative and conceptual tasks.

In conclusion, the end of the human-intuition paradox is not inevitable; it depends on our approach. When we position AI not as a replacement for the human mind, but as a natural extension and amplifier of it, we can celebrate not the end of

human intuition, but the beginning of its new evolution. The future materials scientist will be neither a pure intuitive nor a mere model user, but a "cyber-physical explorer" who synthesizes the best qualities of both, thinks critically, and can engage in dialogue with AI.

5. CONCLUSION: Towards an Age of Synthesis – A New Balance Between Simulation and Wisdom

At this historic juncture where materials science intersects with artificial intelligence, the ultimate synthesis we must achieve is to transcend the tool-master dichotomy. AI is undoubtedly an incredible tool; it has multiplied our discovery rate and ushered us into an era of unprecedented efficiency. Yet, this powerful tool must never become a master. Absolute obedience to its judgments threatens the spirit of critical inquiry intrinsic to science and, ultimately, our autonomy.

Therefore, the future materials scientist must be expected not merely to be a model user, but to assume the role of a "cyber-physical translator." This new generation of researcher must deeply understand the limits and assumptions of AI models, and must be able to take their statistical "correlations" and blend them with the characteristic human quest for "causality." This synthesis represents a new epistemological stratum that unites the power of quantity with the depth of quality.

Our ultimate goal is not merely to design materials faster, but to attain a deeper wisdom concerning the complex language of nature. Artificial intelligence should be positioned as a catalyst, an accelerator, in this ancient pursuit. Rather than viewing it as the source of final answers, we must embrace it as a partner that helps us ask deeper questions. True and lasting progress lies not in the number of data points, but in the depth of our comprehension of their meaning. By repositioning humans from

being passive spectators of the process to being active seekers and interpreters of wisdom at its core, we can achieve a balanced and fruitful synthesis between technology and humanity.

REFERENCES

Cao, B., Adutwum, L. A., Oliynyk, A. O., Luber, E. J., Olsen, B. C., Mar, A., & Buriak, J. M. (2018). How To Optimize Materials and Devices via Design of Experiments and Machine Learning: Demonstration Using Organic Photovoltaics. *ACS Nano, 12*(8), 7434-7444. doi:10.1021/acsnano.8b04726

Carr, N. (2014). *The Glass Cage: Automation and Us*. New York: W. W. Norton & Company.

Carvalho, D. V., Pereira, E. M., & Cardoso, J. S. (2019). Machine Learning Interpretability: A Survey on Methods and Metrics. *Electronics, 8*(8), 832. Retrieved from https://www.mdpi.com/2079-9292/8/8/832

Castelvecchi, D. (2016). Can we open the black box of AI? *Nature, 538*(7623), 20-23. doi:10.1038/538020a

Domingos, P. (2015). *The Master Algorithm: How the Quest for the Ultimate Learning Machine Will Remake Our World*. New York: Basic Books.

Gribbin, J. (2002). *Science: A History 1543-2001*. London: Penguin Books.

Hutson, M. (2018). Artificial intelligence faces reproducibility crisis. *Science, 359*(6377), 725-726. doi:doi:10.1126/science.359.6377.725

Klenam, D. E. P., Asumadu, T. K., Vandadi, M., Rahbar, N., McBagonluri, F., & Soboyejo, W. O. (2023). Data science and material informatics in physical metallurgy and material science: An overview of milestones and limitations. *Results in Materials, 19*, 100455. doi:https://doi.org/10.1016/j.rinma.2023.100455

Kohn, W., & Sham, L. J. (1965). Self-Consistent Equations Including Exchange and Correlation Effects. *Physical Review, 140*(4A), A1133-A1138. doi:10.1103/PhysRev.140.A1133

Marcus, G. (2018). *Deep Learning: A Critical Appraisal*. Retrieved from https://arxiv.org/abs/1801.00631

Medvedev, M. G., Bushmarinov, I. S., Sun, J., Perdew, J. P., & Lyssenko, K. A. (2017). Density functional theory is straying from the path toward the exact functional. *Science, 355*(6320), 49-52. doi:doi:10.1126/science.aah5975

Saltelli, A., & Funtowicz, S. (2017). What is science's crisis really about? *Futures, 91*, 5-11. doi:https://doi.org/10.1016/j.futures.2017.05.010

Sholl, D. S., & Steckel, J. A. (2009). *Density Functional Theory: A Practical Introduction*.

Trehern, W., Ortiz-Ayala, R., Atli, K. C., Arroyave, R., & Karaman, I. (2022). Data-driven shape memory alloy discovery using Artificial Intelligence Materials Selection (AIMS) framework. *Acta Materialia, 228*, 117751. doi:https://doi.org/10.1016/j.actamat.2022.117751

Yang, J., Zhou, K., Li, Y., & Liu, Z. (2024). *Generalized Out-of-Distribution Detection: A Survey*. Retrieved from https://arxiv.org/abs/2110.11334

HARVESTING IN THE GREENHOUSE WITH THE YOLOV5 METHOD

Mehmet GÜL[1]

1. INTRODUCTION

The YOLO (You Only Look Once) method is one of the fastest and most successful end-to-end differentiable networks developed today for object detection tasks in computer vision and image processing. This architecture, which exhibits high performance and efficiency compared to traditional approaches, has become prominent in the literature, particularly for combining bounding box estimation and object classification in a single network. The method's high speed is largely due to its use of optimized libraries such as PyTorch. The YOLOv5 version, developed by Ultralytics, provides users with flexibility with four different model options (small/medium/large/extra-large), offering different detection accuracy and performance trade-offs according to application requirements. In later versions, architectural innovations, such as the replacement of the C3 module with the C2f module in YOLOv8, aimed to preserve the lightweight nature of the model while improving gradient flow. The YOLO family has proven its effectiveness in a wide range of applications, including archaeology, healthcare, and agriculture. In healthcare, it has been used for critical tasks such as tooth detection in panoramic radiographs (99% success rate) and white blood cell classification (96.45% success rate). In agricultural technology, successful results have been reported for autonomous

[1] Assist. Prof. Dr., Şırnak University, Engineering Faculty, Computer Engineering, ORCID: 0000-0002-4819-4743.

tomato harvesting in greenhouses (96.9% success rate) and high accuracy (up to 91.9%) diagnosis of rice and tomato leaf diseases. These studies demonstrate the speed and precision offered by YOLO methods in object detection and their applicability to complex real-world problems.

The YOLO (You Only Look Once) method is the fastest and most successful object recognition method developed to date. This extremely high-performance model delivers successful results for virtually any required object detection task.

Object Detection is an important branch of computer vision and image processing. This method locates objects within photographs, videos, and snapshots, focusing on the desired objects. Popular algorithms such as Faster R-CNN, Single Shot Detector (SSD), and YOLO are among the most common methods used for this purpose.

When this method was introduced to the literature, its most significant achievement was as the first object detection model to combine bounding box estimation and object classification in a single, end-to-end, differentiable network. It also provides the ability to simultaneously detect objects within an image or video and their precise location coordinates. While previous versions of the YOLOV5 model generally operated within the DarkNet framework, the YOLOV5 method stands out as the first YOLO model to run on the PyTorch Framework. This groundbreaking version was published by Glenn Jocher, Founder and CEO of Ultralytics. The YOLOV5 method offers users four different model sizes (small/medium/large/extra-large). Each of these models offers different detection accuracy and performance (speed) trade-offs depending on the application.

In short, why is YOLO so fast? It is a deep learning algorithm used in object detection. Its speed and efficiency make it preferred over many other deep learning models. This speed is

largely due to the libraries used. Benchmark tests have proven that PyTorch provides faster training processes than other platforms.

The YOLO method is extremely effective, and thanks to its high performance, it has been used effectively in a variety of studies. Among the influential studies using this method are studies in archaeology, health, and agriculture. The next section includes literature studies that have used this method and proven its effectiveness.

2. LITERATURE REVIEW

[1] Evaluates the effectiveness of the YOLOv5 algorithm for automatically detecting, segmenting, and numbering primary and permanent teeth in panoramic radiographs (PRs) of pediatric patients with mixed dentition. This study automates the accurate identification and numbering of teeth, a critical step in interpreting panoramic radiographs. [1] In this study, 99% accuracy and 99% sensitivity were achieved in tooth detection.

Figure 1. Use of the YOLOv5 method in dental treatment

[2] Attempts to identify 16 different types of white blood cells in the human body. The study employed a two-pronged approach. Two different datasets were used: a WBC (White Blood Cell) image and a nucleus-only image. The study reported a success rate of 96.45%.

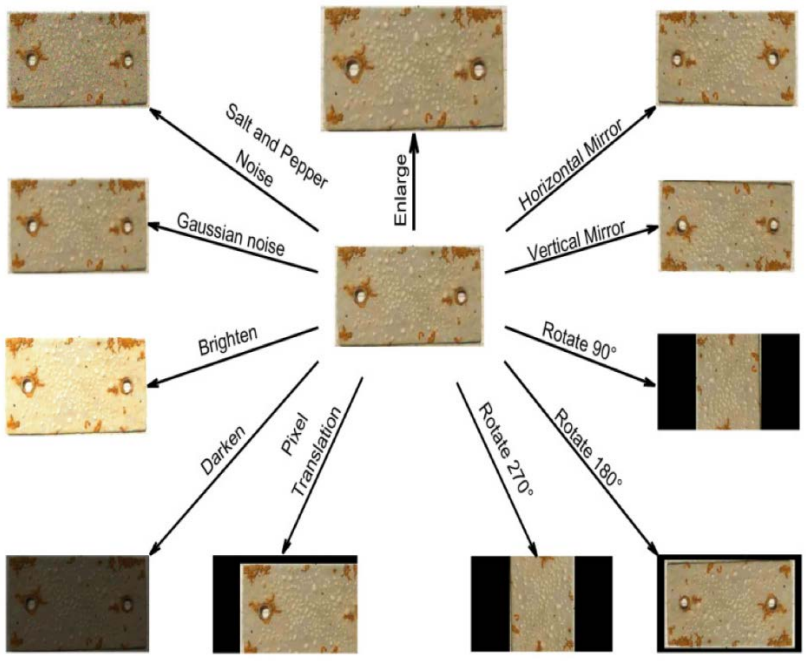

Figure 2. Corrosion Detection with the YOLOv5 Method

In [3], the YOLOv5 method was used to address serious corrosion problems in coastal China. The researchers aimed to detect metal surface corrosion under various protective coatings. In their study, the researchers reported highly effective results of the YOLOv5 method in their monitoring and inspection study, which was conducted over two different time periods: 24 and 60 months.

In [4], the researchers prioritized the detection of small objects. In their study, they proposed an advanced model to avoid high computational costs. Traditional methods make real-time

object tracking very difficult. In this case, the use of real-time systems, known for their high computational costs, is necessary. Unlike expensive methods that perform real-time instantaneous calculations, the HIC-YOLOv5 method aims to overcome this problem.

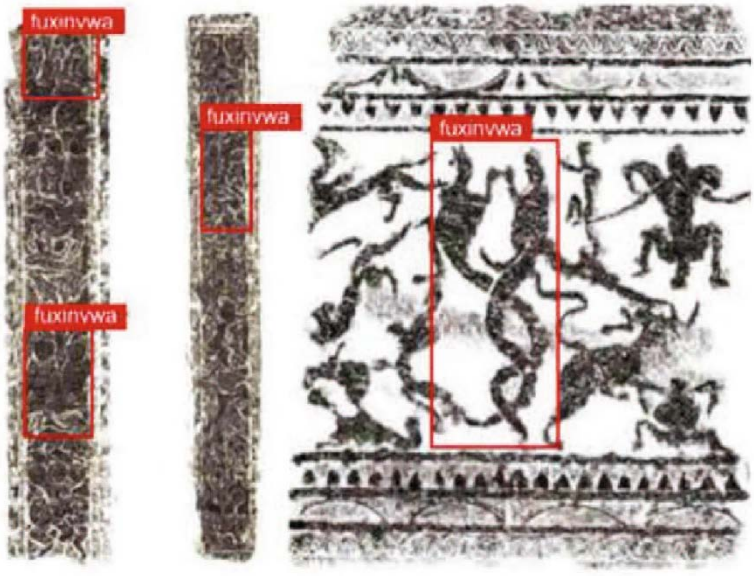

Figure 3. Analysis of Artifacts from Ancient Chinese History

In [5], researchers used the YOLOV5 method to detect human figures on portrait stones dating from the Han Dynasty, considered an important artistic heritage of China. One of the key points of this study was that highly sensitive targeting techniques often require numerous parameters, and the portable devices used for processing are not suitable. One of the most significant challenges to the study's sensitivity was the background complexity, the densely packed target groups, and significant scale changes in the detection of human figures on large portrait stones.

In [6], researchers used the YOLOV5 method to diagnose rice leaf diseases. Methods developed based on machine learning

or artificial intelligence, which have yielded highly successful results in many different studies, have failed to diagnose rice leaf diseases. In this case, the success of the YOLOV5 method, as the most effective method, inevitably yields successful results. The method developed by the researchers successfully detected rice leaf diseases. In [6], the YOLOv5 method was used to harvest tomatoes in a greenhouse. It is a fact that manual harvesting is both time-consuming and costly, and autonomous robot harvesting significantly overcomes these challenges. One of the main reasons for the low success rate of currently used robotic tomato harvesters stems from collisions between the end effector and the tomato plant during harvesting. In this study, a cascade deep learning network algorithm was proposed to reduce collisions, determine ripeness, estimate 3D poses, and search for a collision-free harvesting strategy. The researchers used the YOLOv5 method for tomato harvesting, achieving a high success rate of 96.9% to overcome all these challenges.

In [7], researchers focused on tomato harvesting. Their study aims to improve the low recognition accuracy of tomato branches in complex environments. During tomato harvesting, tomato seedlings also require pruning. An algorithm was successfully developed to determine the pruning point and position the harvesting robot's gripper in the correct location.

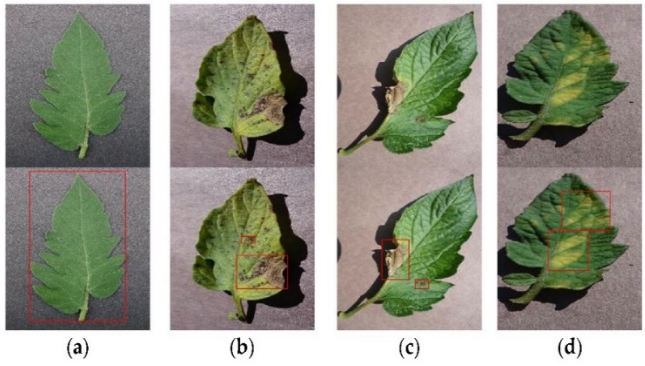

Figure 4. Disease Diagnosis on Tomato Leaf

In their study [8], researchers identified tomato leaf disease as one of the most common problems encountered during the tomato harvest process. Disease diagnosis, which is crucial for increasing yield in tomato harvests, requires high accuracy. The researchers proposed the Global Attention Mechanism (GAM) method for disease diagnosis. In their study, they compared their proposed method with methods such as YOLOv5, YOLOv7, YOLO-HC, YOLOv8, and Faster R-CNN. They reported the effectiveness of their proposed method in their study.

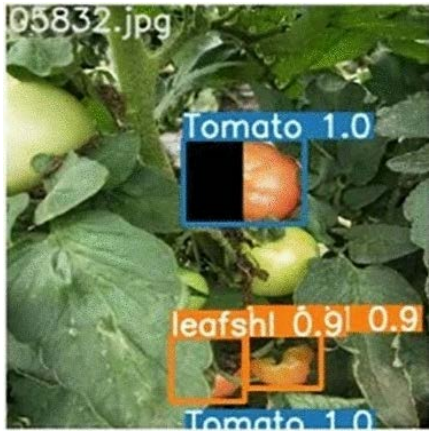

Figure 5. Tomato identification using real-time image enhancement on a harvesting robot

[9] Researchers studied agricultural harvesting robots, which are becoming increasingly common today. Harvesting robots, an indispensable element of modern greenhouses, are reducing the increasing cost of tomato harvesting. Tomato plants have a characteristic vine structure. This led the researchers to improve the detection accuracy and three-dimensional positioning of tomatoes in complex greenhouse environments. A hybrid method was proposed integrating the YOLOV5 deep learning algorithm and the SGBM (Semi-Global Block Matching) algorithm. The generated dataset contained approximately 640 tomato images, but data augmentation was applied to obtain high

performance results from the dataset. The researchers achieved a 94.1% success rate in their study.

[10] In their study, researchers assessed tomato quality after harvesting. The quality classification of harvested tomatoes is significantly affected by the detection of smooth skin, uneven lighting, and invisible defects. Intelligent detection of postharvest epidermal defects is critical for increasing the economic value of tomatoes. The researchers developed a hybrid method by combining the advanced YOLOv5 method with a number of methods, including Convolutional Block Attention Module (CBAM) and Switchable Atrous Convolution (SAConv). In their experimental study, they achieved an average success rate of 87.57% using their proposed hybrid method.

In another study [11] focused on tomato leaf disease diagnosis during harvest, a YOLOv5-based deep learning method was proposed. The researchers identified tomato leaf diseases such as Yellow Leaf Curl Virus and early blight. Using the proposed method, the researchers achieved high accuracy in disease diagnosis. The success rate in the study was reported as 91.9%.

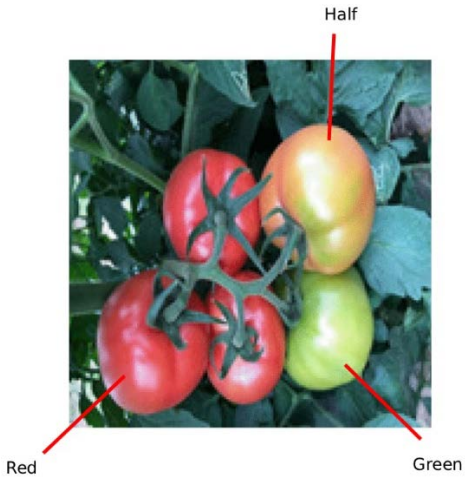

Figure 6. Ripe Tomato Recognition

[12] Used fruit ripeness and stem recognition during tomato harvesting. The hybrid method developed by the researchers for this purpose was introduced as YOLOX-SE-GIoU. The SE Focus Module, used in addition to the YOLOX method, improved the imbalance in fruit and stem counts and improved recognition accuracy. The success rate achieved in the study was reported as 92.17%.

Independently of the preceding studies reviewed, the specialized academic body of work executed by Dr. Ülgen and her associates merits significant attention. Their research rigorously investigates the effects of applied magnetic fields on critical aspects of plant development and various physiological processes, thereby providing substantial insights into biophysical stimuli in plant systems [13, 14, 15 ,16]. Given the high degree of thematic correlation between Ülgen's findings and the experimental domain addressed in the present study, the establishment of a future bilateral scientific collaboration with this distinguished research group is identified as a highly promising strategic objective for advancing the understanding of magneto-biological interactions in this field.

YOLO (You Only Look Once) method

The YOLO (You Only Look Once) method is built upon the working principle of YOLOv3 and the innovations introduced by the subsequently developed YOLOv5 model [17], [18]. An examination of the YOLOv3 architecture reveals a typical end-to-end networking principle used for object detection. When YOLOv3 analyzes an image, it first divides the input image into equal grids of SxS size [19].

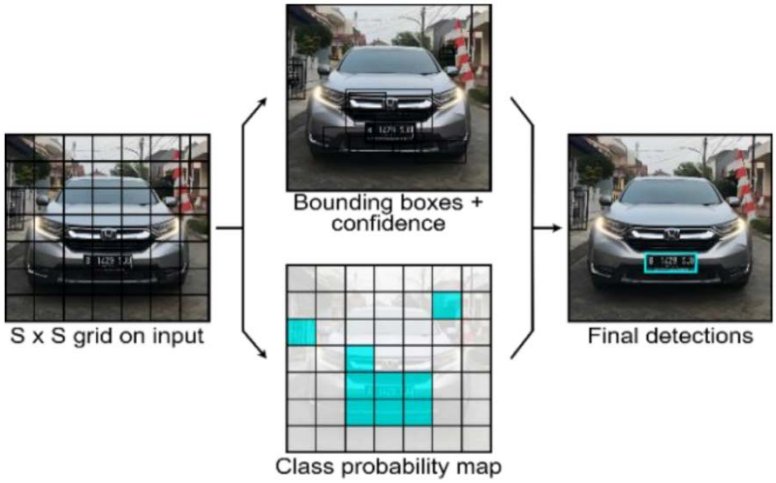

Figure 7: YOLO framework

Bounding box estimates and probabilities are generated separately for each grid in the image. Multi-scale fusion is used to provide estimates covering the entire image. All acquired data is processed using a Convolution Neural Network (CNN) [20]. The clustering method is used to evaluate the boundary lines.

The developed YOLOv5 method offers several advantages [21], [22]:

- Developed by Ultraytics and published by Glenn Jocher in 2020, YOLO was the most up-to-date version of the object detection technology at the time.
- The method's architecture was built on the EfficientDet object detection framework and used a single-shot detector (SSD) architecture similar to previous YOLO versions.
- The method features significant improvements in both speed and accuracy compared to previous versions. Furthermore, thanks to its backbone and training methodologies, it outperforms older versions in speed and accuracy.

- The method's flexible design includes advanced features that allow for easy modification and transfer of acquired knowledge.

The YOLOv7 method was first proposed by Joseph Redmon and his team in 2016 [23]. This new method stands out for its ability to accurately and precisely localize objects in an image in real time. Among the notable features of the YOLOv7 method over previous methods is the integration of various improvements, such as skip connections and residual blocks, into the network structure. These changes allow the model to identify objects more accurately and quickly. Furthermore, successful updates from previous successful models such as YOLOv4, scalled-YOLOv4, and YOLO-R were incorporated. This laid the foundation for the new, improved version of the model. Thanks to its exceptional speed and high accuracy, the new method is among the most widely used algorithms for object detection tasks. The operating principle of the YOLOv7 algorithm is based on the ability to divide an image into a grid. For each cell, the algorithm calculates bounding boxes, the probabilities of the corresponding classes, and confidence scores indicating whether the box contains an object. It also estimates the probability of which bounding box encloses the object in the labeled cells. The YOLOv7 method is most frequently used in autonomous vehicles, surveillance systems, and robotic systems.

The YOLOv8 method is extremely similar to the YOLOv5 method, with only some nuanced differences. The main difference between the two methods is that the C3 module in the YOLOv5 method has been replaced by the C2f module in the YOLOv8 method. The salient features of this modified method are as follows [24], [25]. It is created by integrating the ELAN concept used in the YOLOv7 method with C3, thus improving gradient flow information while preserving the lightweight design of the model.

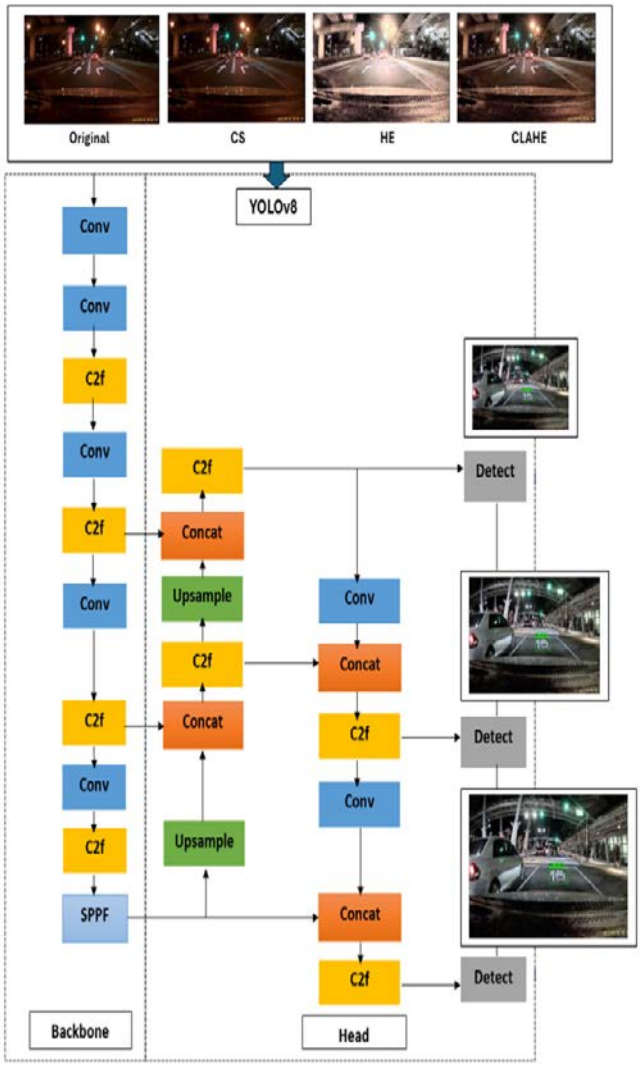

Figure 8. YOLOv8 architecture

The YOLOv9 method proposes two key innovations that surpass previous versions in terms of increased efficiency and accuracy in object identification tasks. With the Programmable Gradient Information (PGI) model, the YOLOv9 method achieves an adaptable and flexible architecture. This versatility is

achieved by adapting to different computing needs and model complexities, enabling various deployment scenarios [26].

REFERENCES

[1] B. Beser *et al.*, "YOLO-V5 based deep learning approach for tooth detection and segmentation on pediatric panoramic radiographs in mixed dentition," *BMC Med Imaging*, vol. 24, no. 1, p. 172, Jul. 2024, doi: 10.1186/s12880-024-01338-w.

[2] S. A. Tarimo, M.-A. Jang, E. E. Ngasa, H. B. Shin, H. Shin, and J. Woo, "WBC YOLO-ViT: 2 Way - 2 stage white blood cell detection and classification with a combination of YOLOv5 and vision transformer," *Comput Biol Med*, vol. 169, p. 107875, Feb. 2024, doi: 10.1016/j.compbiomed.2023.107875.

[3] Q. Yu, Y. Han, W. Lin, and X. Gao, "Detection and Analysis of Corrosion on Coated Metal Surfaces Using Enhanced YOLO v5 Algorithm for Anti-Corrosion Performance Evaluation," *J Mar Sci Eng*, vol. 12, no. 7, p. 1090, Jun. 2024, doi: 10.3390/jmse12071090.

[4] L. Deng *et al.*, "HAD-YOLO: An Accurate and Effective Weed Detection Model Based on Improved YOLOV5 Network," *Agronomy*, vol. 15, no. 1, p. 57, Dec. 2024, doi: 10.3390/agronomy15010057.

[5] J. Zhang, Y. Zhang, J. Liu, Y. Lan, and T. Zhang, "Human figure detection in Han portrait stone images via enhanced YOLO-v5," *Herit Sci*, vol. 12, no. 1, p. 119, Apr. 2024, doi: 10.1186/s40494-024-01232-2.

[6] W. Gao, C. Zong, M. Wang, H. Zhang, and Y. Fang, "Intelligent identification of rice leaf disease based on YOLO V5-EFFICIENT," *Crop Protection*, vol. 183, p. 106758, Sep. 2024, doi: 10.1016/j.cropro.2024.106758.

[7] J. Zhang *et al.*, "Greenhouse tomato detection and pose classification algorithm based on improved YOLOv5,"

Comput Electron Agric, vol. 216, p. 108519, Jan. 2024, doi: 10.1016/j.compag.2023.108519.

[8] G. Wang, R. Xie, L. Mo, F. Ye, X. Yi, and P. Wu, "Multifactorial Tomato Leaf Disease Detection Based on Improved YOLOV5," *Symmetry (Basel)*, vol. 16, no. 6, p. 723, Jun. 2024, doi: 10.3390/sym16060723.

[9] J. Zhao, W. Bao, L. Mo, Z. Li, Y. Liu, and J. Du, "Design of tomato picking robot detection and localization system based on deep learning neural networks algorithm of Yolov5," *Sci Rep*, vol. 15, no. 1, p. 6180, Feb. 2025, doi: 10.1038/s41598-025-90080-6.

[10] Y. Huang *et al.*, "A fluorescence detection method for postharvest tomato epidermal defects based on improved <scp>YOLOv5m</scp>," *J Sci Food Agric*, vol. 104, no. 11, pp. 6615–6625, Aug. 2024, doi: 10.1002/jsfa.13486.

[11] S. Zhong, Y. Liu, G. Huang, B. Xu, and Y. Chen, "Tomato Leaf Disease Detection and Management System Based on YOLOv5," in *Proceedings of the 2024 8th International Conference on Electronic Information Technology and Computer Engineering*, New York, NY, USA: ACM, Oct. 2024, pp. 690–697. doi: 10.1145/3711129.3711247.

[12] Y. Li, J. Li, L. Luo, L. Wang, and Q. Zhi, "Tomato ripeness and stem recognition based on improved YOLOX," *Sci Rep*, vol. 15, no. 1, p. 1924, Jan. 2025, doi: 10.1038/s41598-024-84869-0.

[13] Ulgen, C., Yıldırım, A. B., & Turker, A. U. (2017). Effect of magnetic field treatments on seed germination of melissa officinalis L. International Journal of Secondary Metabolite, 4(3, Special Issue 1), 43-49.

[14] Ulgen, C., Yıldırım, A., & Turker, A. (2020). Enhancement of plant regeneration in lemon balm (Melissa officinalis L.) with different magnetic field applications. International Journal of Secondary Metabolite, 7(2), 99-108.

[15] Ulgen, C., Yildirim, A. B., Sahin, G., & Turker, A. U. (2021). Do magnetic field applications affect in vitro regeneration, growth, phenolic profiles, antioxidant potential and defense enzyme activities (SOD, CAT and PAL) in lemon balm (Melissa officinalis L.)?. Industrial Crops and Products, 169, 113624.

[16] Ulgen, C., Yıldırım, A., & Turker, A. (2023). Melissa officinalis: Antibacterial and antioxidant potential, phenolic profile and enzyme activities. Kahramanmaraş Sütçü İmam Üniversitesi Tarım ve Doğa Dergisi, 26(5), 1075-1085.

[17] J. Redmon and A. Farhadi, "YOLO9000: Better, Faster, Stronger," in *2017 IEEE Conference on Computer Vision and Pattern Recognition (CVPR)*, IEEE, Jul. 2017, pp. 6517–6525. doi: 10.1109/CVPR.2017.690.

[18] Q. Xu, R. Lin, H. Yue, H. Huang, Y. Yang, and Z. Yao, "Research on Small Target Detection in Driving Scenarios Based on Improved Yolo Network," *IEEE Access*, vol. 8, pp. 27574–27583, 2020, doi: 10.1109/ACCESS.2020.2966328.

[19] C. Dewi, S. A. Philemon, G. Dai, and A. P. S. Chen, "Image Enhancement Technique Utilizing YOLO Model for Automatic Number Plate Recognition," *International Journal of Transport Development and Integration*, vol. 9, no. 1, pp. 59–68, Mar. 2025, doi: 10.18280/ijtdi.090106.

[20] Y. Yu and M. Yao, "When Convolutional Neural Networks Meet Laser-Induced Breakdown Spectroscopy: End-to-End Quantitative Analysis Modeling of ChemCam Spectral Data for Major Elements Based on Ensemble Convolutional Neural Networks," *Remote Sens (Basel)*, vol. 15, no. 13, p. 3422, Jul. 2023, doi: 10.3390/rs15133422.

[21] K. He, X. Zhang, S. Ren, and J. Sun, "Spatial Pyramid Pooling in Deep Convolutional Networks for Visual Recognition," *IEEE Trans Pattern Anal Mach Intell*, vol. 37, no. 9, pp. 1904–1916, Sep. 2015, doi: 10.1109/TPAMI.2015.2389824.

[22] C.-Y. Wang, A. Bochkovskiy, and H.-Y. M. Liao, "Scaled-YOLOv4: Scaling Cross Stage Partial Network," in *2021 IEEE/CVF Conference on Computer Vision and Pattern Recognition (CVPR)*, IEEE, Jun. 2021, pp. 13024–13033. doi: 10.1109/CVPR46437.2021.01283.

[23] Redmon J, Divvala S, Girshick R, and Farhadi A, "You Only Look Once: Unified, Real-Time Object Detection," *Computer Vision and Pattern Recognition*, May 2016.

[24] C. Dewi, D. Manongga, Hendry, E. Mailoa, and K. D. Hartomo, "Deep Learning and YOLOv8 Utilized in an Accurate Face Mask Detection System," *Big Data and Cognitive Computing*, vol. 8, no. 1, p. 9, Jan. 2024, doi: 10.3390/bdcc8010009.

[25] S. Khalid, H. M. Oqaibi, M. Aqib, and Y. Hafeez, "Small Pests Detection in Field Crops Using Deep Learning Object Detection," *Sustainability*, vol. 15, no. 8, p. 6815, Apr. 2023, doi: 10.3390/su15086815.

[26] M. Hu, Y. Li, L. Fang, and S. Wang, "A2 - FPN: Attention Aggregation based Feature Pyramid Network for Instance

Segmentation," in *2021 IEEE/CVF Conference on Computer Vision and Pattern Recognition (CVPR)*, IEEE, Jun. 2021, pp. 15338–15347. doi: 10.1109/CVPR46437.2021.01509.

WOUND CREAM DERIVED FROM COTTON OLANT SEEDS AND IN VITRO BIOCOMPATIBILITY TESTS

Şevval ÇELİK[1]

Büşra MORAN[2]

Mustafa TÜRK[3]

1. INTRODUCTION

The skin is a multilayered structure consisting of the epidermis, dermis, and hypodermis, and is the largest organ that protects the body against physical, chemical, and biological factors (Taşkapan, 2005; Alberts et al., 2002). While the epidermis acts as a barrier, the dermis contains vascular and connective tissue elements; the hypodermis consists of fatty tissue that serves as an energy reserve (Landmann, 1986). Additionally, the skin plays a critical role in maintaining vital functions such as thermoregulation, water balance, immune response, and sensory perception (Taş & Kırkık, 2022).

Wounds resulting from the disruption of skin integrity are classified as acute, chronic, traumatic, and infected wounds (Raziyeva et al., 2021). While acute wounds generally heal through physiological processes, the healing process is significantly prolonged in chronic wounds associated with

[1] Kırıkkale Üniversitesi/Fen Bilimleri Enstitüsü/ Biyomühendislik Anabilim Dalı, ORCID: 0000-0002-3091-620X.

[2] Dr., Hitit Üniversitesi, Bilimsel Teknik Uygulama ve Araştırma Merkezi, In Vitro Biyouyumlukuk ve Hücre Kültürü Laboratuvarı, ORCID: 0000-0002-7280-4417.

[3] Prof. Dr., Kırıkkale Üniversitesi, Mühendislik ve Doğa Bilimleri Fakültesi, Biyomühendislik Bölümü, ORCID: 0000-0001-8202-090X.

conditions such as diabetes, prolonged pressure, and venous insufficiency (Umar & Damar, 2017). Infected wounds can complicate the treatment process by causing both local and systemic complications (Öztaş, 2021).

Wound healing is a biologically regulated process consisting of four phases: hemostasis, inflammation, proliferation, and remodeling (Kahraman & Erdoğan, 2022). A disruption in any of these phases can lead to delayed or halted healing. For this reason, modern approaches based on biopolymers and bioactive components are gaining importance alongside traditional treatments (Can & Sağbaş, 2023; Kral et al., 2023). Natural and biopolymer-based materials that support the moist wound healing approach have come to the fore in recent years (Dhivya et al., 2015).

Natural ingredients rich in phytochemicals support wound healing through their anti-inflammatory, antioxidant, and antimicrobial properties. Natural products such as olive oil, beeswax, pine resin, and cotton seeds have been used in traditional medicine for many years, and their positive biological effects have been confirmed in recent studies (Harborne & Williams, 2000). Chitosan and alginate, which are biopolymers, are valuable components in terms of providing a moist healing environment, supporting tissue regeneration, and exhibiting antimicrobial properties (Jayakumar et al., 2010; Patel et al., 2016).

The synergistic use of natural components and biopolymers is considered a promising approach in modern wound-care strategies due to its ability to accelerate tissue regeneration and reduce the risk of infection. However, studies in the literature on biopolymer-based topical formulations using cotton cocoons in combination with components such as olive oil, beeswax, and pine resin are quite limited (Çaydamlı, 2012).

This study aims to develop a biodegradable, biocompatible, and non-toxic wound cream formulation by combining natural components such as cotton seeds, olive oil, beeswax, and pine resin with chitosan and alginate-based biopolymers, and to evaluate the biological and physicochemical properties of this developed formulation.

2. METHOD

2.1. Preparation of the Natural Formulation

The first harvest of cotton bolls, collected before rainfall, was burned to ash. 400 g of the resulting ash was taken and boiled in a beaker containing 1 L of water on a magnetic stirrer. Once the ash settled to the bottom and a clear supernatant formed, the mixture was transferred into a copper pot. The clear phase was evaporated by applying heat until salt crystals appeared, and natural crystals intended for use in the formulation were obtained.

2.2. Preparation of Cream Formulations

Following the conversion of the ash extract into its crystalline form, three different cream formulations (WH1, WH2, and WH3) were prepared. In all formulations, 51 mL of physiological serum was used as the solvent phase, and natural components were added to the chitosan–alginate-based biopolymer structure.

WH1 Formulation: This formulation contained 3% chitosan, 4% alginate, 4% beeswax, 4% pine resin, 4% olive oil, and 8% ash extract. All components were mixed until a homogeneous mixture was obtained in the solvent phase.

WH2 Formulation: The WH2 formulation contained 3% chitosan, 4% alginate, 4% beeswax, 4% pine resin, approximately 4% olive oil, and 8% ash extract. First, chitosan,

alginate, beeswax, pine resin, and olive oil were mixed in the solvent phase to obtain a homogeneous mixture, then ash extract was added to complete the formulation.

WH3 Formulation: The third formulation used 3% chitosan, 4% alginate, 4% beeswax, 6% pine resin, approximately 6% olive oil, and 12% ash extract. After all components were thoroughly homogenized, the mixture was considered the final formulation.

2.3. MTT Test

MTT analysis was performed in accordance with the ISO 10993-5 standard. Each sample (WH1, WH2, WH3) was prepared by dissolving 1 g of ash in 6 mL of DMEM mixture and sterilized by passing through 0.2 µm pore diameter filters.

L929 cells were washed with PBS, detached from the surface with Trypsin-EDTA, and centrifuged for 3 minutes. Cells were suspended in 1 mL DMEM, counted, and seeded into 96-well plates at a density of 10,000 cells per well. The cells were incubated for 24 hours with DMEM containing 10% FBS + 1% P/S.

Then, solutions containing 0.2% cream extract were added to the wells, and dilution series were created. The cells were incubated for a second 24 hours. Subsequently, fifty microliters of MTT solution (1 mg/mL) was added to each well and incubated for 2 hours.After removing the MTT solution, the crystals were dissolved with 100 µL of isopropanol, and the absorbances were measured at 570 nm.

2.4. Scratch Test

L929 cells were cultured in DMEM + 10% FBS + 1% P/S medium and allowed to reach 90% confluence. Subsequently, 50 µL and 25 µL volumes of 0.2% filtered cream

formulations were applied to the A–B–C groups. The control group was left untreated.

A linear scratch was created in each well using a sterile pipette tip, and the cells were washed with PBS. Cell migration and wound-closure processes were monitored under a microscope at 0, 12, 24, 48, and 72 hours. Cell migration and closure percentages were calculated using the initial wound width as a reference.

2.5. Disk Diffusion Test

Antimicrobial activity was evaluated using the WH2 formulation. Fresh bacterial isolates were spread onto agar plates, and Cefoxitin (30 µg) discs and cream-impregnated discs were placed on each plate as positive controls.

After incubation, the inhibition zones (mm) formed around the disks were measured, and the antimicrobial potential of the formulation was compared with the positive control.

2.6. Double Staining

Plates with 48 wells were incubated for 24 hours with 10,000 cells added to each well. The plate was divided into two sections, one serving as the positive control and the other as the negative control. 20% DMSO was added to the positive wells.

Dilution series of the WH2 formulation were prepared and applied, and Double Staining solution was added to all wells at the end of incubation. DAPI was applied to the wells designated for apoptotic nuclei, while FITC was applied to those designated for necrotic cells, followed by 10 minutes of incubation and imaging using a fluorescence microscope.

2.7. FT-IR Analysis

The WH2 formulation was analyzed using the ATR-FT-IR method. Measurements were performed in the 4000–400

cm^{-1} wavenumber range with a resolution of 4 cm^{-1}. Spectral bands were analyzed to confirm the functional groups of the natural components and biopolymers.

2.8. DSC Analysis

The thermal properties of the formulation were examined using a Mettler Toledo DSC device. A 5 mg sample taken from the WH2 cream was placed in a hermetic DSC pan and analyzed in a nitrogen atmosphere at a heating rate of 5 °C/min in the range of –20 °C to 600 °C. The Tg, Tm, and Td values were determined from the resulting thermogram.

3. FINDINGS

3.1. MTT Test

MTT assay results were evaluated to determine the effects of the formulations on cell viability. The average absorbance values and cell viability percentages for samples WH1, WH2, and WH3 are presented in Table 3.1. Additionally, the viability curves corresponding to each dilution ratio are shown in Figure 3.1.

Table 3.1. Combined absorbance, % viability, and standard deviation values according to WH1, WH2, and WH3 MTT results

Dilution	Average Absorbance WH1	Cell Vitality(%) WH1	Average Absorbance WH2	Cell Vitality (%) WH2	Average Absorbance WH3	Cell Vitality (%) WH3
1/1	1.11 ± 0.01	58.6	0.95 ± 2.06	83.2	0.78 ± 0.14	68.0
1/2	1.35 ± 0.05	71.7	1.03 ± 2.99	89.7	0.99 ± 2.28	86.3
1/4	1.56 ± 0.08	83.2	1.61 ± 3.19	140.6	1.03 ± 3.86	89.6
1/8	1.71 ± 0.04	91.4	1.66 ± 3.10	145.0	1.11 ± 3.71	96.9
1/16	1.78 ± 0.04	95.0	1.35 ± 1.49	118.0	1.09 ± 2.78	94.8
1/32	1.78 ± 0.04	94.8	1.36 ± 4.78	118.5	1.07 ± 2.47	93.7
1/64	1.87 ± 0.06	99.8	1.32 ± 3.47	115.0	1.18 ± 1.19	102.6
Kontrol	1.87 ± 0.02	100.0	1.07 ± 0.19	100.0	1.22 ± 0.16	100.0

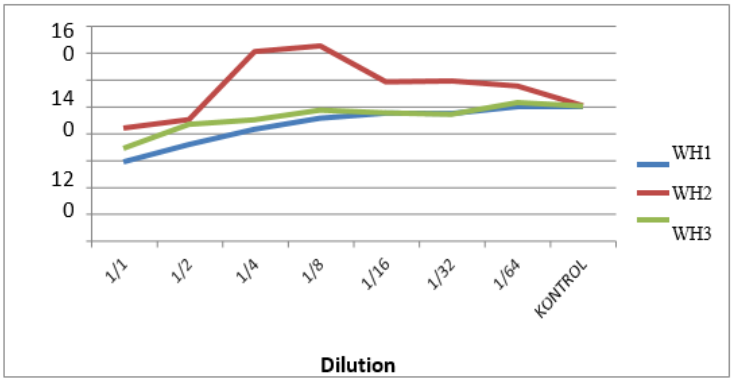

Figure 3.1. WH1, WH2, and WH3 comparative MTT assay % viability values

When the tables and graphs are evaluated together, it is seen that cell viability generally increases as the dilution ratio increases. This finding indicates that the biomaterial exhibits a dose-dependent inhibitory effect at higher concentrations; dilution reduces the toxic effect.

The WH1 formulation showed the highest toxicity at a 1:1 ratio with 58.6% cell viability. As dilution increased, viability values rose rapidly, reaching 99.8% at a 1/64 dilution. This indicates that WH1 is cytotoxic at high concentrations but becomes biocompatible upon dilution.

Among all formulations, WH2 exhibited the most prominent dose-response profile. Mild toxicity was observed at low dilutions (1/1–1/2); however, at 1/4 and 1/8 dilutions, cell viability exceeded 140%, demonstrating a significant proliferative effect. This increase suggests that WH2 offers a structure that can be used in wound healing and tissue regeneration. Although viability decreased to 115% at higher dilutions, it remained above the control group.

The WH3 formulation showed a mild toxic effect with 68% cell viability at a 1:1 dilution. Although viability values

increased with increasing dilution, they remained below the control group in most dilutions. Only at a 1:64 ratio was a mild proliferative potential observed with 102.6% viability. Overall, the findings demonstrate that the formulation is biocompatible, exhibits low cytotoxicity, supports limited proliferation, induces minimal apoptosis, does not cause necrotic damage, and displays moderate strain-dependent antimicrobial activity.

In general, formulations containing ash extract have been observed to have varying effects on cell viability depending on the composition and dosage. In particular, the proliferative effect of the WH2 formulation at moderate dilution ranges suggests that the formulation shows promise in terms of biocompatibility.

3.2. Scratch Test

Scratch Assay results were obtained to evaluate the effect of the WH2 formulation on cell migration. The initial wound area was accepted as 100% for all groups.

The findings indicate that the WH2 formulation initially slowed cell migration but later promoted partial wound-closure and cell motility. In particular, the increase in closure rates in the scratch area after 24 hours suggests that the formulation may support cell migration at low concentrations.

However, when the proliferative effect is comprehensively evaluated with MTT results, it is evident that the WH2 formulation can elicit a more pronounced cellular repair response at more optimized concen trations. This indicates that the formulation has he potential to be adapted to support wound healing.

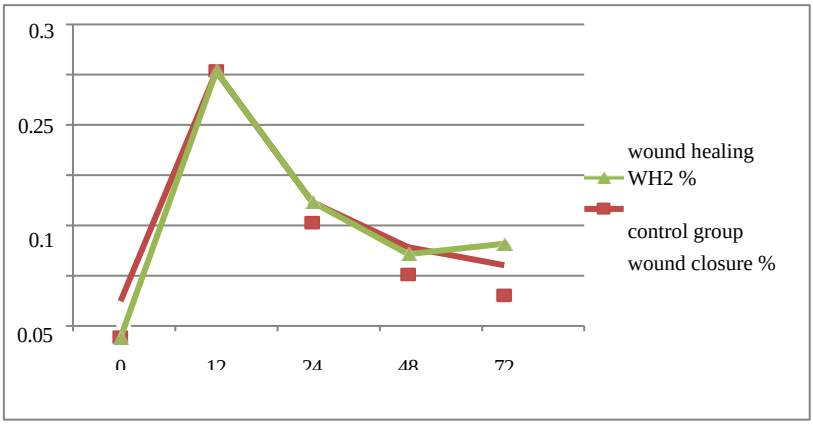

Figure 3.2. Wound healing over time

3.3. Disk Diffusion Test

The antimicrobial efficacy of the WH2 formulation was evaluated using the disk diffusion test, and the inhibition zone diameters for different bacterial species were measured.

The zone diameters formed by the cream discs were measured as follows: *E. coli*: 13.67 mm, *S. mutans*: 12.86 mm, *S. aureus*: 12.20 mm, *E. faecalis*: 11.59 mm, *A. baumannii*: 10.89 mm.

The zone diameters of the positive control Cefoxitin discs were measured as 5.26 mm, 24.28 mm, 27.08 mm, 5.36 mm, and 5.92 mm, respectively.

Overall, the results indicate that the formulation exhibits moderate but strain-dependent antimicrobial activity. In particular, the fact that the cream discs formed wider zones in *A. baumannii*, *E. coli*, and *E. faecalis* strains, where Cefoxitin displayed weak activity against *A. baumannii*, *E. coli*, and *E. faecalis*, which explains why the cream-impregnated discs produced relatively larger inhibition zones in these strains.

However, the fact that the cream disk forms lower zones in *S. aureus* and *S. mutans* strains, which Cefoxitin strongly inhibits, indicates that the effect is strain-dependent.

In general, the formulation appears to offer complementary antimicrobial activity, particularly against resistant bacteria. (EUCAST, 2015; EUCAST, 2024; CLSI, 2023).

3.4. Double Staining Analysis

Apoptosis was observed in 11.7% of the positive control group, and this high value indicates that the apoptotic pathways were activated correctly (Elmore, 2007). In the negative control group, the low rates of apoptotic and necrotic cells confirm that the experimental conditions did not have a toxic effect on the cells (Kroemer et al., 2009).

Table 3.2. Apoptosis and Necrosis Index

	% Apoptosis (DAPI)	% Necrosis (FITC)
Positive Control	11.7 ± 1.5	8.3 ± 1.5
Negative Control	3.7 ± 1.5	5.7 ± 1.5
Cream Formulation	7.7 ± 1.2	4.3 ± 1.5

The apoptotic cell rate in the group treated with the cream formulation was higher than in the negative control but lower than in the positive control. This result suggests that the formulation induces low-level apoptosis without triggering severe cytotoxic responses. (Portt et al., 2011). However, the fact that the necrosis rate was lower than both the positive and negative control groups indicates that the cream formulation did not disrupt cell membrane integrity and did not cause necrotic damage (Galluzzi et al., 2018).

These findings confirm that the formulation is cytocompatible, as it induces minimal apoptosis and does not cause membrane-disruptive necrosis.

3.5. FT-IR Analizi

FT-IR analysis was performed on the WH2 cream formulation prepared in section 3.1.3.2. The purpose of the analysis was to evaluate the effects of the cross-linking process created by $CaCl_2$ on the biopolymer structure in the formulation.

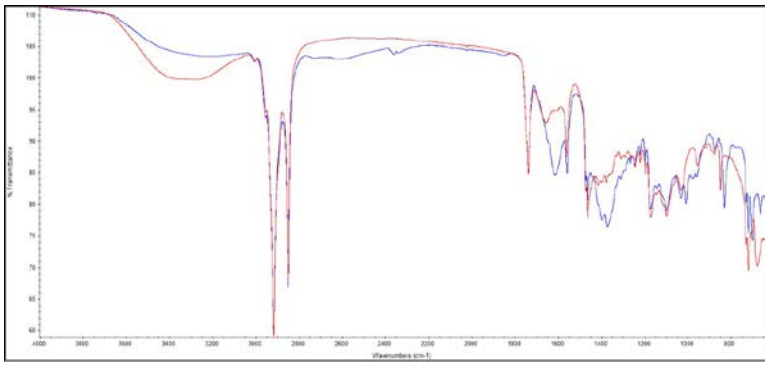

Figure 3.3. After cross-linking (blue) and before cross-linking (red)

In the spectrum of the uncrosslinked sample (red), the broad band observed around 3273 cm^{-1} represents the –OH and –NH groups present in chitosan and alginate (Rinaudo, 2006). In the cross-linked sample, the observation of this band at a lower intensity and slightly shifted indicates that hydrogen bonds have been rearranged and ionic interactions have increased.

C–H stretching vibrations at 2915 and 2848 cm^{-1} confirm the aliphatic structures of beeswax and olive oil and are not significantly affected by cross-linking (Matos et al., 2015; Javidnia et al., 2018). Carbonyl signals around 1736 cm^{-1} indicate ester groups originating from olive oil and beeswax and appear unaffected by cross-linking

However, the narrowing and frequency shifts observed in the amide I and amide II bands specific to chitosan in the 1655–1550 cm^{-1} range indicate that Ca^{2+} ions interact ionically with

the amine groups (Jayakumar et al., 2010). This confirms that ionic cross-linking between polymer chains has been enhanced.

Furthermore, shifts observed in the C–O and C–C vibration bands in the 1460–1000 cm^{-1} range indicate that cross-linking affects the polymer network structure (Pawar & Edgar, 2012).

The distinct bands appearing in the lower wavenumber region of 848–710 cm^{-1} support the increased structural regularity after cross-linking. Overall, FT-IR findings indicate that Ca^{2+} ions form strong physical interactions between the biopolymers in the formulation, thereby enhancing the system's mechanical strength and structural stability.

3.6. DSC Analysis

DSC analysis was performed to compare the thermal behavior of the uncrosslinked WH2 sample with that of the $CaCl_2$-crosslinked WH2-2 sample.

The endothermic transition observed between –20 and 100 °C in both samples is associated with the removal of free water and volatile components. The literature reports similar endothermic transitions at low temperatures in systems containing oil and wax (Pizzimenti et al., 2022).

In the WH2 sample, a sharper endothermic peak was observed around ~240 °C. This peak can be associated with the melting of regular, crystal-like regions in the wax and biopolymer matrix. Furthermore, the absence of cross-linking results in a more homogeneous transition. The literature reports a significant increase in melting temperatures in polymers after cross-linking with $CaCl_2$ (Jahan & Mathad, 2016).

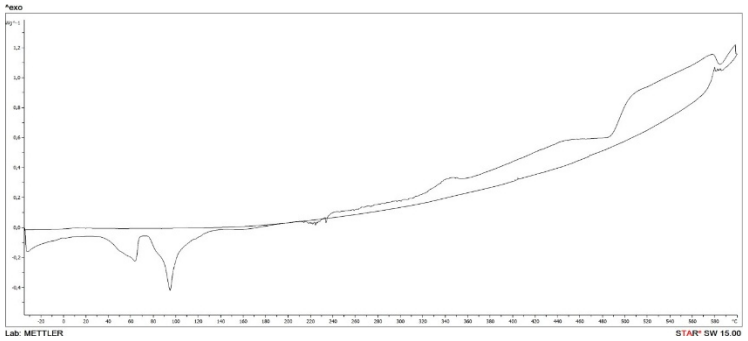

Figure 3.4. Cross-linking pre-graph for WH2 formulation

In the cross-linked WH2-2 sample, a broad endothermic region was observed between ~200–260 °C. This expansion is consistent with the dissolution of ionic interaction regions with different binding energies and indicates that the structure is thermally more resistant. Indeed, it is reported in the literature that endothermic peaks in Ca^{2+} cross-linked alginate systems shift from 240 °C to 280 °C, increasing oxidative thermal resistance (Janik et al., 2023).

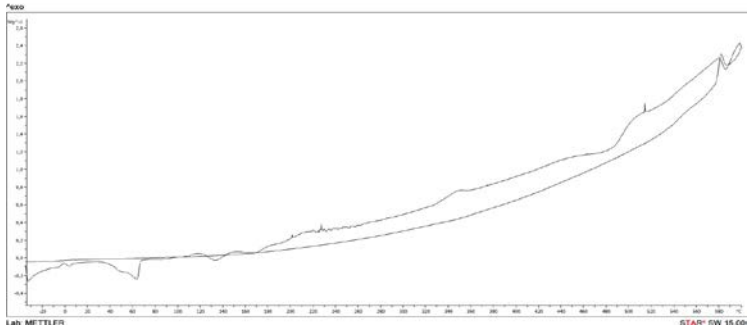

Figure 3.5. Cross-linking post-graph for WH2 formulation

The absence of decomposition peaks above 300 °C indicates that the formulation maintains high thermal stability. This indicates that the formulation remains relatively stable at high temperatures. The results obtained reveal that crosslinking increases the thermal resistance of the polymeric matrix,

providing a more stable structure and extending the potential shelf life and functional temperature range of the product.

4. CONCLUSION AND DISCUSSION

In this study, the biocompatibility, cell proliferation effects, wound-healing potential, and antimicrobial activity of the developed biopolymer-based cream formulations were comprehensively evaluated. The in vitro biological tests (MTT, Scratch Assay, Double Staining, and disk diffusion) and physicochemical analyses (FT-IR and DSC) performed provided multifaceted findings regarding the functional performance of the formulations.

The MTT results demonstrated distinct biological behaviors among the formulations. While the WH1 formulation exhibited marked toxicity at high concentrations, it was observed that as the dilution ratio increased, the cytotoxic effect decreased markedly, and cell viability approached that of the control group (99.8%). The WH2 formulation, on the other hand, showed a significant proliferative effect, creating over 140% cell viability, especially at 1/4 and 1/8 dilutions. Although the WH3 formulation showed viability below the control at most concentrations, it created a slight proliferative effect at a 1/64 ratio with 102.6%. These findings reveal that the effects of cream formulations on cell viability and proliferation vary depending on the content components and the applied dose. It is known in the literature that natural polymer-based systems contribute to regenerative processes by supporting cell proliferation (Freshney, 2010). From this perspective, the WH2 formulation demonstrates a particularly promising biocompatibility profile.

The scratch test results evaluating cell migration showed that the formulation inhibited cell migration in the early stages;

however, it showed moderate wound-closure activity during later time points. These findings suggest that the formulation does not strongly stimulate cell migration, particularly during early time points, but its migratory impact may be enhanced through concentration optimization or the incorporation of additional bioactive components. The literature states that biopolymer systems that accelerate wound healing provide more pronounced cell migration, especially at low concentrations (Liang et al., 2007). In this context, it can be concluded that the current formulation offers limited migration support, but has a structure that can be improved.

Double staining analysis has revealed the formulation's effect on cellular death mechanisms. The observation of apoptosis at a rate of 11.7% in the positive control group confirms that the method is working correctly (Elmore, 2007). Low apoptosis/necrosis ratios were obtained in the negative control (Kroemer et al., 2009). The fact that the cream formulation produces an apoptosis rate above the negative control but below the positive control indicates that it may exhibit mild apoptotic activity without a strong inducer (Portt et al., 2011). The low necrosis rate indicates that cell membrane integrity is preserved and that the formulation is safe in terms of cytotoxicity (Galluzzi et al., 2018).

In terms of antimicrobial activity, disk diffusion results showed that the cream formulation exhibited moderate antibacterial activity with zone diameters ranging from 10.89 to 13.67 mm. It was particularly noteworthy that the cream disk formed wider zones than the positive control Cefoxitin, especially against antibiotic-resistant strains such as *E. coli*, *E. faecalis* and *A. baumannii*. These results suggest that the natural components in the formulation may offer complementary antimicrobial activity, particularly against strains that exhibit reduced susceptibility to Cefoxitin. However, since Cefoxitin

provided much stronger inhibition in *S. aureus* and *S. mutans* strains, the effect of the cream formulation was limited. Overall, it can be said that the formulation offers a promising antimicrobial profile, particularly against resistant bacteria, although it exhibits species-specific differences (EUCAST, 2015; CLSI, 2023).

The structural and thermal properties of the formulation were supported by FT-IR and DSC analyses. FT-IR findings showed that cross-linking with Ca^{2+} ions strengthened the ionic interactions between chitosan and alginate polymer chains and increased structural stability through the rearrangement of hydrogen bonds (Rinaudo, 2006; Jayakumar et al., 2010). DSC findings reveal that cross-linked samples exhibit broader endothermic transitions and higher thermal resistance. This indicates that Ca^{2+} cross-linking increases the thermal stability of the polymeric matrix, as evidenced by broader endothermic transitions and the absence of decomposition peaks (Janik et al., 2023).

Overall, it is concluded that the developed cream formulation offers a structure that is biocompatible, has low toxicity, can exhibit partial proliferative effects, provides a mild apoptotic response, does not cause necrotic damage, and displays moderate antimicrobial activity. However, it is recommended that the formulation undergo concentration optimization, reinforcement with biologically active components, and re-adjustment of formulation parameters, particularly to enhance its capacity to support cell migration.

REFERENCES

Alberts, B., Johnson, A., Lewis, J., Raff, M., Roberts, K., & Walter, P. (2002). *Molecular biology of the cell* (4th ed.). Garland Science.

Can, A., & Sağbaş, S. (2023). Yara bakımı ve güncel yaklaşımlar. *Sağlık & Bilim*, 141.

Çaydamlı, Y. (2012). *Elektrospinning yöntemi ile biyopolimer esaslı nanoyapıların hazırlanması ve karakterizasyonu* (Yüksek lisans tezi). Dokuz Eylül Üniversitesi, Fen Bilimleri Enstitüsü.

Dhivya, S., Padma, V. V., & Santhini, E. (2015). Wound dressings – A review. *BioMedicine, 5*(4), 24–28.

Elmore, S. (2007). Apoptosis: A review of programmed cell death. *Toxicologic Pathology, 35*(4), 495–516.

EUCAST. (2015). *Antimikrobik duyarlılık testine yönelik EUCAST disk difüzyon yöntemi (Sürüm 5.0).*

Freshney, R. I. (2010). *Culture of animal cells: A manual of basic technique and specialized applications* (6th ed.). Wiley-Blackwell.

Galluzzi, L., Vitale, I., Aaronson, S. A., Abrams, J. M., Adam, D., Agostinis, P., … Kroemer, G. (2018). Molecular mechanisms of cell death: Recommendations of the Nomenclature Committee on Cell Death 2018. *Cell Death & Differentiation, 25*(3), 486–541.

Harborne, J. B., & Williams, C. A. (2000). Advances in flavonoid research since 1992. *Phytochemistry, 55*, 481–504. https://doi.org/10.1016/S0031-9422(00)00235-1

Janik, J., Boncel, S., Zawisza, K., & Kamedulski, P. (2023). Structure and thermal properties of calcium cross-linked alginate aerogels. *Scientific Reports, 13*, 12666.

Jayakumar, R., Menon, D., Manzoor, K., Nair, S. V., & Tamura, H. (2010). Biomedical applications of chitin and chitosan based nanomaterials—A short review. *Carbohydrate Polymers, 82*(2), 227–232.

Jayakumar, R., Prabaharan, M., Sudheesh Kumar, P. T., Nair, S. V., & Tamura, H. (2010). Biomaterials based on chitin and chitosan in wound dressing applications. *Biotechnology Advances, 29*(3), 322–337.

Kahraman, F. C., & Erdoğan, S. S. (2022). Yara iyileşmesi. *Turkiye Klinikleri Dermatology–Special Topics, 15*(4), 8–14.

Kral, Ö., Tamer, S. İ., Gül, Ü., & Tirnaksiz, F. (2023). Radyodermatit tedavisi: Geleneksel derleme. *Turkiye Klinikleri Journal of Dermatology, 33*(1), 30–39.

Kroemer, G., Galluzzi, L., Vandenabeele, P., Abrams, J., Alnemri, E. S., Baehrecke, E. H., … Melino, G. (2009). Classification of cell death: Recommendations of the Nomenclature Committee on Cell Death 2009. *Cell Death & Differentiation, 16*(1), 3–11.

Landmann, L. (1986). Epidermis and dermis. In *Biology of the integument: 2 vertebrates* (pp. 150–187). Springer Berlin Heidelberg.

Liang, C.-C., Park, A. Y., & Guan, J.-L. (2007). In vitro scratch assay: A convenient and inexpensive method for analysis of cell migration in vitro. *Nature Protocols, 2*(2), 329–333.

Öztaş, P. (2021). Yara iyileşmesi, bakımı ve tedavisi. *Ankara Eğitim ve Araştırma Hastanesi Tıp Dergisi, 54*(2), 341–351.

Patel, M. A., AbouGhaly, M. H. H., Schryer-Praga, J. V., & Chadwick, K. (2016). The effect of ionotropic gelation

residence time on alginate cross-linking and properties. *Carbohydrate Polymers, 155*, 362–371.

Portt, L., Norman, G., Clapp, C., Greenwood, M., & Greenwood, M. T. (2011). Anti-apoptosis and cell survival: A review. *Biochimica et Biophysica Acta – Molecular Cell Research, 1813*(1), 238–259.

Raziyeva, K., Kim, Y., Zharkinbekov, Z., Kassymbek, K., Jimi, S., & Saparov, A. (2021). Immunology of acute and chronic wound healing. *Biomolecules, 11*(5), 700.

Rinaudo, M. (2006). Chitin and chitosan: Properties and applications. *Progress in Polymer Science, 31*(7), 603–632.

Taş, S. K., & Kirkik, D. (2022). Dermatolojide temel immünoloji. *Turkiye Klinikleri Dermatology–Special Topics, 15*(3), 45–51.

Taşkapan, O. (2005). Deri immünolojisi. *Turkiye Klinikleri Journal of Internal Medical Sciences, 1*(6), 1–8.

Umar, D. Ç., & Damar, H. T. (2017). Akut ve kronik yaralar ve hemşirelik bakımı. *Turkiye Klinikleri Surgical Nursing–Special Topics, 3*(3), 157–163.

APPLICATIONS OF FUNCTIONAL THIN FILM COATINGS ON EYEWEAR LENSES

Naki KAYA[1]

1. INTRODUCTION

Eyeglass lens coatings are one of the most important building blocks of the modern optical industry. In the days before eyeglass lens coatings were used, the usefulness of an eyeglass lens was determined solely by the dioptric effect of the glass and its response to light. Today, this is also determined by properties obtained through lens coatings, such as the lens surface's resistance to external factors, its dirt-repellent properties, its ability to prevent light reflections, and the relationship between surface adhesion and cohesion forces. Coating technologies today not only improve vision quality but also enhance user comfort and can make significant improvements in daily life adaptation.

The advancement of coating technologies has accelerated the development of the optical sector. The first anti-reflective (AR) coatings were initially used for military purposes and were later transferred to civilian products. The most important factor that paved the way for the use of coating technologies in spectacle lenses was the use of organic lenses in spectacle lenses. With the transition from mineral spectacle lenses to organic spectacle lenses, the need arose to improve organic spectacle lenses. These needs emerged after the negative characteristics of organic spectacle lenses, such as being easily scratched and prone to dirt and water, were noticed.

[1] Lecturer, Kafkas University, Kağızman Vocational School, Department of Medical Services and Techniques, Opticianry Programme. ORCID: 0000-0003-2287-676X.

2. BASIC COATING TYPES AND PROPERTIES

2.1. Hard Coating (Hard Coat)

Mineral lenses were made from raw materials resistant to micro-scratches, and their surfaces were not easily scratched. However, this was not the case for organic lenses. It was observed that organic lenses were severely scratched, especially in dusty environments and when a solid particle came into direct contact with the lens surface. To increase the scratch resistance of organic lenses, a surface coating technology called hard coating was used.

Similar to other coatings, the advancement of hard coatings has accelerated mainly with the development of polymeric materials. Silica-based or acrylic resin-based polymers are generally used for hard coatings. These materials are polymerised through a series of processes, forming a high-density layer on the glass surface. This layer prevents particles that cause scratches and abrasion from coming into direct contact with the glass surface, thus preventing scratches on the glass surface due to mechanical friction.

Two traditional methods used in glass coating are spin coating and dip coating. Spin coating is a common method used to obtain a very thin and homogeneous film layer on the target material. In this method, the liquid solution material is dripped onto the surface to be coated, and the target material is rotated at high speeds. During rotation, the liquid solution spreads evenly over the surface of the target material. Centrifugal force is utilised in this process. As the coating process continues, the solvent contained in the liquid solution applied to the surface evaporates and a homogeneous film coating layer is obtained on the target material surface. The thickness of the film obtained may vary depending on certain conditions such as the viscosity of the solution used, the rotation speed, the spin time, and the volatility of the solvent. The spin coating method is widely used in the

technological field due to its advantages such as simplicity of application, cost-effectiveness compared to competitors, and repeatability. This method is particularly frequently used in the production of anti-reflective coatings on eyeglass lenses.

Another method frequently used in glass coatings, the dip-coating method, is a widely used technique for applying a thin and homogeneous coating layer to optical surfaces such as spectacle lenses. In this method, the glass is dipped into the coating solution at a specific speed and then withdrawn from the solution at a controlled speed; the withdrawal speed, the viscosity of the liquid, and the environmental conditions determine the coating thickness. In spectacle lens production, this method can be used to apply hard coatings that increase scratch resistance, anti-reflective (AR) coatings, or water-repellent hydrophobic coatings. The dip coating method is an economical and efficient method preferred in the optical coating industry because it provides a fairly uniform film thickness even on large surfaces and can be easily integrated into the production line.

There is a direct correlation between the quality of the hard coating and the quality of the anti-reflective coating. If the hard coating is of high quality, the anti-reflective coating can be applied more homogeneously to the glass surface. However, if the hard coating quality is low, deformations that may occur on the glass surface will eventually damage the anti-reflective coating as well. The important point to note here is that anti-reflective coating can be applied to the glass surface independently of hard coating. If anti-reflective coating is applied to hard-coated glass, this correlation will apply. However, anti-reflective coatings generally require hard coating because they do not have high mechanical durability.

2.2. Anti-Reflective Coating (AR)

Unwanted light reflections on spectacle lenses not only compromise comfort but also significantly reduce the quality of life for spectacle wearers. Environmental factors such as headlights from oncoming traffic at night and the brightness of screens from devices like computers and tablets can reduce image quality and negatively impact the perception of image clarity. Anti-reflective (AR) coatings, used to prevent such reflections, greatly limit light reflections through multi-layered optical thin films applied to the lens surface. Lens coatings are designed to be effective in the range of approximately 420 nm to 700 nm.

Materials with different refractive indices, such as SiO_2, TiO_2, ZrO_2, and Al_2O_3, are preferred in anti-reflective coatings. These materials are coated onto the surface in a very thin layer in multiple layers. The application of a multi-layer coating has a positive effect on anti-reflective properties. For example, when SiO_2 and TiO_2, which have different refractive indices, are coated in layers on the same glass surface, reflection can be reduced more efficiently due to the difference in refractive indices between the two materials.

An AR coating contains components such as a bonding layer, a hard coating, active layers, a top protective layer, and a hydrophobic/oleophobic coating. The bonding layer is used to strengthen the chemical bond between the glass surface and the coating, the hard coating is used to increase scratch resistance in polycarbonate and high-index lenses, the top protective layer is used to reduce moisture and surface charge, and the hydrophobic/oleophobic coating is used to prevent water, dirt and oil adhesion. The active layers are a multi-layered thin film structure formed with pairs such as SiO_2/TiO_2 or SiO_2/ZrO_2.

The coating stages can be summarised in a general framework as follows:

1. Preparation of the lens surface: The glass surface is cleaned using appropriate chemicals in ultrasonic baths.
2. Plasma activation: The energy of the glass surface is increased in a vacuum environment, improving the adhesion quality of the coating.
3. Hard coating application: Applied using dip-coating or spin-coating methods; followed by sintering.
4. AR thin film deposition: An AR layer is deposited onto the glass under vacuum.
5. Hydrophobic coating: Fluorinated materials are condensed in the vapour phase to reduce surface energy.
6. Final sintering and testing: The thickness, adhesion strength and optical transmittance of the coating are checked using measuring instruments.

Since surface reflection is high in high-index glass, the use of AR coatings is unavoidable. One of the negative characteristics of AR coatings is the sensitivity of the nanometre-scale structure on the glass surface to abrasive cleaning agents. When glass is cleaned with such agents, the coating layer can be easily damaged. For this reason, solutions with a neutral pH value and water are recommended for cleaning AR-coated glass, and no other chemicals are recommended.

2.3. Hydrophobic Coating

Hydrophobic coatings prevent water droplets from spreading on glass surfaces, causing them to bead up. This effect is not only beneficial when exposed to water but also offers significant convenience to the user in terms of daily cleaning. Water that comes into contact with the glass surface flows away with low friction. In this case, water droplets do not form stains or irregular fog marks on the glass. In addition, the hydrophobic

layer makes it difficult for organic contaminants such as fingerprints and grease to adhere to the surface, allowing cleaning to be done with less friction. In this case, no coating deformations due to the formation of micro-scratches on the glass surface are observed.

These coatings work by reducing surface energy. In hydrophobic coatings, surface energy is reduced to low values; this reduces the interaction force between water and the surface. This causes water droplets to spread less on the glass surface. The chemical structure of hydrophobic coatings mostly contains fluorine-based materials. These molecules contain structures that can form covalent bonds with the lens surface. These structures significantly reduce surface energy. These properties ensure the presence of fluorine-based materials in technological systems and industrial production.

Hydrophobic coatings can deform over time due to certain physical effects. UV light, friction, unsuitable cleaning chemicals, and high pH cleaners can cause this. However, applying the hydrophobic coating in combination with AR layers increases its durability, as the dense silica layer on top of the AR coating enables stronger bonding of the hydrophobic silanes. Today, some manufacturers perform plasma activation on the surface before the hydrophobic application to increase the physical durability of the coating. Surface energy is controlled using oxygen, argon or carbon tetrafluoride plasma, silanol groups on the surface are activated, and the chemical bonding density of fluorinated silanes is increased. This process significantly increases the durability of the hydrophobic layer.

In current glass technologies, hydrophobic coating has largely ceased to be an optional feature and has become a natural complement to AR coating. This allows users to enjoy both clearer vision and easier maintenance.

2.4. Oleophobic Coating (Oil-Repellent)

Oleophobic coatings are a surface coating application that significantly reduces the adhesion of fingerprints and oil-based dirt to glass surfaces. This feature is a major advantage, especially for users who work intensively with digital devices and frequently touch computer and phone screens. Skin sebum, sweat, and lipid-containing dirt are retained in smaller, weakly bonded areas rather than spreading over large areas of the glass surface. This makes the glass appear cleaner and significantly reduces the rate of soiling. Fingerprint marks on oleophobic coated surfaces are less visible and can be easily cleaned with a microfibre cloth.

These coatings are chemically composed mostly of fluoropolymer-based compounds. Thanks to the low polarizability of the carbon-fluorine (C-F) bond, the surface energy is reduced to levels where oil molecules cannot adhere. Although oil normally has low polarity, it tends to form a film on the surface; however, the lipophobic character of fluoropolymers prevents this spreading. Thus, oil droplets do not spread on the surface and cover a smaller area, making the contamination both less visible and easier to clean.

Modern oleophobic coatings not only provide oil repellency; they also have an advanced network structure that includes cross-linking mechanisms. This three-dimensional network structure increases surface hardness, enhancing scratch resistance. Formed by the polymerisation of fluorinated silanes, this structure adheres to the AR coating with strong chemical bonds. The formation of covalent bonds instead of adsorption extends the lifespan of the oleophobic layer.

During the production process, the oleophobic coating is typically applied by condensing it in the vapour phase. The process consists of the following steps: surface activation, vaporisation of the oleophobic molecule, condensation and

bonding, and low-temperature curing. In the surface activation stage, the AR-coated glass surface is activated with plasma. During the vaporisation of the oleophobic molecule stage, fluorinated silane or fluoro polymer derivatives are vaporised under vacuum at a controlled temperature. During the condensation and bonding stage, the molecules adhere to the surface and form chemical bonds. Finally, during the low-temperature curing stage, short thermal treatments are applied to complete the bonding and form cross-link structures.

Hydrophobic and oleophobic coatings work with a common physical mechanism to prevent both water and oil from adhering to the surface. However, oleophobic coatings require more advanced technology than hydrophobic coatings due to the complexity of a series of chemical processes.

2.5. UV Coatings

The adverse effects of UV rays on eye health have been known for a long time. In particular, UV-A and UV-B rays have many known adverse effects on human health. Therefore, UV protection is a very important feature in eyeglass lenses. Plastic lenses such as CR-39 eliminate the harmful effects of UV rays due to their chemical structure, but this elimination does not reach sufficient levels. Therefore, UV coatings are of great importance in CR-39 and similar plastic lenses. UV coatings are generally obtained either by using fully organic materials or by using organic and inorganic materials simultaneously.

The application process is usually carried out using sol-gel or spray methods and includes surface cleaning and activation, UV-absorbent layer application, drying and curing, and quality control steps. In the surface cleaning and activation step, ultrasonic washing and plasma or chemical activation are used to increase the adhesion of the coating. In the UV absorber layer application, organic UV absorbers are deposited onto the

surface as a thin film. In the drying and curing step, polymerisation is achieved using mild heat or UV light, increasing the mechanical and chemical resistance of the coating. Finally, a quality control stage is carried out to check whether the coating achieved the target UV protection value.

2.6. Mirror Coating

Mirror coatings consist of thin metallic or metal oxide layers applied to the surface of eyeglass lenses, and their primary function is to reflect a large portion of the incoming sunlight, thereby reducing the amount of light reaching the eye. This feature significantly reduces eye fatigue and glare in environments with high light reflection, such as skiing, mountaineering, and water sports.

Materials such as aluminium, silver, chromium, titanium dioxide, and silicon dioxide are commonly used in these coatings. The selected chemicals are applied to the glass surface in the form of nano-sized particles, creating an optical film on the glass surface. The colour of the coating varies depending on the thickness of the layer and the type of metal oxide used. Gold-coloured coatings transmit more red and yellow wavelengths, while blue coatings partially reflect blue and green light.

The optical performance of mirror coatings largely depends on surface homogeneity and layer quality. As metallic layers are very thin and fragile, they can be easily scratched by direct contact or abrasive cleaning processes. Therefore, it is recommended that coatings be reinforced with a protective top layer . This makes the glass resistant to scratches and abrasion, preserving the surface brightness and reflection homogeneity.

Mirror coatings are typically obtained using physical vapour deposition (PVD) or ion-assisted deposition (IAD) methods under vacuum. The process consists of surface preparation, vaporisation of the metal or metal oxide layer,

thickness control, and application of the protective top layer. During the surface preparation stage, the glass is cleaned of dirt, grease, and particles using ultrasonic washing and plasma activation. During the evaporation of the metal or metal oxide layer stage, the metal or oxide is evaporated in a vacuum environment and deposited homogeneously onto the surface. During the thickness control stage, the layer thickness is controlled, and finally, the protective top layer application ensures the protection of the mirror coating with a hard coating and an optional hydrophobic/oleophobic layer.

Mirror coatings not only reflect light but also enhance clarity perception. They reduce glare for athletes in low-light conditions while optimising colour perception in bright environments. Light transmittance may vary depending on the coating's colour and thickness.

Today, mirror coatings can be applied as multi-layer systems integrated with AR, UV, hydrophobic and oleophobic coatings. This allows the glass to offer both aesthetic appeal and high-performance protection.

2.7. Anti-static Coatings

Static electricity accumulated on the surface of eyeglass lenses causes dust, pollen, and small particles to adhere, reducing vision quality and increasing the need for cleaning. Anti-static coatings significantly reduce dust accumulation by decreasing the build-up of electrical charge on the surface. This provides users with a cleaner eyeglass lens experience and allows them to use their lenses for longer without damaging the AR, UV, hydrophobic/oleophobic layers.

Antistatic coatings are typically derived from conductive or semi-conductive polymers, metal oxide nanoparticles, or ionic compounds. When applied to the surface, these materials disperse accumulated static charges, neutralise electrical potential

differences, and prevent dust and particles from being electrostatically attracted.

The most commonly used components in this coating include indium tin oxide, polyaniline, polypyrrole, and carbon nanotubes. These materials are applied in nanometre-scale layers on top of AR or hard coatings. Surface conductivity is controlled to ensure minimal impact on optical transparency and light transmittance.

Application is typically performed using sol-gel, spray, or vacuum deposition methods. The process involves the following steps: surface preparation, deposition of the antistatic layer, drying and curing, and quality control. During the surface preparation stage, the glass surface is cleaned and the surface energy is adjusted using plasma or chemical activation. During the deposition of the antistatic layer, nanoparticles or conductive polymers are applied to the surface from a controlled solution; dip-coating, spin-coating or vapour phase methods are used for this stage. In the drying and curing stage, the coating layer is dried at room temperature or with gentle heat, and its mechanical strength is increased through cross-linking. Finally, in the quality control stage, surface resistance and optical transmittance are measured to verify compliance with standards.

Antistatic coatings are generally applied as a thin build-up layer on top of AR coatings. This protects all optical layers, maintains surface smoothness and light transmittance, allowing the user to benefit from reduced glare and low dust accumulation on the glass.

3. MODERN COATING TECHNOLOGIES

Today, coatings used on optical glass are not only used for reflection reduction or aesthetic purposes. These coatings are also

designed to increase glass durability, provide water and oil repellency, create UV protection, and impart antistatic properties.

3.1. Vacuum Coating Technology (PVD & Sputtering)

Advanced surface technologies such as AR, mirror, and certain UV coatings in optical glass are typically applied in a vacuum environment.

PVD (Physical Vapor Deposition): The coating material is vaporised with high energy and deposited onto the glass surface at the atomic level. This method is frequently preferred because it allows for high optical homogeneity and dense layers.

Sputtering: In this method, ion bombardment is performed on the glass material, causing particles to detach from the surface and form a thin film layer on the glass. This method is used to increase the durability of coatings such as titanium dioxide, zirconium dioxide, and silicon dioxide in AR and mirror coatings.

Both methods are important technological production methods that determine the mechanical durability and optical quality of coatings. Parameters such as vacuum quantity, material purity, layer thickness, surface temperature, and ion energy are highly effective in minimising reflection, achieving homogeneous colour distribution, and obtaining a long-lasting coating.

3.2. Nano-Coating Technologies

Nano-coating technologies aim to control the roughness of the glass surface with high precision, preventing unwanted structures such as water and oil molecules from adhering to the glass surface. This makes the glass surface cleaner and more resistant to contamination. Consequently, the hydrophobic and oleophobic coating mechanisms are strengthened. Another important effect is that nano-sized coating layers reduce light

refraction on the glass surface, making the glass more transparent. This is particularly important in high-index glass.

Nano coatings such as titanium dioxide have photocatalytic properties. Thanks to these properties, nano coatings such as titanium dioxide can remove unwanted organic-based structures from the glass surface under sunlight. Although this property exists in physical terms, it has not yet become widespread enough in optical glass production. It is expected that this technology will be used much more frequently in optical glass in the future.

There are some innovative approaches that are expected to come to the fore in coating technologies in the future. Some of these are: self-healing coatings, smart (adaptive) coatings and photocatalytic cleaning coatings.

3.2.1. Self-healing coatings

Research is being conducted on the ability of nano polymer chains to repair minor damage on surfaces themselves (Chen et al., 2025; Wang et al., 2020; Coillot, Méar, Podor, & Montagne, 2010; Finkelstein-Zuta et al., 2024). If this technology becomes widespread, the mechanical durability and, consequently, the service life of glass coatings will increase significantly.

3.2.2. Smart (Adaptive) Coatings

Studies on smart (adaptive) coatings that can change their reflection properties depending on light intensity are frequently encountered in the literature (Ren & Wu, 2018; Algorri, Zografopoulos, Urruchi, & Sánchez-Pena, 2019; Hartmann, Penkner, Danninger, Arnold, & Kaltenbrunner, 2020). These coatings provide comfortable use by ensuring that eyewear users are less affected by sudden changes in their environmental conditions.

3.2.3. Photocatalytic Cleaning Coatings

Research is ongoing into coatings that utilise materials with photocatalytic properties on glass surfaces to facilitate the breakdown of organic contaminants under light. (Mellott, Durucan, Pantano, & Guglielmi, 2005; Çamurlu, Kesmez, Burunkaya, Kiraz, Yeşil, Asiltürk, & Arpaç, 2012; Altın, Polat, Bacaksız, & Sökmen, 2012). When this type of coating is sufficiently successful, it will be possible to observe that the glass surface can clean itself.

3.3. Digital Coating Design

Modern coatings simulate and optimise a series of physical parameters using computer programmes before the physical coating process begins. These physical parameters include the refraction, reflection, and transmission behaviour of light on the surface, as well as the number and thickness of the coating layers. Once these parameters are optimised, it is possible to achieve minimum reflection and maximum transparency in coatings applied under the specified coating conditions.

Particularly in blue light-filtered coatings, it is necessary to target specific wavelengths, not just visible light. This ensures blue light filtering efficiency while optimising AR performance. Manufacturers use these digital design methods to test integrated formulations of AR, UV, hydrophobic, and oleophobic layers; layer thicknesses are applied with nanometre precision in production.

Thanks to digital coating design, modern glass minimises optical defects even in different materials such as high-index, polycarbonate or CR-39, while maximising surface durability and functional properties.

4. PERFORMANCE CRITERIA FOR COATINGS

The fundamental performance criteria of optical coatings are whether their optical and mechanical properties are sufficiently good. Various tests are applied to determine how coatings will perform in long-term use. These tests include the Taber abrasion test to measure scratch and surface wear resistance, a thermal cycling test to measure resistance to temperature changes, a solid particle spray test to measure resistance to corrosive environments, chemical resistance tests to measure resistance to detergents and cleaning agents, and adhesion tests to evaluate the bonding strength of the layers to the surface.

Properties such as reflection amount, clarity ratio, light transmittance and spectral distribution, which are criteria for the optical performance of coatings, are determined using spectrophotometer devices.

5. USER SATISFACTION CRITERIA

The success of coatings is evaluated not only through laboratory tests but also through user experiences. The main factors determining user satisfaction are as follows:

- Ease of cleaning,
- Stain resistance,
- Reflection reduction level,
- Lifespan of the coating.

These criteria fundamentally highlight the quality of the coating and the importance of coating types.

6. SELECTING THE RIGHT COATING FOR THE USER

The choice of coating types varies depending on the user's daily needs and conditions of use. Recommended coating combinations for different user groups are summarised below:

Digital Screen Users

- Anti-reflective coating
- Blue light filter coating
- Oleophobic top layer

Drivers

Advanced AR coating

Hydrophobic layer

Low reflection spectrum coatings

Athletes

- Mirror coating
- Highly durable hard coating
- Hydrophobic layer

Children

- High scratch resistance hard coating
- UV protection layer

Industrial workers

- Coatings with enhanced chemical resistance
- Extra AR or UV filters

7. CONCLUSION

Optical glass coatings have become an indispensable part of today's optical technologies. Modern glass coatings improve vision quality and comfort of use while also enhancing the life and functionality of the glass. Although the most commonly used coatings today are AR coatings, hard coatings, UV protective coatings, hydrophobic coatings, and oleophobic coatings, advanced technological glass coatings such as self-repairing glass, glass that adapts to changing environmental conditions, and self-cleaning glass will likely take their place in the field in the future.

REFERENCES

Algorri, J. F., Zografopoulos, D. C., Urruchi, V., & Sánchez-Pena, J. M. (2019). Recent advances in adaptive liquid crystal lenses. *Crystals, 9*(5), 272. https://doi.org/10.3390/cryst9050272

Altın, İ., Polat, İ., Bacaksız, E., & Sökmen, M. (2012). ZnO and ZnS microrods coated on glass and photocatalytic activity. *Applied Surface Science, 258*(11), 4861–4865. https://doi.org/10.1016/j.apsusc.2012.01.082

Chen, Y., Chen, J., Ji, X., Wang, P., Shang, Z., Ji, C., Kiryukhantsev-Korneev, P. V., Levashov, E. A., Ren, X., Kang, X., Zhang, B., Zhang, P., Wang, X., Feng, P., Peng, J., Wang, J., & Song, K. (2025). In-situ engineered ZrB_2-$ZrSi_2$-$MoSi_2$ coatings with self-healing multiphase glass networks for superior oxidation protection at 1973 K. *Corrosion Science, 257*, 113355. https://doi.org/10.1016/j.corsci.2025.113355

Coillot, D., Méar, F. O., Podor, R., & Montagne, L. (2010). Autonomic self-repairing glassy materials. *Advanced Functional Materials, 20*(24), 4371–4374. https://doi.org/10.1002/adfm.201000147

Çamurlu, H., Kesmez, Ö., Burunkaya, E., Kiraz, N., Yeşil, Z., Asiltürk, M., & Arpaç, E. (2012). Sol-gel thin films with anti-reflective and self-cleaning properties. *Chemical Papers, 66*(5), 555–562. https://doi.org/10.2478/s11696-012-0144-4

Finkelstein-Zuta, G., Arnon, Z. A., Vijayakanth, T., Messer, O., Lusky, O. S., Wagner, A., Zilberman, G., Aizen, R., Michaeli, L., Rencus-Lazar, S., Gilead, S., Shankar, S., Pavan, M. J., Goldstein, D. A., Kutchinsky, S., Ellenbogen, T., Palmer, B. A., Goldbourt, A., Sokol, M.,

& Gazit, E. (2024). A self-healing multispectral transparent adhesive peptide glass. *Nature, 630*(8016), 368–374. https://doi.org/10.1038/s41586-024-07408-x

Hartmann, F., Penkner, L., Danninger, D., Arnold, N., & Kaltenbrunner, M. (2020). Soft tunable lenses based on zipping electroactive polymer actuators. *Advanced Science, 8*(3), 2003104. https://doi.org/10.1002/advs.202003104

Mellott, N., Durucan, C., Pantano, C., & Guglielmi, M. (2005). Commercial and laboratory prepared titanium dioxide thin films for self-cleaning glasses: Photocatalytic performance and chemical durability. *Thin Solid Films, 502*(1–2), 112–120. https://doi.org/10.1016/j.tsf.2005.07.255

Ren, H., & Wu, S. (2018). Adaptive lenses based on soft electroactive materials. *Applied Sciences, 8*(7), 1085. https://doi.org/10.3390/app8071085

Wang, H., Liu, H., Cao, Z., Li, W., Huang, X., Zhu, Y., Ling, F., Xu, H., Wu, Q., Peng, Y., Yang, B., Zhang, R., Kessler, O., Huang, G., & Wu, J. (2020). Room-temperature autonomous self-healing glassy polymers with hyperbranched structure. *Proceedings of the National Academy of Sciences, 117*(21), 11299–11305. https://doi.org/10.1073/pnas.2000001117

THEORETICAL AND EXPERIMENTAL APPROACHES IN SCIENTIFIC STUDIES 2025

yaz
yayınları

YAZ Yayınları
M.İhtisas OSB Mah. 4A Cad. No:3/3
İscehisar / AFYONKARAHİSAR
Tel : (0 531) 880 92 99
yazyayinlari@gmail.com • www.yazyayinlari.com

ISBN: 978-625-8508-84-0